Effect of Soil Arching on Stress Developments in Underground Mine Stopes, Drives and Barricades

Submitted by

Seneth Udara Jayakodi, B.Sc. (Eng.) Hons

in fulfilment of the requirements for the degree of

Doctor of Philosophy

College of Science and Engineering

James Cook University

September 2024

Statement of access

I, the undersigned, the author of this dissertation, understand that James Cook University will make it available for use within the University Library and, by microfilm or other means, allow access to users in other approved libraries.

All users consulting this dissertation will have to sign the following statement:

In consulting this dissertation, I agree not to copy or closely paraphrase it in whole or in part without the written consent of the author; and to make proper public written acknowledgement for any assistance which I have obtained from it.

Beyond this, I do not wish to place any restriction on access to this dissertation.

…… ……

Signature Date

Statement of sources

DECLARATION

I declare that this dissertation is my own work and has not been submitted in any form of another degree or diploma at any university or other institution of tertiary education. Information derived from the published or unpublished work of others has been acknowledgement in the text and a list of references is given.

…… ……

Signature Date

Statement of the contribution of others

Grants	This research work was financially supported by the James Cook University Postgraduate Research Scholarship (JCUPRS) offered by the Graduate Research School of JCU, and also, the Doctoral Completion Grant provided from the Primary Advisor's funds. The participation for the international conferences was sponsored by the Primary Advisor's JCU Discretionary Budget Allocation (DBA) account.
Supervision	This research was mainly guided and facilitated by A/Prof. Nagaratnam Sivakugan as the primary advisor, and the additional supervision and support was provided by Dr Peter To as the secondary advisor.
Editorial assistance	The editorial assistance for both dissertation and research articles was provided by the A/Prof. Nagaratnam Sivakugan and Dr Peter To.

Acknowledgements

Numerous people have supported to the successful completion of this research. It is my great pleasure to acknowledge their contribution.

Firstly, I'm truly grateful to my primary advisor Associate Professor Nagaratnam Sivakugan for his patience, motivation and continuous advice and support throughout my PhD research. His immense knowledge and invaluable guidance helped me in all the time of research work and writing of this dissertation. Thank you, Prof. Siva, without your untiring efforts and guidance, my PhD research would not have been a success. Besides Prof. Siva, I would like to appreciate my secondary advisor Dr Peter To for his valuable comments on my written work and presentations, and for his support especially during the pressure sensor selection for my model apparatus. In addition, my sincere thanks go to all laboratory technicians in the Geomechanics and Structures laboratories as well as to the technical specialists in the JCU Advanced Analytical Centre and workshop.

I also wish to acknowledge the JCU postgraduate research scholarship, which covered the tuition fees and provided a living allowance during my studies as well as the financial support received from my HDR account and my primary advisor's funds to support my academic and conference travel expenses. My sincere appreciation goes to the Graduate Research School team, College of Science Engineering team, International Student Support team and the Library staff for their various support throughout my candidature.

Finally, and importantly, I would like to thank my beloved wife Ashani for her patience and for keeping my priorities in perspective. I also wish to express my sincere love and gratitude to my dearest parents for supporting me spiritually throughout my studies and life.

To my parents, wife and teachers

Abstract

Mine backfilling with processed mine tailings is a widely used method to fill the large underground voids created as a result of mining, to ensure the regional stability of the mining area. During backfilling, stress is developed within the fill in the mine stope, and that is influenced by soil arching. Prior to backfilling, the horizontal drives of the mine are barricaded with competent retaining walls to prevent backfill material entering other working areas of the mine. The failure of a barricade can be catastrophic causing interruptions to mining operations resulting financial loss and potential fatalities. Barricade failures have been reported worldwide during the past two to three decades with the increasing trends in mine backfilling processes. Therefore, it is significant to determine the stress behaviour within backfilled mine stopes as it paves the way to design safe backfill systems for mines. Accordingly, this research critically analysed the stresses within a hydraulic fill mine stope and quantified the lateral loading on the drive barricade through analytical, laboratory and numerical approaches.

Geotechnical characterisation of mine tailings is initially done to determine its potential suitability for backfill material. Accordingly, the Ernest Henry Mine (EHM) tailings used in this study was characterised to use as Hydraulic fill (HF) material in the laboratory models for backfill stress analysis. Further, fine sand was tested for geotechnical properties and confirmed to be use as an alternative material for HF research studies where the access and supply of real HFs from mines is difficult or not possible at all. The self-weight settling column tests carried out over the entire natural drying process of Pajingo mine tailings revealed that the large clay content in the Pajingo fill induced lateral shrinkage of the fill causing a complete fill-wall detachment leading to loss of arching in the stope and possible increase of barricade stress. Hence, the importance of analysing the long-term settlement behaviour of backfills and the changes of fill settling characteristics, was confirmed and addressed. The shrinkage curves were developed mimicking the fill settling in stope, to estimate the volume variation and final settlement of the fill, for any fill height in the stope.

The stress generation within mine stopes is directly influenced by soil arching. A general expression was developed to determine the shear stress on stope wall at any depth of the fill. Accordingly, the variation of shear stress with fill depth was modelled analytically for square and circular shaped stopes, introducing two coefficients to account the fill properties and stope wall roughness. These coefficients were used in developing analytical models for the variation of vertical normal stress within the fill along depth, which were then validated with laboratory stope arching model data. It confirmed that the vertical normal stress within the fill increases continuously with fill depth, but the shear stress is high at lower fill depths and then becoming asymptotic with the increase of depth. Analytical solutions suggested that taking interfacial friction angle of the fill-wall equal to the friction angle of the fill, gives better approximations to the stresses within the stope. Moreover, it was determined that the variation of earth pressure coefficient with fill depth is not constant as suggested in analytical solutions, however, the use of at-rest earth pressure coefficient in the analytical equations was found to be conservative. Numerical simulations with continuum approach have suggested that the normal stress becomes asymptotic after a certain fill depth. In contrast, particulate modelling has shown a continuous increase of normal stress within the fill throughout the depth, correlating better with laboratory test data.

The arching developed in horizontal drive and an accurate estimation of stress on the drive barricade is an important aspect of barricade design. Barricades can fail around the wall-rock interface and/or at the barricade centre due to different failure mechanisms. Hence, it is important to investigate the stress formation on the entire barricade surface due to the fill load in the stope. Accordingly, barricade surface pressure mapping was done with a laboratory model setup, to visualise and determine the distribution of load that comes from the surcharges applied at the fill top representing the fill mass in the stope. Then the barricade stresses were analysed using the pressure sensors attached in the model, for varying parameters such as barricade size and offset distance. It was found that the barricade stress near the drive top is minimum agreeing with low stress transformation at drive top region associated with the flow pattern of the fill.

Further, the maximum fill load is transferred and concentrated at the barricade centre suggesting that the barricade may likely to fail at centre due to punching failure mechanism. The barricade stress near the drive floor region is less compared to that at the centre, suggesting the frictional immobilization at drive floor and thus the arching within the drive caused the reduction of fill load on barricade near the drive bottom. The barricade stress comparison with analytical solutions reconfirmed that the at-rest earth pressure coefficient is the appropriate parameter to use in analytical equations. It was also revealed that the barricade stress variation with offset is non-linear, which showed a good agreement with analytical and numerical solutions. Moreover, an empirical equation is proposed to determine the barricade stress for any drive size located at any offset, after comparing with the analytical and numerical solutions.

Table of Contents

List of Figures

List of Tables

Chapter 1

1 Introduction

1.1 General

The vertical stress at a point in an ideal geotechnical assessment is calculated using the product of soil unit weight and depth. However, in underground mine stopes, behind retaining walls and in grain and pharmaceutical silos, the vertical stress at a point can be much less. The reduction in vertical stress is due to the development of shear stress at the interface of the material and walls (Fahey et al., 2009). The phenomenon that describes this reduction in vertical stress is known as 'soil arching'. Soil arching was first quantified by Terzaghi (1943) with his trap door experiment (Pirapakaran and Sivakugan, 2007b). Researchers including Janssen (1895), Marston (1930) and Sivakugan and Widisinghe (2013) have conducted research and developed analytical expressions to predict vertical stress in a variety of void situations, including silos, trenches and underground mine stopes.

This research will aim at extending the current knowledge of the arching theory in regard to stress distribution in underground mine stopes, drives and at barricades. The operational stress prediction methods discussed in this dissertation will be investigated and tested using a laboratory vertical stope model and barricade model apparatus developed at James Cook University.

Laboratory testing will attempt to confirm the accuracy of analytical expressions and numerical models currently in-use to predict the stresses in the underground mining environment. The continuum approach based numerical modelling methods used in predicting the stress behaviour within backfilled stopes will be compared in terms of the real stress developments in a particulate medium. The appropriate use of the lateral earth pressure coefficient (K) in vertical and horizontal stress predictions will be a focus point of the analysis, along with the determination of relationships including the stress variation with increased barricade offset, barricade pressure variation with drive size and the soil friction angle effect on the reduction of lateral stress on the barricade.

1.2 Mining

The Australian mining industry is essential to the growth of the economy and our way of life. Mining of all resources from 379 operating mines contributes about 13 % to Australia's GDP and around 60 % of exports. The Australian mining industry directly employs more than 300,000 people throughout Australia, with many more benefiting indirectly. The mining industry is particularly important to the economic and social wellbeing of the regional and indigenous communities. The continued economic performance, community involvement and workplace health and safety in the mining industry are imperative to a strong national economy and quality of life in Australia.

The 'open cut' and 'underground' mining are the two main mining methods used in Australia as well as in other countries for ore recovery. The main difference between the two is the method of ore removal (Sivakugan, 2008). The underground mining technique is utilised when there are large volumes of overburden to be removed to reach the typical narrow and steep ore body that is extending into the ground with high dipping angle, rather than laterally. Hence, the ore is accessed by shafts and tunnelling through the earth (Sivakugan, 2008). This research focusses on the geotechnical aspects of backfilling of underground voids resulted after mining of the ore.

1.3 Mine waste management

Mining and processing involve extracting valuable concentrate of minerals and metals from the ore reserves being mined out. During this process, a large amount of waste is generated which is inevitable but should be managed properly and responsibly complying with the sustainable goals. There are three main types of mine wastes based on the source of generation namely overburden/waste rock, tailings and mine wastewater. Overburden and waste rock are accumulated during blasting, scaling, mining and overburden removal activities while the mine tailings and wastewater are generated during the processing stage. Mine waste management is a crucial part in the mining life cycle and therefore execution of a well-defined mine waste

management and disposal plan is utmost important. It is essential that the mine waste management plan should be strategically designed before any mining activities are commenced but it can be updated as required when the project progresses. The waste disposal plan should be a custom-tailored document which accounts for the individual circumstances of each mining site such as mining method and type of ore being mined, space availability for disposal, socio-economic and environmental aspects, etc. Mine wastewater is often reused in the processing cycle and in dust suppression. When it comes to solid mine waste management such as waste rock and dewatered tailings, there are different methods currently in practice worldwide as below.

- Direct disposal
    - Riverine tailing disposal (RTD)
    - Submarine tailing disposal (STD)
- Tailing Storage Facilities (TSFs) (Figure 1.1)
- Underground backfilling of voids
- Ground improvement works
- Dry stacking
- On-site rehabilitation (landfills)
- Use as construction materials (aggregates) and in other processes and industrial applications

Figure 1.1. Sarsfield pit used as a TSF in Ravenswood gold mine, Queensland

Nowadays, mining is being carried out extensively in most of the countries due to high demand of mineral commodities in the manufacturing and other industries to fulfil human needs and services. As a result, mine waste generation has also been increased progressively in the past few decades. With the recent technological advancements in the mining and processing industry, low-grade ore processing is becoming popular which leads to even more tailing accumulation down the line. Therefore, sustainable approaches for tailing management are highly encouraged to reduce negative socio-environmental impacts. The reduce, reuse, recycle and reprocess/recover concepts play vital roles for outlining a greener tailing management plan for a successful implementation. Backfilling of voids is a widely accepted and utilised method of reuse of mine tailings where it helps to minimise tailing dam constructions and at the same time it supports the underground mining operations.

1.4 Mine backfilling

The removal of ore in underground mining creates large cavities, known as stopes. The stopes are accessed through horizontal drives that allow machinery to remove the ore. Underground mine stopes have base dimensions of 20 m – 60 m and heights in excess of 200 m (Sivakugan et al., 2014) and they are assumed rectangular for analytical purposes. Once the rock has been removed and processed, the stope requires backfill for surrounding stability and continued production. The backfilling of stopes can represent up to 20% of underground mining costs (Grice, 2001). The three main types of backfill used include hydraulic, paste and rock or aggregate fill which utilise excess waste rock or tailings (Grice, 2001). The granular soil or backfill used in laboratory testing of this study resembles an Australian dry hydraulic fill.

The horizontal drives that access the stope for ore removal need to be barricaded or capped to allow for the backfill process to take place. An idealised underground mine stope is shown in Figure 1.2. The construction and performance of these barricades is a major topic in the mining industry today. The correct calculation of the stress state in the backfill and the associated pressures exerted on the barricade is a critical engineering challenge (Li and Aubertin, 2009a).

Barricade failures in underground mines lead to serious consequences including damage to machinery, flooding and in some cases injury or death to workers. A barricade failure in 2000 at the Bronzewing mine in Western Australia resulted in 18000 m^3 of hydraulic fill being released into the working area, claiming three lives (Rankine et al., 2007). The analysis of backfill stress developments within the stope is required first, before attempting to determine the stress state in the barricade. This can pave the way to improving the prediction of barricade stress and the effective design of drive barricades (Sivakugan et al., 2014).

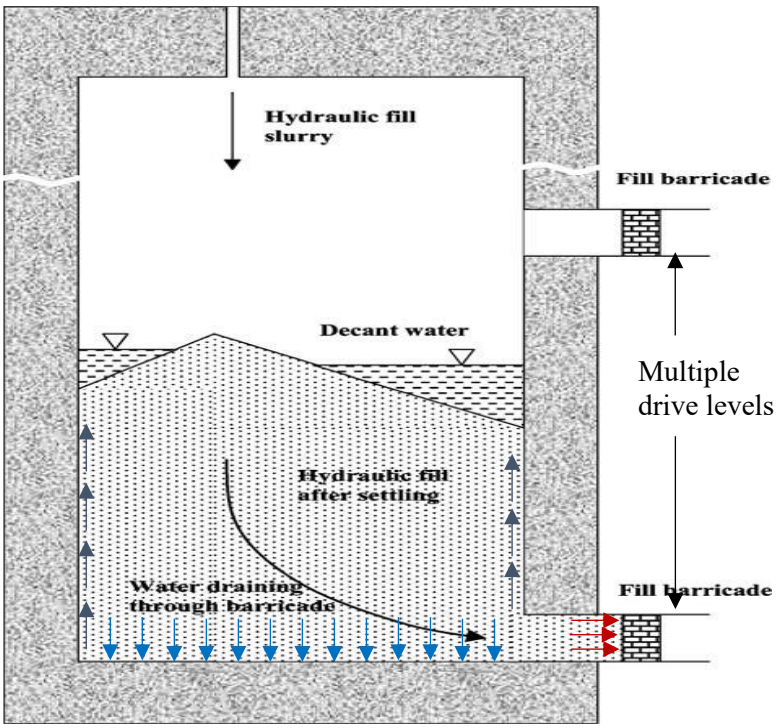

Figure 1.2. Idealised underground mine stope (Fahey et al., 2009; Rankine et al., 2006)

1.5 Problem statement and research significance

Analytical expressions and numerical modelling for vertical stress with depth have been studied and extended numerous times, however, in-situ ('real world') results of average vertical stress in a backfilled mine stope are rare. Analytical and some numerical methods are based on an approach that treats the mine backfill as a continuum, whereas in reality the fill is a particulate medium, thus a prediction methods encompassing both approaches may be optimal. Belem et al. (2004) conducted in-situ measurements of these in cemented paste fill backfill, however, not with

hydraulic fill. The laboratory vertical stope and barricade pressure models developed at James Cook University will allow scale in-situ testing and comparison of results from the different approaches. The intent of this research is to investigate these operational stress developments in underground mine stopes, drives and at barricades in relation to the soil arching phenomenon. The study of arching in drive and barricade, and the methods used to predict operational stress is critical due to the catastrophic nature of barricade failures. A few examples of barricade failures reported in Australia, are presented in Table 1.1.

Table 1.1. Examples of barricade failures occurred in Australia

Year	**Incident/ Mine**	**Location**	**Consequences**	**References**
2000	Osborne Mine	Queensland	Rehabilitation	Duffield, Gad, and Bamford (2003)
2000	Bronzewing Mine	Western Australia	Three fatalities	Rankine et al. (2007)
2003-2006	Twelve barricade failures	Multiple locations	Not reported	(Helinski, Fahey, and Fourie (2011)
2007	Two mines- five barricade failures	Not reported	Not reported	Revell and Sainsbury (2007b)

Mine backfilling strategies in slurry form can be of different types, namely, Hydraulic fills (HF), Paste fills (PF), Cemented Hydraulic fills (CHF) and Cemented Paste backfills (CPB) owing to their unique characteristics for particle size distribution, consistency (solid content), binding effect, permeability, rheological properties, and etc. Hydraulic fills are the deslimed coarser fraction of mine tailings consisting sand and silt with the solid content of 60-70 % by weight allowing for faster drainage and fill settlement in the stope. In contrast, paste fills are the thickened tailings comprised of the finer fraction of mine tailings including clay particles and its high solid content of 70-85 % by weight lead the fill to undergo the consolidation process, resulted in higher drainage and fill settlement time. Cemented backfills are produced when 3-6 % binding agent such as cement, lime or gypsum is added to HF or PF. In comparison to other backfill types, HFs have favourable characteristics for backfilling such as cost effectiveness, less preparation

work and time only with tailings and water, easy handling especially during transportation in pipelines due to absence of fill stratification and clogging, faster filling schedules due to quicker drainage process, etc. Different backfill types and their characteristics are discussed in detail in Chapter 2 (Jayakodi et al., 2023).

Investigations into stress developments within HF stopes have not been fully covered to date particularly in relation to shear stress distribution along the fill-wall interface of the stope due to arching. The shear resistance developed along the stope wall is the main influencing factor in governing the variation of the vertical normal stresses within the fill in the stope and the horizontal normal stress onto the barricade in the drive. Therefore, this research study attempts to fill the gap aforementioned by formulating a new arching equation for shear stress determination at a given depth of the fill in the stope and then analysing stress variations within the stope and on the barricade surface, integrating analytical, experimental and numerical approaches. Most of the existing numerical modelling work on HF stopes are based on continuum approach, confirming an asymptotic nature of the fill stress after a certain depth of the fill. However, mine tailings are particulate matter thus requiring the stope to be modelled numerically embedding solid particles in the simulation process. Hence, the continuum and particulate modelling of a laboratory tested HF stope are compared in this study to highlight the differences in stress variations from the two modelling methods and to confirm the degree to which the particulate modelling agrees with the stresses generated from the experimented stope that mimics the nature of HF behaviour in an actual mine stope.

Results from the laboratory tested HF stope will be compared to Pirapakaran and Sivakugan (2007a) analytical expressions and the finite difference numerical modelling code from FLAC (Fast Lagrangian Analysis of Continua) to determine their accuracy, and the suitable application of the lateral earth pressure coefficient. The investigation of these ‘real’ stress developments is extended to determine the horizontal stresses acting on access drive barricades using the laboratory barricade model. Barricade testing results will be compared with Li and Aubertin (2009a), Kuganathan (2002) analytical expressions. Numerical solutions from FLAC

will be compared with the laboratory barricade model test results. The results and analysis conducted throughout this research will attempt to evaluate the accuracy and reliability of current prediction methods assisting the mining industry to efficiently, economically and safely design and construct engineered backfill and drive barricade structures dependant on operational stresses.

1.6 Research aim and objectives

The aim of this research is to critically investigate the arching and stress developments within backfilled stopes and drives and to develop a methodology to estimate the loads onto barricades synthesizing analytical, numerical and laboratory studies. The following objectives are set in order to estimate loads onto backfilled barricades.

1. To revisit the stress transfer mechanisms in hydraulic backfilled stopes
2. To quantify the geotechnical characteristics of materials used in this study and suggest alternative materials for granular hydraulic fills
3. To measure vertical stress in backfilled stopes and develop alternative analytical solutions to verify the test results
4. To measure the variation of the barricade stress with the change of barricade location within the drive and the effect of barricade dimension on stresses in laboratory tests
5. To verify the laboratory model tests with numerical modelling methods
6. To determine the appropriate lateral earth pressure coefficient for backfill stress estimation

1.7 Thesis outline

Chapter 1 introduces the soil arching theory and the underground mining process. The importance of predicting stresses in the backfilled stope and at drive barricades are discussed and the research problem statement and research significance are also covered.

Chapter 2 reviews the literature related to previous research on the soil arching theory and applications to the underground mine backfill process. The limitations of analytical methods in predicting stresses in backfilled stopes are identified and discussed. The identified research gaps with analytical and numerical modelling approaches in the accurate determination of the backfill stresses are also covered. Mine fill types, behaviour of a backfill system, barricade types and failure mechanisms are also discussed.

Chapter 3 presents a complete geotechnical characterisation of real mine tailings and other alternative materials. The correlation between actual mine tailings and other experimental materials which can be used for physical modelling of mine fill stopes and barricades for research purposes, is also discussed. The effect of soil shrinkage phenomena in a self-weight consolidated fill on arching and thus stress developments within the fill, influenced by the fine content in the fill, are investigated experimentally. A proper understanding of the fill properties and fill settling behaviour are important for analysing and interpreting the fill stress models.

Chapter 4 focuses on stress developments in underground mine stopes. The vertical stope testing apparatus and interpretation methods are discussed, and results are displayed. A novel analytical expression is proposed for shear stress determination followed by analytical models and generalised plots for vertical normal stress estimation are proposed and validated with laboratory test results. The analytical and numerical values of vertical stress are compared to laboratory results. The correct application of the lateral earth pressure coefficient in backfill stress equation is discussed. The importance and credibility of particulate approach in stress simulations of backfilled stope compared to the continuum approach, are also presented in this chapter.

Chapter 5 focuses on the analysis of drive stresses and estimation of lateral loadings on barricades. The barricade testing method and apparatus are covered with special attention given to the barricade stress distribution using the surface pressure mapping sensors used in the physical model. A section of results and analysis is given with the main discussion points including the relationship of lateral barricade stress and barricade offset, lateral earth pressure coefficient and the application of analytical and numerical prediction methods. Finally, a methodology is

proposed to determine barricade stress using analytical and empirical equations developed in this dissertation.

Chapter 6 summarises the full research study, discussing all testing methods (i.e. fill properties, vertical stope and barricade) and research findings from each chapter are put forward. Finally, to conclude the dissertation, recommendations for future research are outlined.

Chapter 2

2 Literature Review

2.1 General

The literature related to mine backfilling strategies and stress developments within backfilled stopes as analysed with analytical and numerical approaches are presented in this chapter identifying their limitations and approximations. Furthermore, the potential of accurate and reasonable stress estimation within a backfilled stope, drive and on barricade by means of laboratory model tests with real tailings, replicating an actual backfill conditions, is discussed.

2.2 Geotechnical aspects of mine backfilling

A detail review of the current literature pertaining to this research study is presented in the published article titled “Geotechnical Considerations of Mine Tailings Management through Mine Backfilling” in appendix A.

Chapter 3

3 Geotechnical Characterisation of Mine Tailings for Potential Use as Backfills

3.1 General

A proper geotechnical characterisation of mine tailings is an important aspect of mine backfill design and it must be done at first. Stress developments within the backfilled stopes, drives and at barricades, and also the shear stresses generated along the stope walls are primarily based on tailing properties and particulate behaviour. Three types of materials were used in this study as shown in Figure 3.1. The geotechnical characteristics of these materials are extensively discussed in this chapter covering the following objectives.

1. Fine sand - to find the suitability for backfill analysis as an alternative material for real mine tailings
2. Ernest Henry Mine (EHM) tailings from a gold-copper mine in Queensland - to find the potential use as backfill material
3. Pajingo mine tailings from a gold mine in Queensland - to compare the tailing settlement behaviour with EHM tailings and to determine its suitability for backfill material

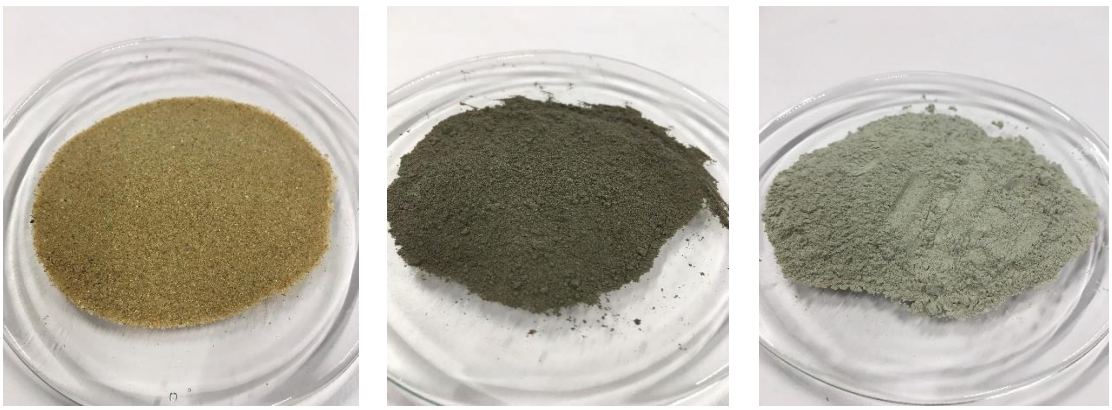

(a) (b) (c)

Figure 3.1. Materials used in this study (a) Fine sand (b) EHM tailings (c) Pajingo tailings

From the visual identification properties of EHM and Pajingo tailings, it was determined that the EHM tailings consist of larger grains which were able to see by naked eye and have silty

nature, implying it may be suitable for HF backfilling, whereas Pajingo tailings are of very fine grains with clayey texture, suggesting its potential use as Paste fill (PF). In order to justify this argument, quantification and comparison of geotechnical characteristics of the tailings were carried out. Accordingly, Grain size distribution (GSD), Atterberg limits, Specific gravity, Friction angle, settling characteristics, other index properties, and mineralogical properties will be discussed in this chapter.

3.2 Grain size distribution

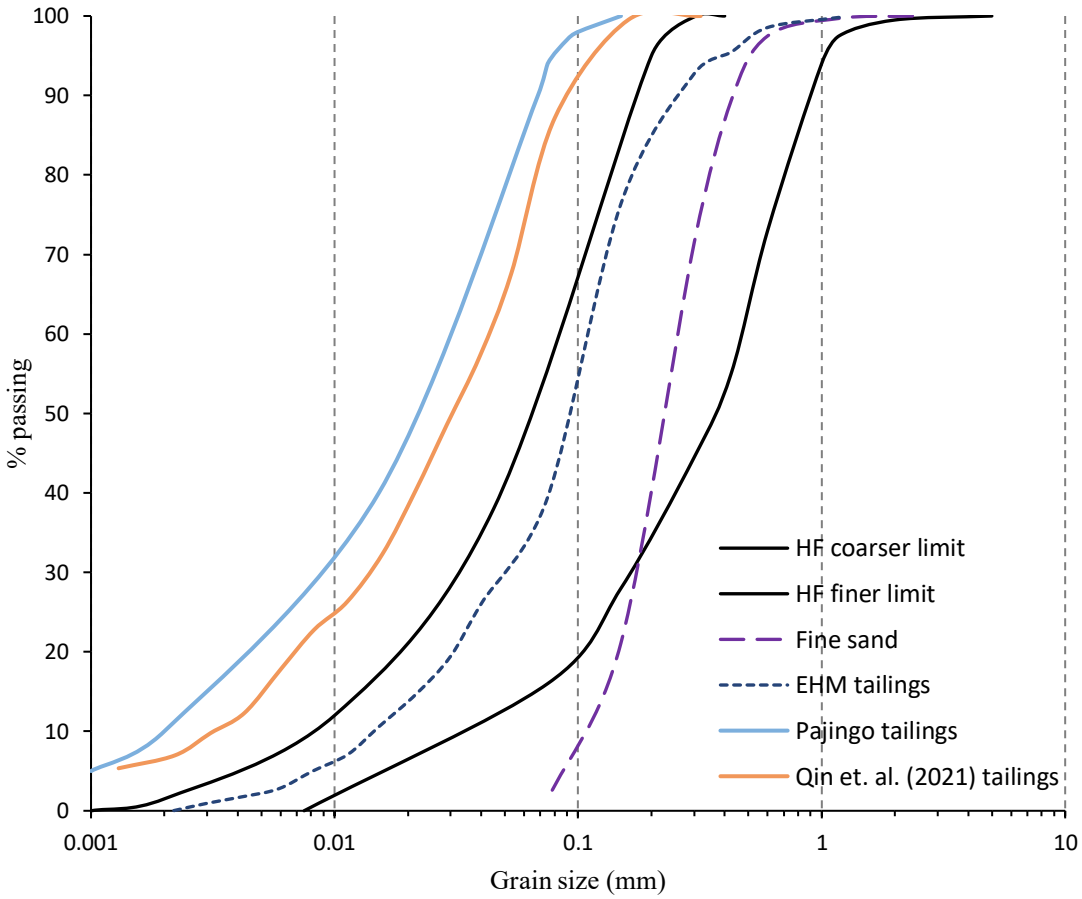

Figure 3.2. Grain size distribution of materials

Sieve analysis and hydrometer test were carried out for all test materials as per AS 1289.3.6.1 and AS 1289.3.6.3, respectively to obtain GSD curves as shown in Figure 3.2.

It can be seen that fine sand is coarser than the EHM tailings and it has only about 1.4 % passing 75 µm particle size. Therefore, fine content analysis with Liquid limit (LL) and Plastic

limit (PL) tests was not required for fine sand. The GSD curve of EHM tailings falls within the zone established for Hydraulic Fills (HF) by Rankine et al. (2006) after testing about 25 HF samples from different mines around Australia. Although EHM tailings have a significant fine content of 39.4 % passing 75 μm particle size, it has no clay fraction once deslimed, and thus it is considered as granular material like fine sand. It was determined that the EHM tailings has LL of 21.3 % and PL of 14.5 % from the tests carried out by Fall cone method (AS 1289.3.9.1) and Rolling thread method (AS 1289.3.2.1), respectively. The Plasticity index (PI) was calculated as 6.8 %. The Unified Soil Classification System (ASTM D2487) was used to classify materials based on GSD and Atterberg limits data. The shrinkage behaviour of Pajingo tailings is compared with the tailings used by Qin et al. (2021) in section 3.9.1 from page 40 to 42. Table 3.1 compares the GSD properties of materials used in this study with general HF properties.

Table 3.1. GSD properties of materials

Property	**Fine sand**	**EHM tailings**	**Pajingo tailings**	**General HF**
D_{10} (μm)	115	16	2	>10
D_{50} (μm)	220	92	11	>65
C_u	2.3	7.2	5.9	3.7-13.3
C_c	1.12	1.4	3.4	0.6-2
Classification (USCS)	SP	SM*	CL	SM or ML

*As per the AS 1726 amended in 2017, EHM tailings are classified as ML.

D_{10} – Effective grain size

D_{50} – Median grain size

C_u – Coefficient of uniformity

C_c – Coefficient of curvature

Hydraulic fills consist mostly uniformly graded tailings which have grains in a narrow range on GSD. The GSD properties of EHM tailings compared well with the general HF properties and thus EHM tailings can be used in potential HF backfilling operations. Furthermore,

the tested fine sand can also be used as an alternative material in laboratory model testing to replicate backfill mine stopes and drives, when the real mine tailings are limited in quantity or not available at all.

3.3 Specific gravity

The specific gravity (G_s) tests by AS 1289.3.5.1 showed that the EHM tailings has G_s of 2.85 whereas the fine sand has G_s of 2.60, and they are compared with the typical specific gravity values in the literature. Generally, tailings have higher specific gravity than normal soils because of the presence of heavy minerals and metals. As tested by Rankine et al. (2006), specific gravity of tailings lies in the range of 2.8-4.4, and thus EHM tailings align with the range. Rankine et al. (2006), based on laboratory and in-situ measurements of dry density and specific gravity of more than 20 HFs, showed that the dry density of the settled tailings is directly proportional to specific gravity of the tailing material as per the following relationship.

$$Dry\ density\ (g/cm^3) = 0.56\ \times Specific\ gravity \qquad \text{Eq. (3.1)}$$

It was determined that the EHM tailings settle at dry density of 1.656 g/cm^3 as discussed in the settling column test presented in Section 3.8.3 in page 34. Accordingly, the red dot in Figure 3.3 indicates where the EHM tailing is placed on the plot. The dry density values of lab data of 20 HFs in Figure 3.3 are from settling of tailing slurry as reported in Rankine et al. (2006).

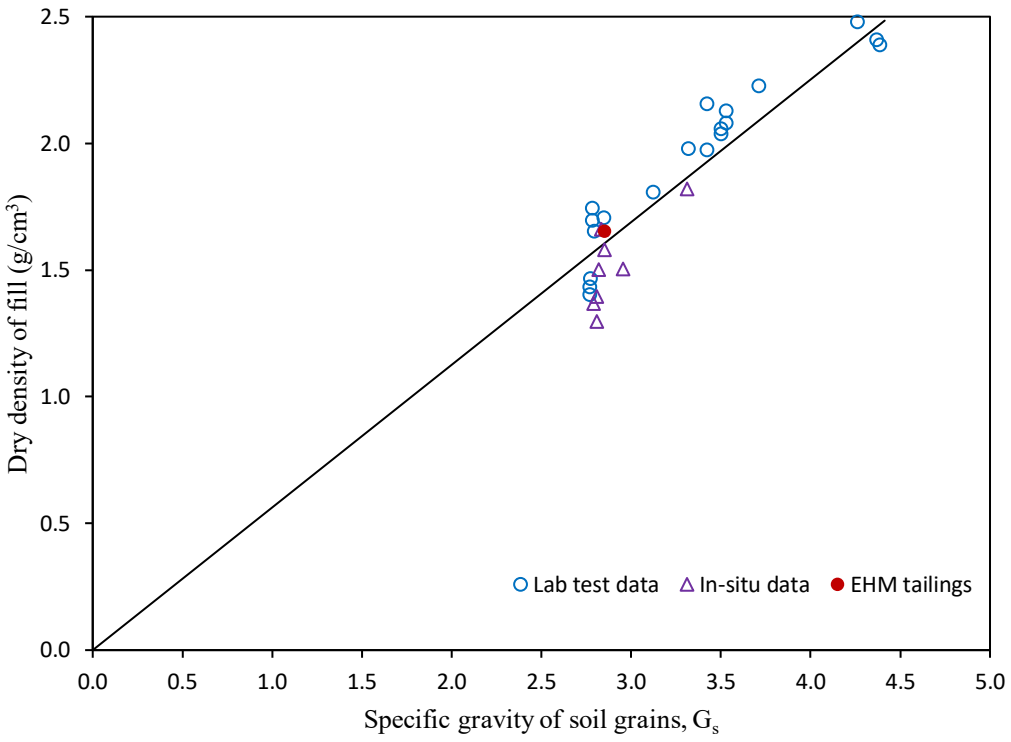

Figure 3.3. Dry density vs. specific gravity of tailings

According to Equation 3.1, settling dry density of EHM fill can be calculated as $0.56 \times 2.85 = 1.596\ g/cm^3$ which is very close to the dry density value obtained from the settling column test, 1.656 g/cm^3.

3.4 Maximum and Minimum densities

The maximum and minimum density tests were performed as per the AS 1289.5.5.1 to find the maximum and minimum void ratios and dry densities as shown in Table 3.2.

Table 3.2. Index properties of materials

Soil index property	**Fine sand**	**EHM tailings**
Minimum dry density (kgm^{-3})	1298	1452
Maximum dry density (kgm^{-3})	1591	1915
Minimum void ratio, e_{min}	0.633	0.488
Maximum void ratio, e_{max}	1.003	0.963

It was revealed that the HFs settled at relative density of 45-80 % and at void ratio ranging 0.6 to 0.8 based on in-situ data and lab tests carried out by Rankine et al. (2006) as shown in Figure 3.4. From the EHM tailing settling column test, it was found that the void ratio and relative density of the settled dry EHM tailings were 0.7207 and 51 % respectively, correlating well with the literature data.

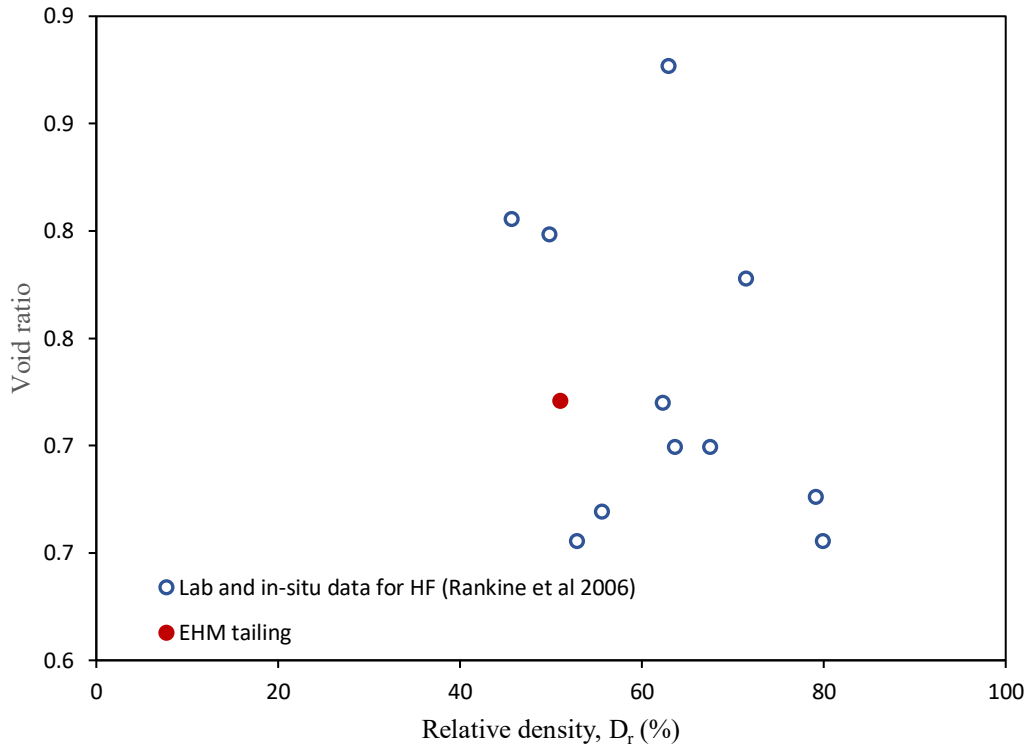

Figure 3.4. Void ratio vs. relative density of settled tailings

3.5 Friction angle

Soil internal friction angle (ϕ) is a crucial parameter that directly influences soil arching and stress developments within backfilled stopes. A series of direct shear tests was performed for test materials according to AS 1289.6.2.2. The variation of peak internal friction angle with the relative density (D_r) of the material was determined and compared with the data from Rankine et al. (2006) as presented in Figure 3.5.

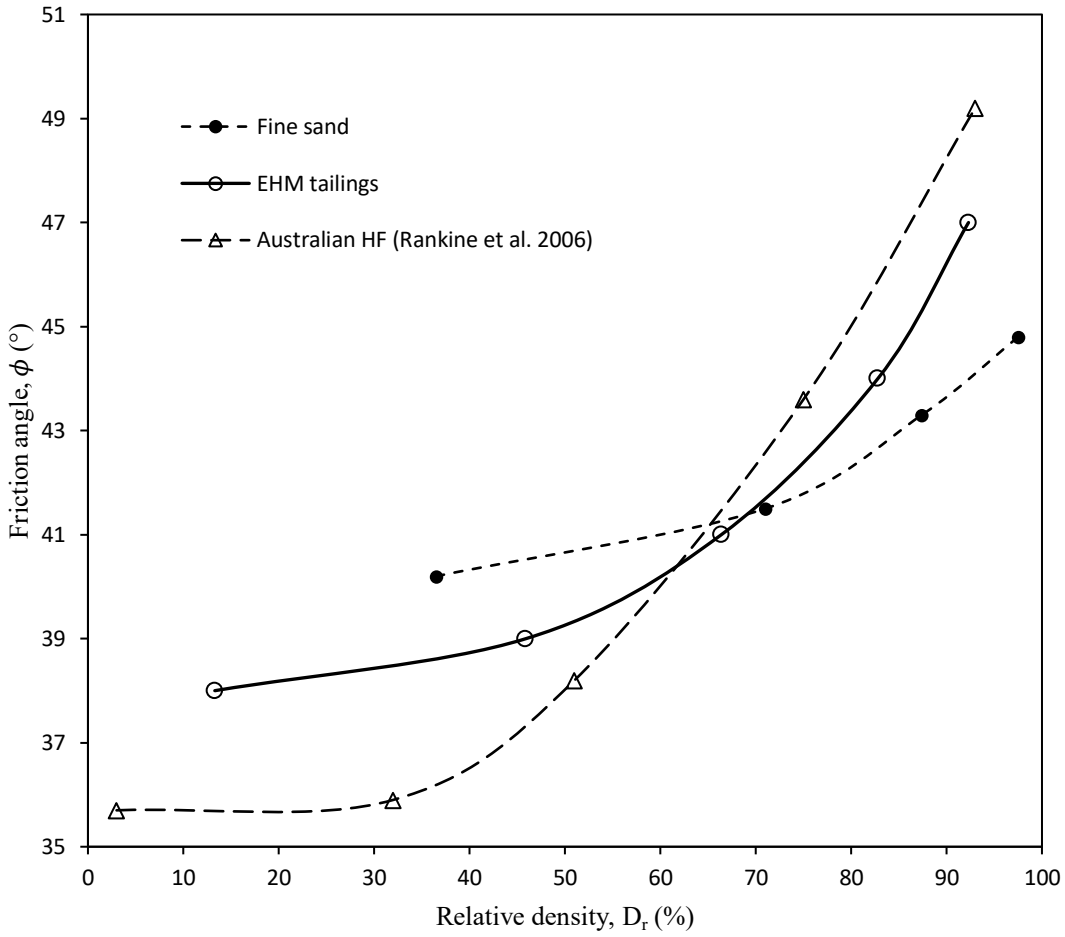

Figure 3.5. Variation of peak friction angle with relative density

It is well known that the friction angle of any soil increases with the relative density. That is, when the relative density is high, the soil grains are tightly packed with low void ratio and therefore, the frictional resistance of grain-grain slip surface is becoming larger and that resulted in an increase of friction angle of soil. The friction angle varies in a narrow range (40°-45°) for fine sand than that of EHM tailings and other Australian HFs which show a variation from 36°-49° for the full spectrum of relative density. Furthermore, friction angle of mine tailings is larger than that of fine sand, especially for relative densities above 60 %. The reason for difference in friction angle variation range for sand and tailings can be attributed to the angularity of particles. Fine sand has sub-rounded grains and hence grain packing is restricted to a certain extent. In contrast, mine tailings are comprised of sub-angular to angular particles, mainly due to the presence of heavy metals, because the tailings are freshly ground, and have not undergone any

geological erosion process, they remain angular, and therefore, interlocking of grains is more when the packing density is increased. On the other hand, the sand has been there for 1000s years and the grains have become sub-rounded through geological processes. The angularity of grains was evident in the images obtained from Scanning Electron Microscopy (SEM) analysis of EHM tailings as shown in Figure 3.6.

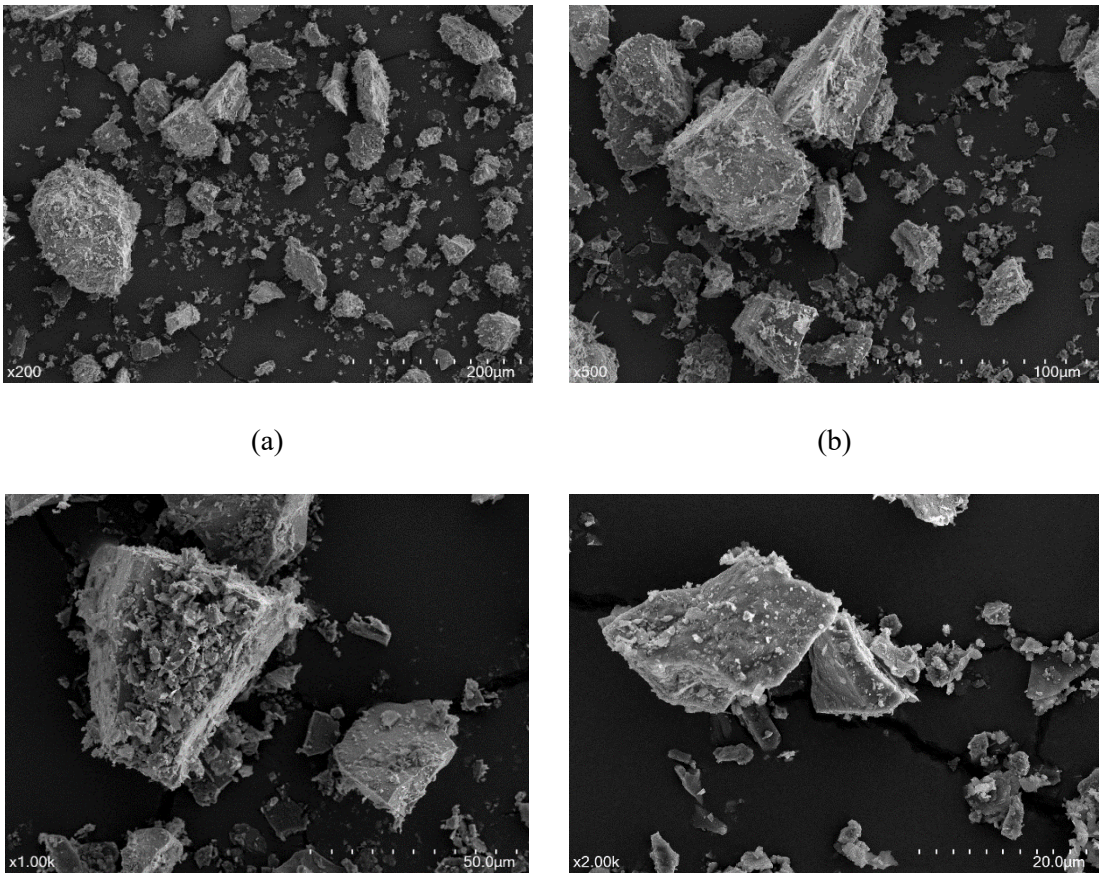

(a) (b)

(c) (d)

Figure 3.6. SEM images of EHM tailings with different magnifications: (a) 200X (b) 500X (c) 1000X (d) 2000X

Table 3.3. Particulate properties of materials

Material	**Friction angle, ϕ°**	**Angularity**	**C_u**	**D_{10} (µm)**
Fine sand	40-45	Sub-rounded	2.3	115
HF (EHM)	38-47	Angular	11	16
Australian HF (Rankine)	36-49	Angular	12	>10

3.6 Interfacial friction angle

During filling of a containment (stope, silo, etc.) with material, shear stresses are developed along the stationary walls of the structure due to frictional resistance at the fill-wall interface. This interfacial friction angle (δ) is embedded in analytical equations for arching within backfilled stopes. Mine stope walls are rough with rugged surfaces after blasting of ore and hence the slip surface is at few grains away from the wall, on fill-fill interface (Figure 3.7). Thus, for backfilled structures with rough wall, interfacial friction angle is taken as backfill's internal friction angle. An experimental study was conducted with direct shear tests to see the effect of wall roughness on interfacial friction angle. A glued P40 (40 grit) coarse sandpaper surface (Figure 3.8) and an acrylic surface were used to simulate the rough wall condition and smooth wall condition, respectively. These two surfaces are used in the laboratory stope arching models for backfill stress analysis which will be discussed in Chapter 4. Figure 3.9 shows the variation of interfacial friction angle of rough walls and smooth walls, with the relative density of the fill.

Figure 3.7. Mine stope wall roughness after blasting

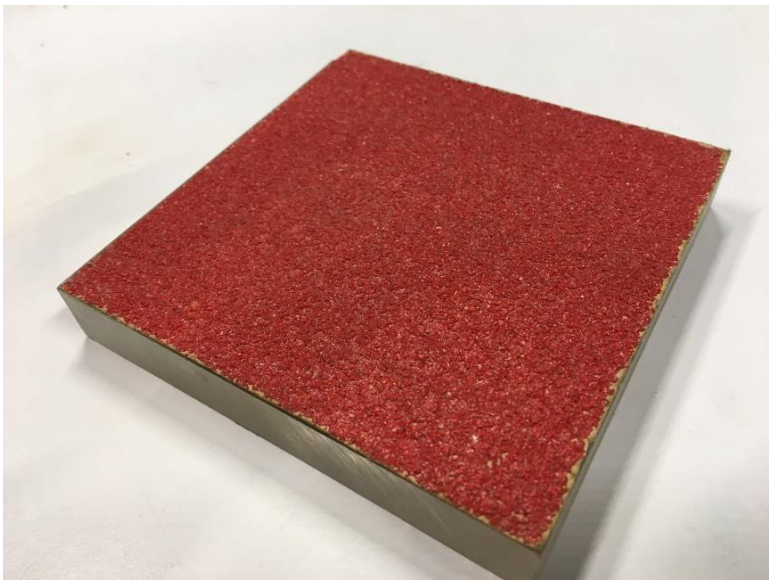

Figure 3.8. Glued sandpaper plate to mimic wall roughness

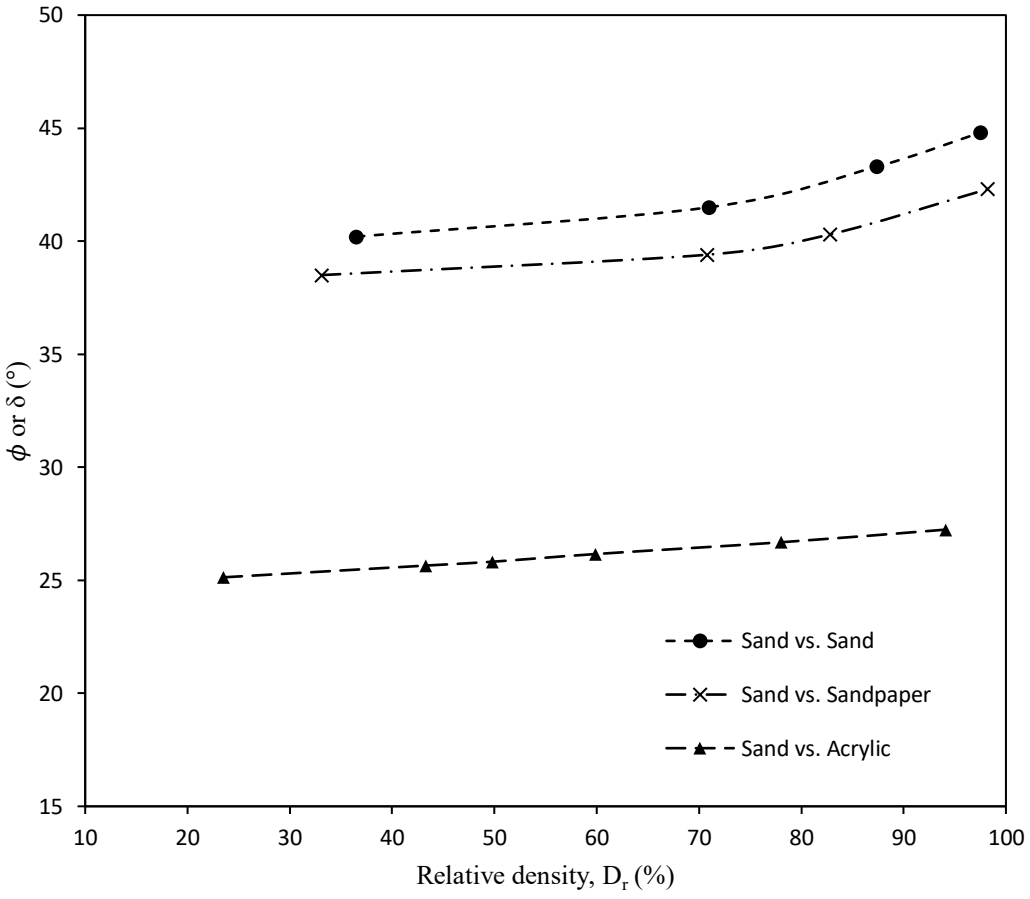

Figure 3.9. Effect of wall roughness on interfacial friction angle

It can be seen that the interfacial friction angle for the rough wall varies from 38-42 degrees whereas for smooth wall the variation is from 25-27 degrees. The variation of interfacial

friction angle for rough wall is comparable with the sand friction angle, justifying the argument $\delta = \phi$ for backfilled stopes. It confirms that the interfacial friction angle for smooth wall is considerably low compared to the rough wall and the values suggest $\delta_{smooth} = {}^{2}/_{3}\,\phi_{sand}$.

Variability in soil properties

Unlike other civil engineering materials, soil variability is quite significant. The scatter is introduced by inherent spatial variability in the soil properties and the test methods. Every soil parameter such as unit weight, specific gravity, friction angle, etc are random variables following specific probabilistic distributions. For simplicity, normal distribution is considered for many soil variables with mean and standard deviation. Therefore, accounting for spatial variability of soil is crucial for accurate design and analysis of geotechnical projects (foundations, slopes, retaining walls, etc). In Reliability-Based design, probabilistic methods are used to account for spatial variability, allowing engineers to make more informed decisions under uncertainty. Typical standard deviation values for some soil properties are given below (Sivakugan, 2021).

Soil property	**Standard deviation**
Unit weight (γ) (kN/m^3)	0.3135
Specific gravity (G_s)	0.0275
Friction angle (ϕ) (degrees)	3.03

3.7 Mineralogical analysis

A qualitative analysis to determine the presence and abundance of mineral species and their phases in EHM tailings was performed using the X-ray Diffractometer (XRD) method. A semi-quantitative analysis of smart oxides was carried out using X-ray Fluorescence (XRF) method as an elemental study of chemical compositions of the minerals present in EHM tailings. Results are shown in Figure 3.10 and Tables 3.4 and 3.5.

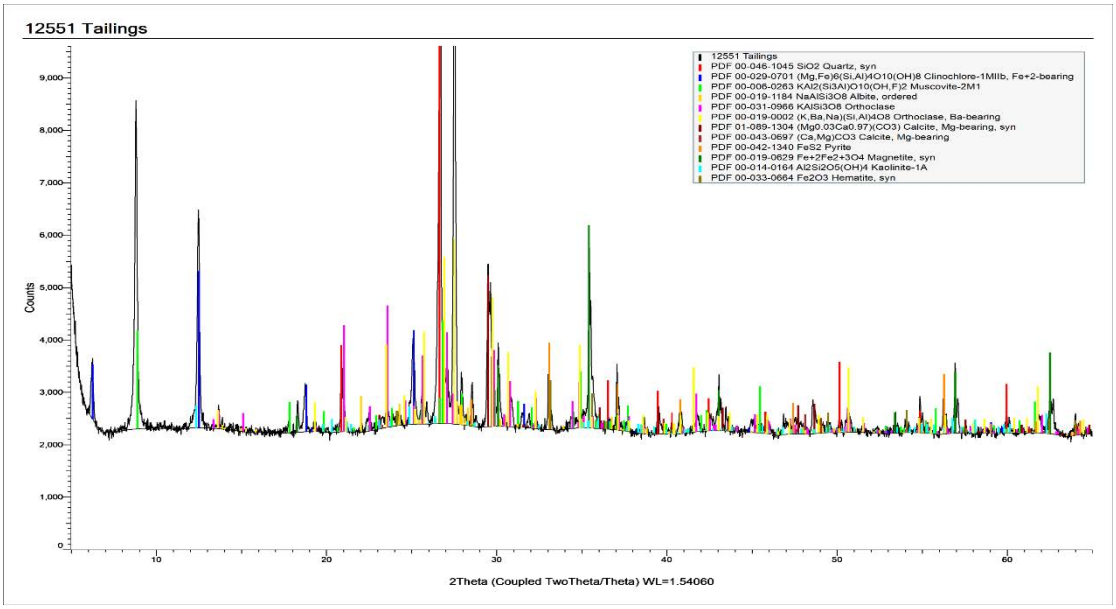

Figure 3.10. Qualitative XRD analysis of EHM tailings

Results from XRD analysis revealed that the EHM tailings consist of major minerals such as quartz, chlorite and muscovite whereas orthoclase feldspar, Mg-bearing calcite and magnetite are low-abundance minerals. Elemental analysis with XRF shows that Fe_2O_3 and SiO_2 are predominantly present in tailings with weight percentages of 37.7 % and 32.9 %, respectively.

Table 3.4. Minerals present in EHM tailings

Mineral phase	**Formula**	**Abundance**
Quartz	SiO_2	Major
Chlorite	$(Mg,Fe)_6(Si,Al)_4O_{10}(OH)_8$	Major
Illite/Muscovite	$KAl_2(Si_3Al)O_{10}(OH,F)_2$	Major
Plagioclase feldspar	$NaAlSi_3O_8$	Trace
Potassium feldspar	$KAlSi_3O_8$	Minor
Calcium-Magnesium Carbonate	$(Ca,Mg)CO_3$	Minor
Pyrite	FeS_2	Trace
Magnetite	Fe_3O_4	Minor
Kaolinite	$Al_2Si_2O_5(OH)_4$	Possible trace
Hematite	Fe_2O_3	Possible trace

Table 3.5. Elemental composition of minerals present in EHM tailings

Chemical compound/Element/State	Concentration/Weight percentage (%)
Na_2O	0.27
MgO	1.74
Al_2O_3	7.85
SiO_2	32.9
P_2O_5	0.35
SO_3	3.6
Cl_2O	0.05
K_2O	3.85
CaO	5.35
TiO_2	0.63
MnO	0.52
Fe_2O_3	37.73
As_2O_3	0.04
BaO	1.77
Ta_2O_5	0.07
LOI (Loss on Ignition)	3.27

3.8 Self-weight settlement of tailings in a backfilled stope

Underground mine stopes are filled with backfills in slurry form having solid content of 50-70 %, considering the fill properties mainly GSD, permeability and rheology that determine the flowability of the fill during transportation through pipelines. Fine sand used in this study is coarse-grained granular soil and hence quick drainage leaves the fill settled instantaneously, without developing any pore water pressure. Therefore, settlement analysis of pure granular sand is not a concern and hence it will not be discussed in this section.

EHM tailings have a fine fraction of 39.4 % and all that is silt, thus classified as silty sand (SM) according to USCS. Although EHM tailings are coarse-grained granular (non-cohesive)

soil, the relatively high silt content in the fill can cause some delay in the drainage process and thus fill may undergo sedimentation-consolidation settlement over a certain time period. Pajingo tailings are essentially fine-grained soil with D_{50} of 15 μm and D_{10} of 2 μm. That confirms it has 10 % of clay fraction which makes tailings to become cohesive. The sedimentation-consolidation settlement of cohesive fills can take a considerable time period with slow draining process. Therefore, it is vital to analyse the settlement behaviour and properties of EHM tailings and Pajingo tailings settling in a backfilled stope.

3.8.1 Laboratory simulation of tailing slurry settlement

The water loss from the fill settling in a backfilled stope is a simultaneous process through drainage and evaporation. Accordingly, 145 mm diameter cylindrical column made of Perspex with a perforated bottom which allows for drainage, was used in the laboratory exercise for simulating backfills settling in a stope. Doubly drained condition was ensured by the drain holes at the bottom of the column and open area at the top, with water evaporation from the top of the fill. After filling the column with the tailing slurry, the soil particles in the fill started to settle under gravity activating the sedimentation phase with a decant water layer formed at the top of the settled fill. During sedimentation, layer stratification occurred due to larger and heavier grains settling first, and smaller and finer grains on top of them in a layered manner.

Once the sedimentation stage is completed, the self-weight consolidation phase begins where the fill volume is decreased with the expulsion of pore water from the fill through drainage and evaporation. During consolidation settlement, fill properties such as void ratio, porosity are decreased while strengthening the soil structure with the increase in effective stresses as a result of dissipation of excess pore water pressure. Consolidation stage is ceased when the tailings reaches its shrinkage limit beyond which the soil skeleton does not shrink any more thus decreasing in volume no longer occurred.

The time and behaviour of the fill settlement are highly influenced by the amount of fine fraction and clay content in the fill. Life of Mine of an underground mine is typically in decades.

Backfilling of underground mine stopes are carried out as a simultaneous process to the ongoing mining operations to ensure the safe and continuous operation of the mining activities. Re-mining of mine tailings and selective mining of low-grade ore deposits from the mines which ceased operations for years, has become popular nowadays with the recent technological advancements which have proven more resource recovery efficiency. In the first instance, the accurate estimation of final settlement and volume variation of backfill slurry in backfilled stope is required to determine the correct fill mass needed to fill the stope completely thereby avoiding any gap forming between the fill and stope roof in the post-settlement phase. Among many other accidents reported in Australia and elsewhere, the recent fatal accident that happened in Dugald river mine in Queensland which costed two lives, triggered the need of reassurance of the safety of backfilled structures in underground mines. Investigations have reported that the accident was due to collapsing of a backfilled stope subjected to long-term settlement of the fill. Therefore, both short-term and long-term settlements of backfills should be thoroughly addressed when designing a safe backfill system.

Accordingly, laboratory simulations were carried out to study and analyse the behaviour and characteristics of EHM tailings and Pajingo tailings settling in a column in separate tests, mimicking a backfilling of a stope. The settlement variations of the two fills were also compared. The tailing slurry was poured into the settling column and allowed to consolidate and settle under its own weight. A filter paper was placed at the bottom of the column to prevent the loss of tailing particles from the fill slurry though drain holes. Unlike many of the studies that were done before, the fill settlement was observed throughout the spectrum from saturated fill just after pouring the column to the completely dry state of the fill where there was no change in the settled fill mass for two consecutive days. That ensured the long-term settlement analysis of backfills in mine stopes in a laboratory environment. Required readings were taken every 24 hours throughout the test which were then used for calculating the properties of the settled fill. The settlement variations of the two fills over the entire natural drying process from saturated state to fully dry state are shown in Figure 3.11.

EHM fill

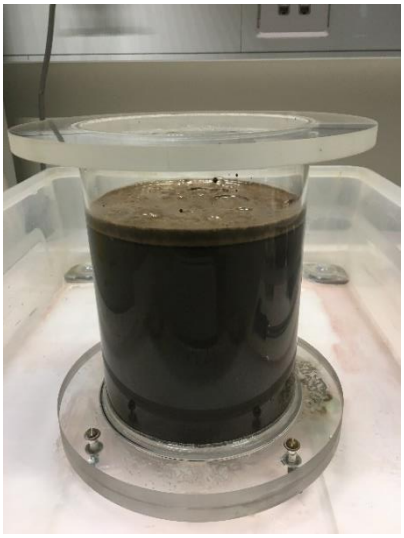

Pajingo fill

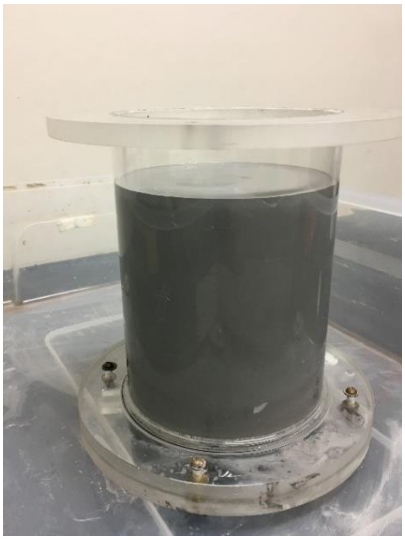

This was just after filling the settling column ($t = 0^{+}$)

t = 0.5 hr

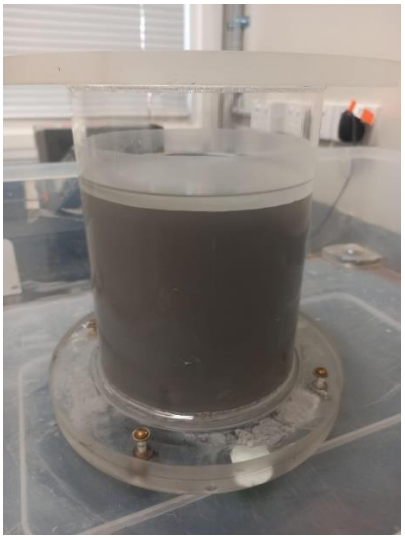

t = 1 day

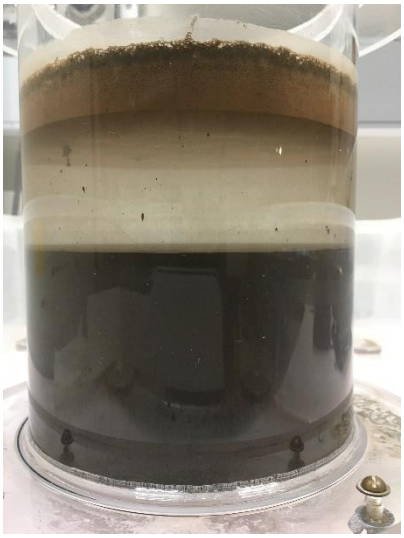

t = 1 hr

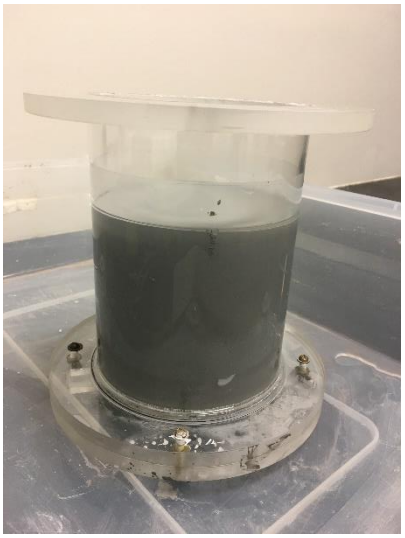

t = 2 days

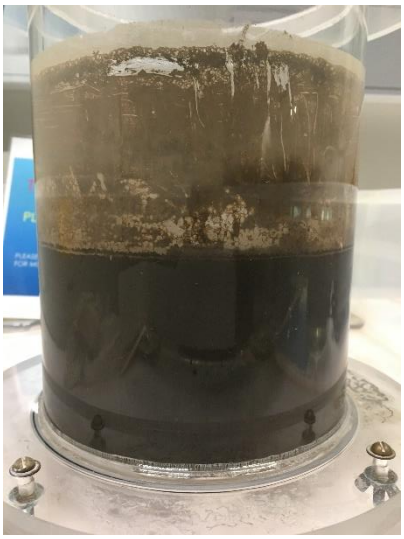

t = 1 day

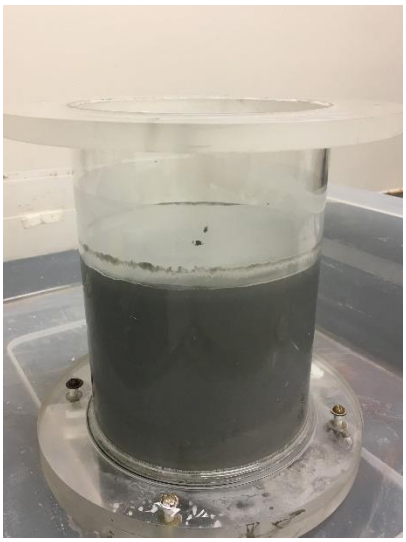

t = 7 days

t = 45 days (end of test)

t = 104 days (end of test)

Figure 3.11. Settling behaviour of EHM and Pajingo tailings in column test

3.8.2 Settling behaviour of EHM and Pajingo tailings

It is clear that much of the EHM fill has settled quickly within the first 30 minutes with a decant water layer containing fine particles, on top of the deposited fill. All that decant was removed within 12 hours, by the faster draining process which confirmed the granular nature of the fill. For the Pajingo fill, the drainage process was lot slower and hence it took about 7 days for all the decant water to be drained out from the fill, confirming that the fill contains a large amount of fines which contributed in delaying the draining process.

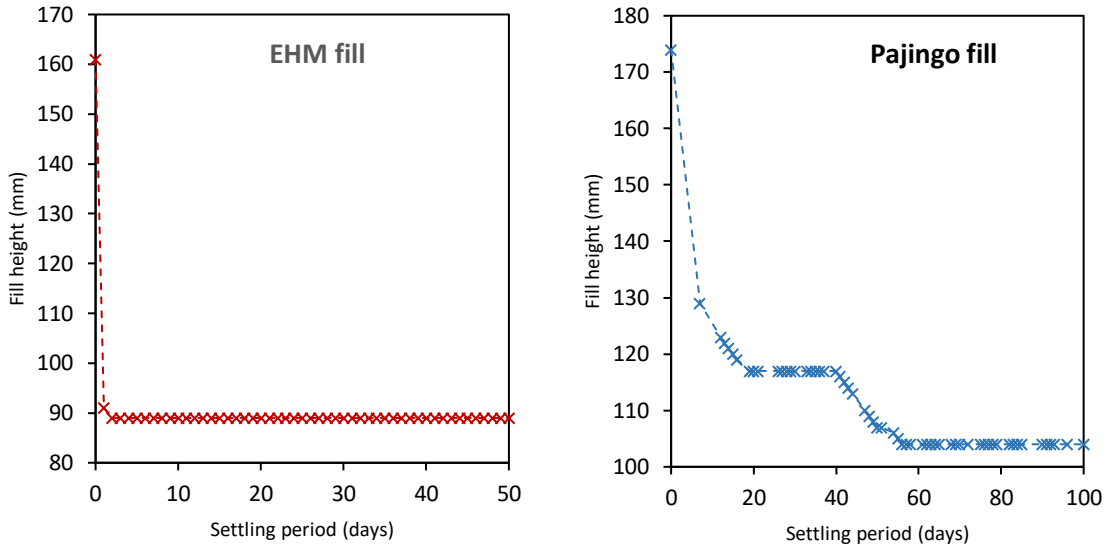

Figure 3.12. Settling height variation with time

In practice, it is difficult to differentiate the end of sedimentation phase and the start of self-weight consolidation phase during tailing slurry settlement as there is no such clear boundary between these two processes. The sedimentation process can be faster and hence completed more quickly with the coarse particles than the finer particles resulting in the accumulation of coarse particles in the lower part of the sediment cake while the fine particles still remained in the suspension and will be slowly settling down. Hence, both sedimentation and self-weight consolidation phenomenon are generally taking place simultaneously along the entire height of the tailing slurry. According to Figure 3.12, it can be determined that the EHM fill has undergone a fast settlement process with a total settlement of 7.2 cm whereas for the Pajingo fill, the total settlement was 7 cm which has occurred in two stages. The fill volume variation for the Pajingo tailings during settling process was not only due to decrease in fill thickness but also due to reduction in fill diameter resulted from the lateral contraction of the fill with tailing shrinkage process, which will be discussed later in this section. For the EHM fill, the entire sedimentation and self-weight consolidation processes completed in the first 2 days as confirmed with no fill volume variation until the fill became completely dry by 45 days, based on observations and readings taken throughout the test. In contrast, Pajingo fill behaved very differently which took 20 days for the completion of sedimentation and consolidation phases followed by the fill volume

reduction due to the combined effect of lateral contraction and consolidation settlement which appeared to have started 10 days later and completed on 56th day. Afterwards, no fill volume variation occurred until the fill became fully dry on 104th day.

The mass of the settled fill continuously decreased with time due to loss of fill water by drainage and evaporation, and reached a constant value at the dry state as depicted in Figure 3.13. EHM fill reached the dry state quicker than the Pajingo fill. A separate exercise was carried out with a water beaker having same diameter as the fill column to determine the water evaporation rate, and the values were compared with the rate of fill water loss as shown in Figures 3.14 (a) and (b) for both fills. As opposed to the case with just water in the beaker, the fill grains in the settling column occupy significant surface area leaving only a fraction of the cross section exposed to the atmosphere for evaporation. With water draining downwards, the water present at the top of the fill is also reducing which then starting to slower the fill water loss until the fill becomes completely dry.

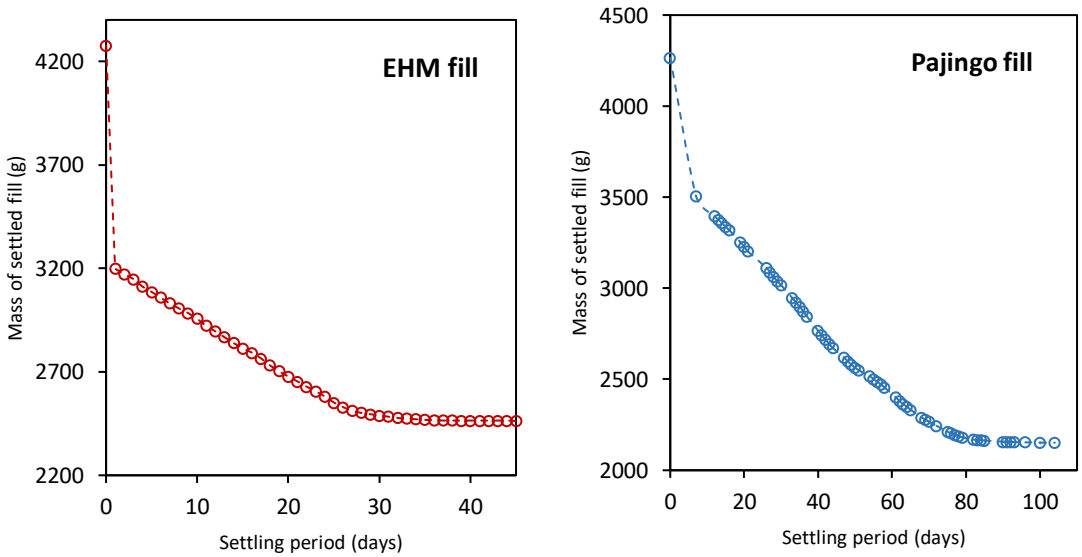

Figure 3.13. Settling fill mass variation with time

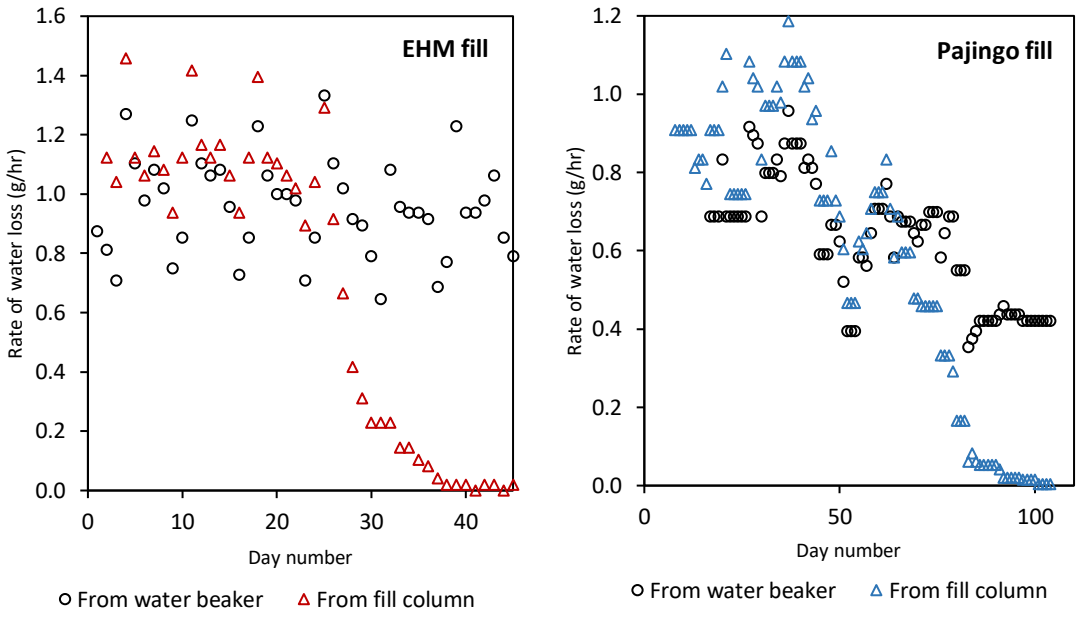

(a) (b)

Figure 3.14. Fill water evaporation rate

3.8.3 Variations of fill settling characteristics

In EHM fill, the bulk density increased initially but then started to decrease with the reduction in settled tailing mass. The volume variation of the settled tailing stopped on the 2nd day since the commencement of fill settlement and the dry density of the fill reached a constant value of 1.656 g/cm^3. For Pajingo fill, the bulk density fluctuated over the settling period with the variations of settled tailing mass and volume. However, the dry density of the fill increased continuously strengthening the soil skeleton and reached the final value of 1.746 g/cm^3. While the tailing skeleton kept becoming denser with time, thus increasing the dry density, the presence of water within the voids makes the bulk density increase and decrease during the sedimentation-consolidation process. All these variations of fill characteristics for EHM and Pajingo fills are presented in Figures 3.15 and 3.16, respectively.

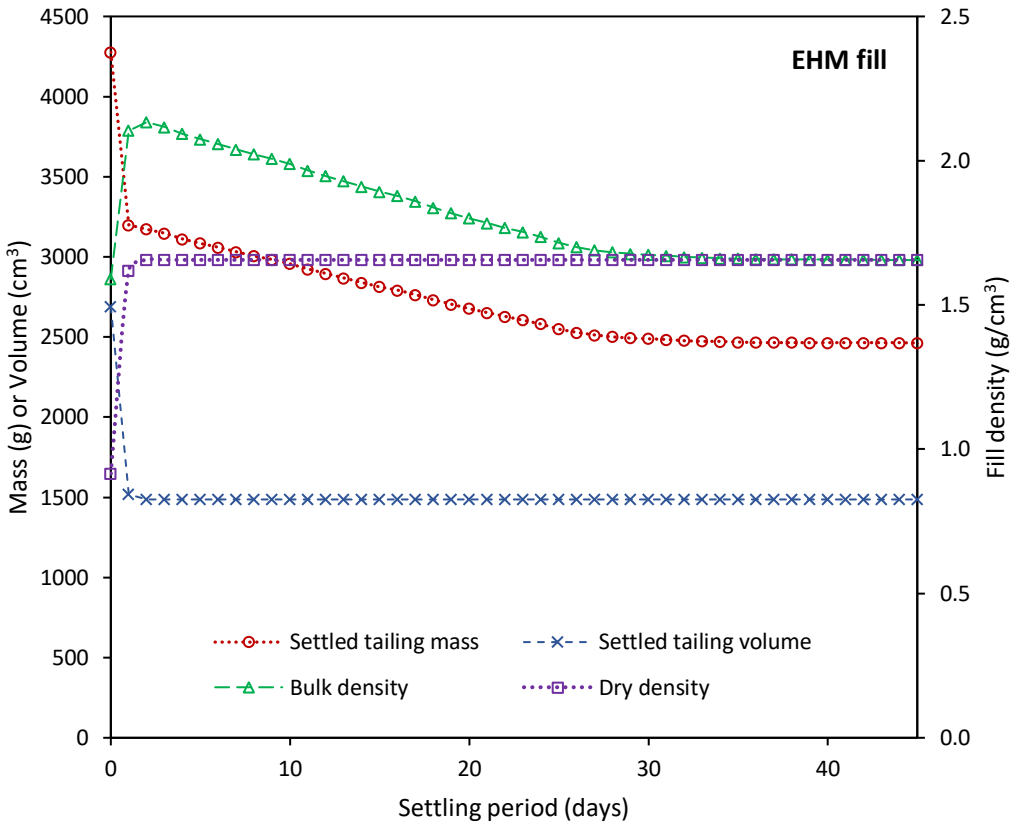

Figure 3.15. Settling mass, volume, density variation with time for EHM fill

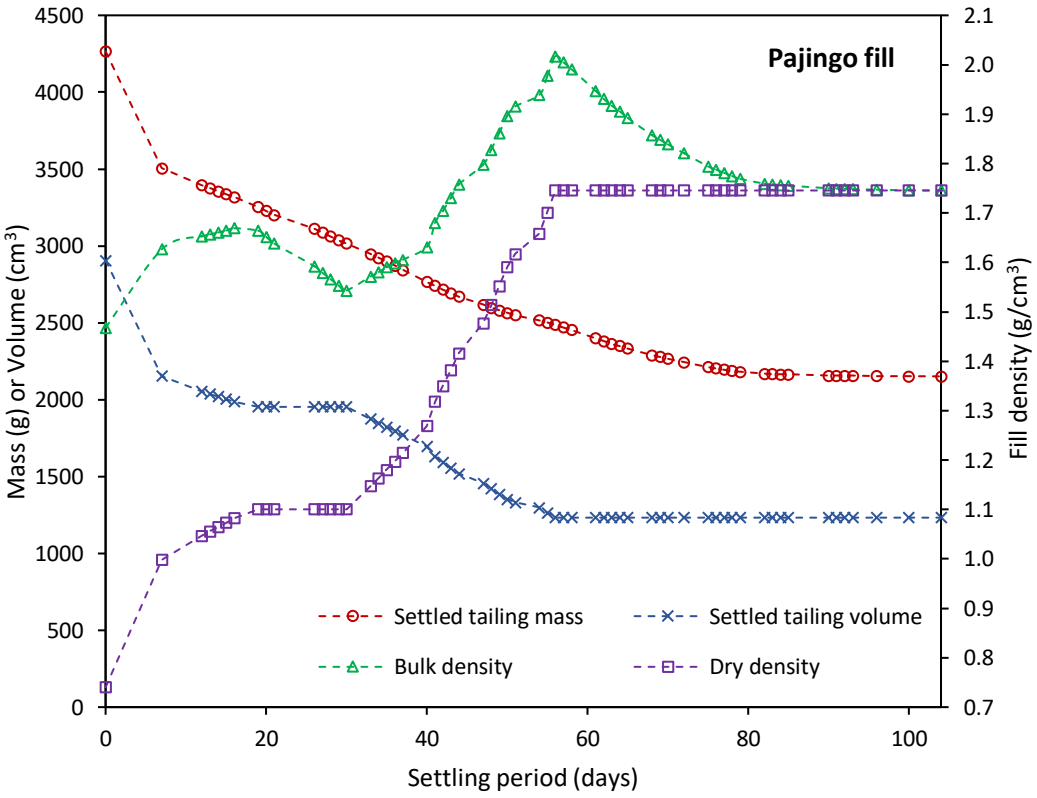

Figure 3.16. Settling mass, volume, density variation with time for Pajingo fill

Depending on the fine content and the coefficient of permeability of the fill, the rate of moisture loss from the fill changed. The variation of fill water content and degree of saturation with the settling time is shown in Figure 3.17 for both fills.

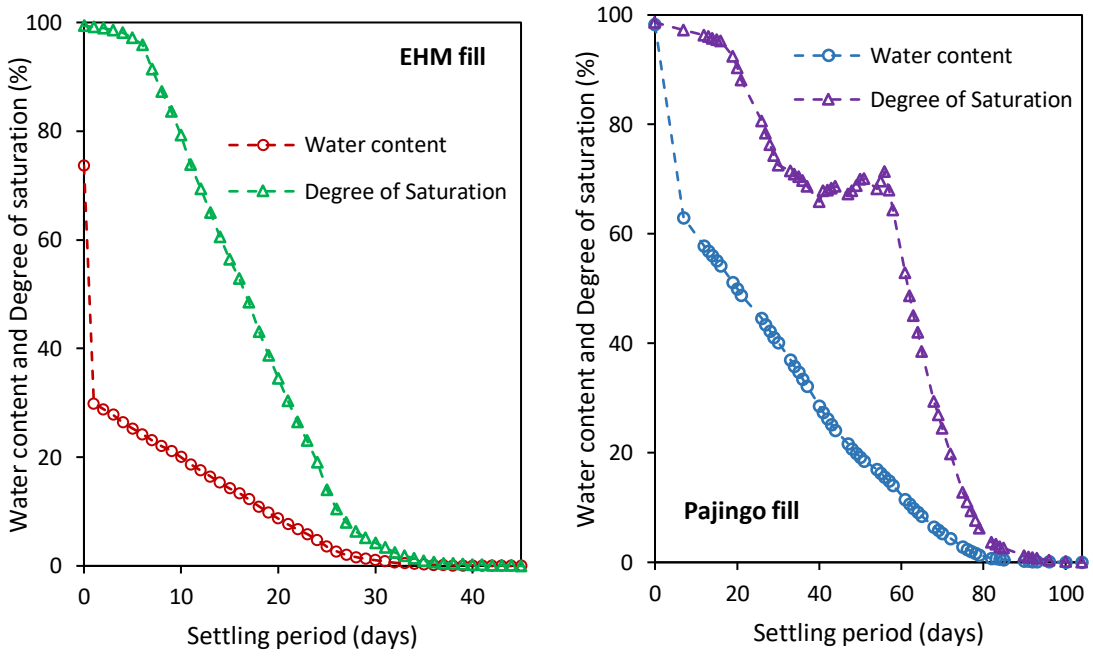

Figure 3.17. Fill water content and degree of saturation variation with time

The variation of porosity of the fill and the degree of saturation, with the fill water content is shown in Figure 3.18. The EHM and Pajingo fills settled to porosities of 42 % and 38 %, respectively at the end of consolidation process.

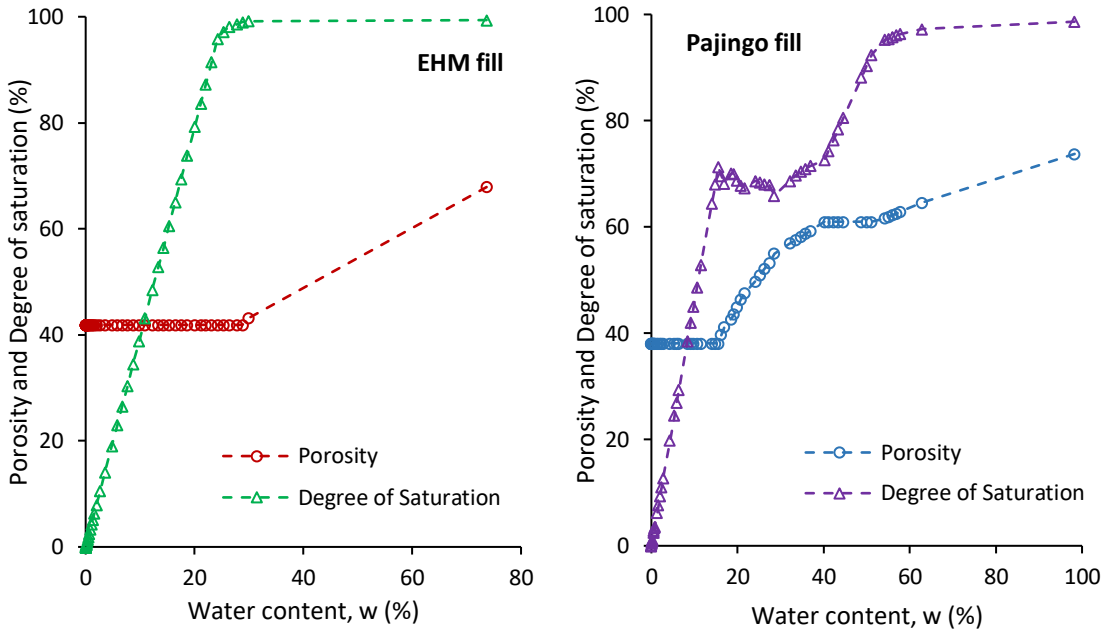

Figure 3.18. Fill porosity and degree of saturation variation with fill water content

The variation of fill void ratio over the settlement period is shown in Figure 3.19. The EHM fill quickly settled to a final void ratio of 0.7207 within two days whereas the Pajingo fill took a longer time (60 days) due to slow draining process to reach the final void ratio of 0.6155.

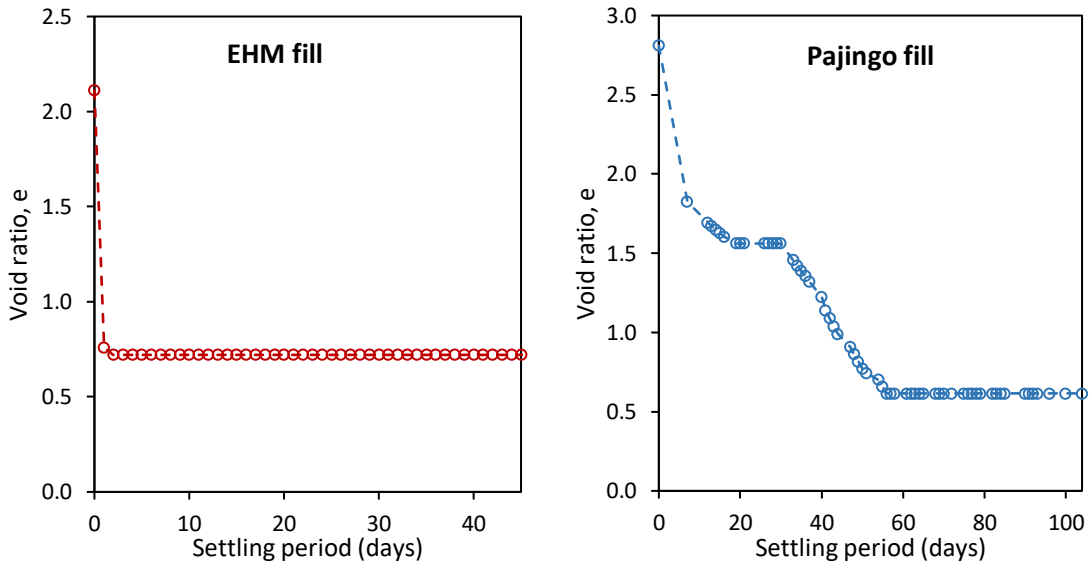

Figure 3.19. Variation of fill void ratio with settling time

The properties of settled fill for EHM tailings and Pajingo tailings were compared with the typical HF characteristics obtained by Rankine et al. (2006) after testing more than 20 HFs

collected from different mines in Queensland, as shown in Table 3.6. It is evident that the properties of settled EHM tailings correlated well with the general HF properties. Due to high fine fraction in the Pajingo fill, it settled at lower void ratio and porosity compared to EHM fill.

Table 3.6. Comparison of fill characteristics

Property	**Australian HF**	**EHM fill**	**Pajingo fill**
Specific gravity, G_s	2.8-4.4	2.85	2.82
Void ratio, e	0.6-0.96	0.7207	0.6155
Porosity, n (%)	38-49	42	38
Water content, w (%)	17-35	28.8	15.6
Dry density, (gcm^{-3})	1.41-2.42	1.67	1.75
Relative density, D_r (%)	45-80	51	-

3.9 Backfill slurry settling mechanism with natural drying process

Initially, the tailing slurry is oversaturated with an initial void ratio of e_0 and the particles not in contact, where the particles start to settle down under gravity while forming the fill sediment over time. During the normal shrinkage stage, the tailing particles get closer to each other with the expulsion of pore water pressure through drainage process and fill water loss due to evaporation. At the end of normal shrinkage stage, the tailing particles start to contact each other and the void ratio at this critical state is called air entry value (AEV) void ratio e_{AEV}. After this point, effective stresses generate within the fill and the residual shrinkage starts. During the residual shrinkage stage, the effective stresses become larger with more water dissipation through draining and evaporation, resulting further decrease of the fill volume. This will continue until the grain-grain contacts are tight enough, where further loss of fill water does not result in anymore fill volume reduction with the final void ratio being e_f. The water content at this second critical state is called the shrinkage limit w_s. From this point onwards, the zero-shrinkage stage begins while the void ratio remains constant at e_f which is called the final void ratio of the settled

fill. This slurry settling mechanism during the natural drying process is schematically shown in Figure 3.20.

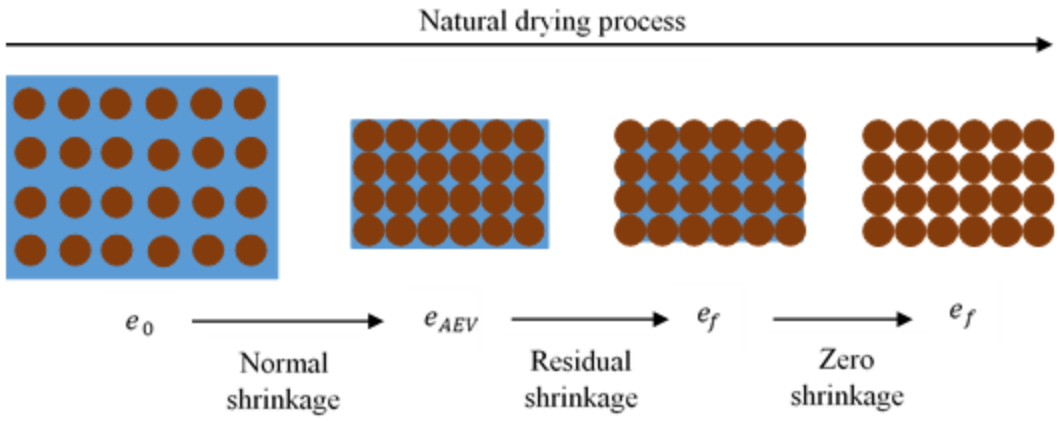

Figure 3.20. Natural drying process of tailing slurry settlement

A typical shrinkage curve of tailing material is shown in Figure 3.21. During the normal shrinkage stage, the void ratio of the fill gradually decreases along the saturation line from e_0 to e_{AEV} due to sedimentation settling of the fill and then during the residual shrinkage stage the fill void ratio continues to decrease until e_f due to the consolidation settlement of the fill. The critical void ratios (e_0, e_{AEV} and e_f) which can be obtained from the shrinkage plot are useful for settlement calculations.

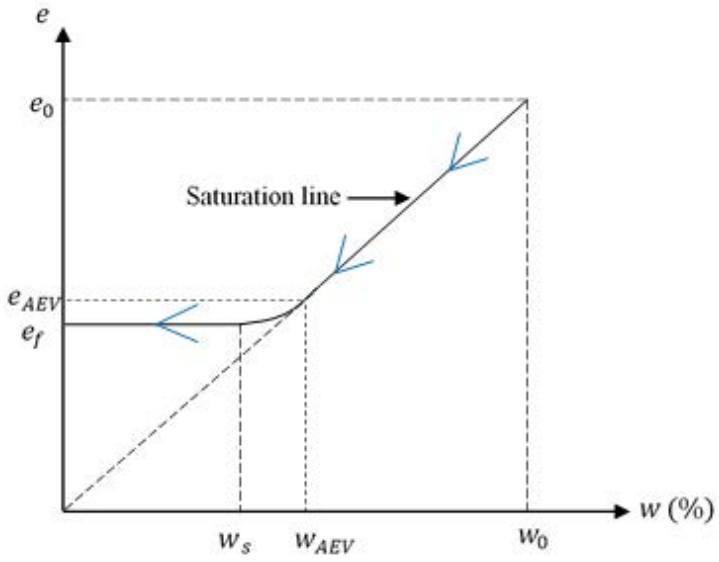

Figure 3.21. Typical shrinkage curve of tailing material

3.9.1 Shrinkage curves and settlement equations

Qin et al. (2021) has presented analytical solutions to calculate settlement and volume variations caused by sedimentation and consolidation of a backfill slurry settling in a column, mimicking a backfilled stope. A shrinkage test has been carried out in a rectangular shaped PVC (polyvinyl chloride) mold to plot the shrinkage curve ($e\ vs. w$) of the tailing which was then used in the sedimentation settlement (S_s) calculations, while the consolidation settlement (S_c) has been calculated using the compression curve ($e\ vs. \sigma'$) obtained from standard 1D odeometer test. The calculated total settlement ($S_t = S_s + S_c$) was then compared with the settlement value obtained from the tailing slurry settling column at which the measured fill thickness remained unchanged for a day, but before the fill became unsaturated. Therefore, the analytical solutions proposed by Qin et al. (2021) have not been validated for the entire natural drying process until the fill becomes completely dry. The GSD properties of tailings used in Qin et al. (2021) study and Pajingo tailings used in this study are very similar as shown in Table 3.7. More importantly, Qin et al. (2021) study does not replicate the long-term self-weight consolidation settlement of a backfill slurry with large fine fraction in a mine stope satisfactorily. Therefore, as discussed in Section 3.8.1 on page 28, it is important to analyse the settlement and volume variations of a backfill slurry settling in a mine stope especially with large fine fraction, caused by the combined effect of sedimentation and self-weight consolidation considering the entire natural drying process. This was evident in the Pajingo settling column test which will be discussed later in this section.

Table 3.7. Properties of different tailing materials

Property	**Qin et al. (2021) tailings**	**Pajingo tailings**
% fines (D < 75 μm)	85	94
% clay (D < 2 μm)	7	10
D_{10} (μm)	3.3	2
G_s	2.73	2.82

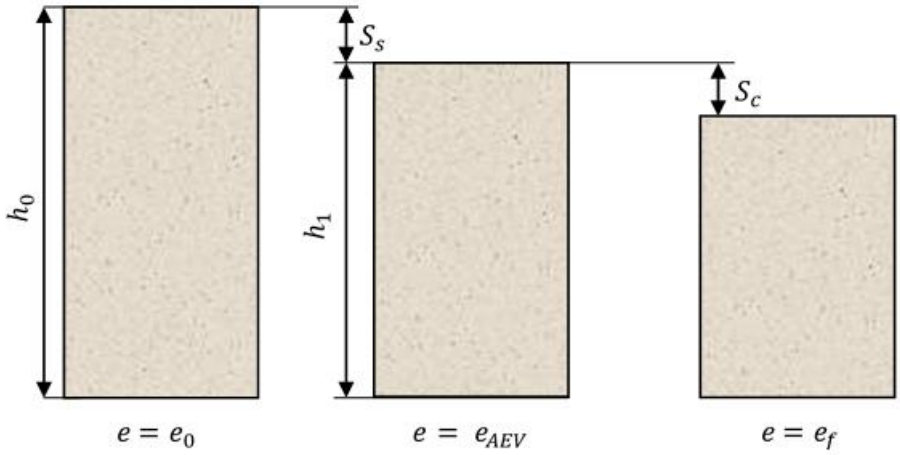

Figure 3.22. Schematic diagram of tailing slurry settling in a column

Let's consider a tailing slurry deposited in a confining structure like the tailing column in this study with a horizontal cross-sectional area A, where the slurry has an initial void ratio of e_0 and an initial height of h_0 as shown in Figure 3.22. The shrinkage curve ($e\ vs.\ w$) which presents the variation of fill void ratio (e) with the water content (w), is used for fill settlement and volume variation calculations. The settlement variation associated with the sedimentation occurring in the normal shrinkage stage, can be estimated using e_{AEV} obtained from the shrinkage curve, where the sedimentation can be considered as completed and the consolidation of the fill will start taking place. Accordingly, the thickness variation (sedimentation settlement S_s) of the tailing slurry can be calculated as follows.

$$S_s = ((e_0 - e_{AEV})/(1 + e_0)) \times h_0 \qquad \text{Eq. (3.2)}$$

The initial void ratio for the consolidation process is then considered as e_{AEV} and the initial height (h_1) of the fill is taken as ($h_0 - S_s$). Assuming one-dimensional (1D) consolidation of the fill where the fill strain is only in vertical direction, the consolidation settlement (S_c) can be calculated as follows using the final void ratio (e_f) obtained from the shrinkage curve.

$$S_c = ((e_{AEV} - e_f)/(1 + e_{AEV})) \times\ h_1 \qquad \text{Eq. (3.3)}$$

Therefore, the total settlement (S_t) of the fill can be calculated as

$$S_t = S_s + S_c = \frac{(e_0 - e_{AEV})}{(1 + e_0)} \times h_0 + \frac{(e_{AEV} - e_f)}{(1 + e_{AEV})} \times h_1 \qquad \text{Eq. (3.4)}$$

For tailings which has a large amount of coarse particles and less fine fraction, a clear boundary between the sedimentation phase and the consolidation phase cannot be identified because of fast settlement of coarser particles and thus, both the sedimentation and self-weight consolidation take place almost instantaneously, and hence the void ratio drops from e_0 to e_f relatively fast. Hence, e_{AEV} is taken as e_f, and, the total (final) settlement ($S_t = S_f$) is calculated as

$$S_t = S_f = ((e_0 - e_f)/(1 + e_0)) \times h_0 \qquad \text{Eq. (3.5)}$$

3.9.2 Shrinkage behaviour of EHM and Pajingo tailings

EHM tailings

EHM tailings settled very quickly within the first 12 hours with all decant water drained out and evaporated. The complete settlement of the fill was observed at the end of day 2 after which no change of fill diameter and thickness occurred. Thus, the fill volume and void ratio remained unchanged until the fill reached its ultimate dry density of 1.656 kg/m^3 and vertical strain (ε_v) of 44 %. Figure 3.23 shows the appearance of EHM fill just after filling the column and at the end of test.

(a) (b)

Figure 3.23. Appearance of EHM fill during settling (a) just after filling (b) end of test

Pajingo tailings

In contrast to EHM fill, the shrinkage behaviour of Pajingo fill was very different. Initially, only the vertical strain of the fill occurred due to sedimentation and consolidation settlement. After some time, the lateral shrinkage of the fill started along with the vertical strain in the consolidation phase. The vertical strain (ε_v) and lateral strain (ε_h) of the fill at the end of natural drying process were 40 % and 15 %, respectively. As the Pajingo fill contains 94 % fines and about 10 % clay, it is suggested that this lateral shrinkage behaviour can be attributed to the clay content induced lateral contraction of the fill, and a complete detachment of the fill from the wall was observed. The absence of fill-wall contact caused loss of arching which then resulted in shear stresses generated previously on wall during fill settlement will eventually be transferred to the stope bottom as normal stresses and then lateral stress on the barricade will be increased raising high concerns of barricade stability. Hence, the risk of barricade failure will be increased when the barricade stress increases due to tailing shrinkage in the stope. The situation can be more critical when the stresses onto the barricade exceed the bearing capacity (design strength) of the barricade resulting in catastrophic failure of the barricade which can then lead to serious

consequences to the mining operations. The appearance of the Pajingo fill just after commencement of the test and at the end of test is shown in Figure 3.24.

(a) (b)

Figure 3.24. Appearance of Pajingo fill during settling (a) just after filling (b) end of test

Shrinkage curves were developed for both EHM and Pajingo tailings from readings taken from the tailing slurry settling column over the entire natural drying process caused by drainage and evaporation (from normal shrinkage stage to residual shrinkage stage through to zero shrinkage stage) as shown in Figure 3.25.

Tailings which have high amount of fines and especially with a considerable amount of clay are subjected to lateral strain during the residual shrinkage stage in addition to the vertical strain of the fill caused by settling of particles as observed with Pajingo tailings. Hence, the applicability of 1D consolidation theory in calculating self-weight consolidation settlement of backfills within mine stopes during the entire natural drying process may not be appropriate.

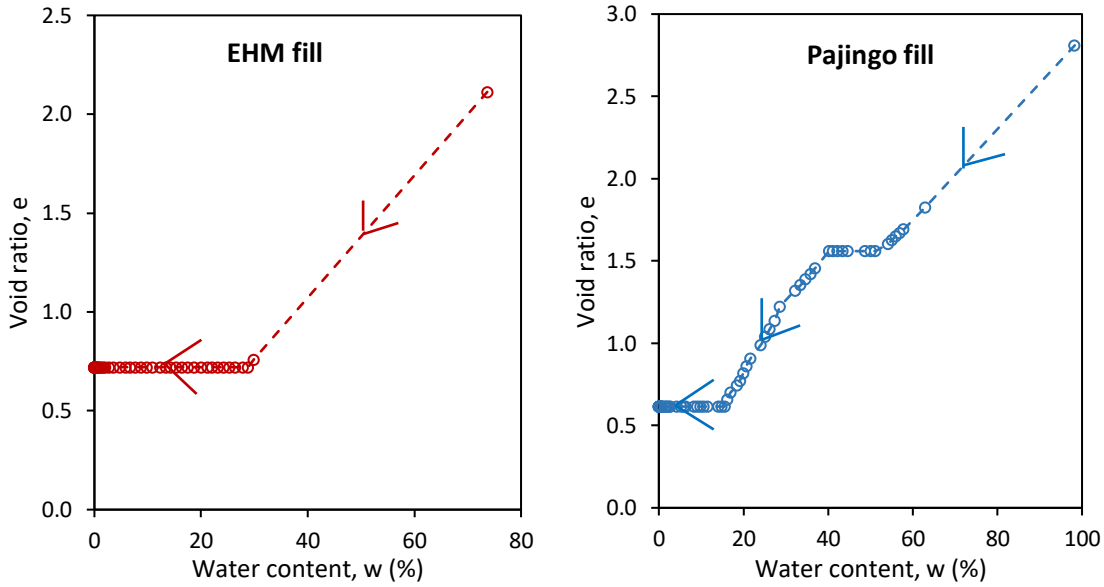

Figure 3.25. Shrinkage curves for EHM and Pajingo fills

3.9.3 Settlement calculations for EHM and Pajingo tailings

Settlement values for both fills can be determined using the Equations 3.2 to 3.5 with the critical void ratios obtained from the shrinkage curves (Figure 3.25), as tabulated in Table 3.8.

Table 3.8. Critical void ratio values for EHM and Pajingo fills

Void ratio	EHM fill	Pajingo fill
e_0	2.1127	2.8098
e_{AEV}	0.7207	1.6712
e_f	0.7207	0.6155

Because of the granular nature of the EHM fill, it settled very quickly in the settling column with both the sedimentation and consolidation processes occurred simultaneously without showing a sharp margin between them. Therefore, from the shrinkage curve, e_f is taken as equal to e_{AEV}. Thus, from Equation 3.5,

$$S_t = S_f = ((2.1127 - 0.7207)/(1 + 2.1127)) \times 161 = 72\ mm$$

In contrast, Pajingo fill exhibited a slow settling rate in the column test, and hence, it shows two values for e_{AEV} and e_f in the shrinkage plot. It is clear that the Pajingo fill has undergone two distinct settlement stages as sedimentation and 1D consolidation with vertical strain together at first and then further consolidation with both vertical and lateral strains of the fill. Hence, the settlement calculations can be done as below.

From Equation 3.2,

$$S_s = ((2.8098 - 1.6712)/(1 + 2.8098)) \times 174 \ = 52\ mm$$

From Equation 3.3,

$$S_c = ((1.6712 - 0.6155)/(1 + 1.6712)) \times 122 \ = 48.2\ mm$$

Thus, the total settlement is calculated as

$$S_t = S_s + S_c = 100.2\ mm$$

However, the total settlement observed from the fill column test was 70 mm. The difference of 30.2 mm can be attributed to the lateral contraction of the fill that occurred in the later stage below water content of 40 % in the Pajingo shrinkage curve plot. The shrinkage curve is based on change in void ratio of the fill over the entire drying process due to both vertical strain and lateral strain of the fill. However, the analytical equations do not account for lateral strain, but only consider vertical strain (1D consolidation), hence giving a large value for S_c for Pajingo fill.

Shrinkage curve is a very important and useful tool in soil science and geotechnical engineering studies. Therefore, if one can develop the shrinkage curve for a given tailing material by means of a laboratory settling column test, then the critical void ratios e_0, e_{AEV} and e_f can be obtained which can then be used in the analytical equations for vertical settlement calculations for any initial height of the fill (h_0) in the backfilled stope, assuming the fill does not undergo any lateral strain. The calculated total settlement is useful in determining the tailing mass or volume required to fill the stope completely.

3.9.4 Shrinkage curve comparison

The shrinkage curve developed by Qin et al. (2021) for Gold mine tailings from Canada, is based on a shrinkage test carried out in a linear mold where the test was terminated when there was no change of specimen volume in two successive days, but before the specimen became completely dry. Therefore, shrinkage curve by Qin et al. (2021) does not reflect the complete drying process of the fill. In contrast, the shrinkage curve developed for Pajingo tailings in this study was based on the settling column test of the fill covering the entire natural drying process, mimicking the sedimentation and self-weight consolidation of the fill in an actual backfilled stope. This also replicated the long-term settlement of tailing slurry in a backfilled stope. The shrinkage curves are compared in Figure 3.26.

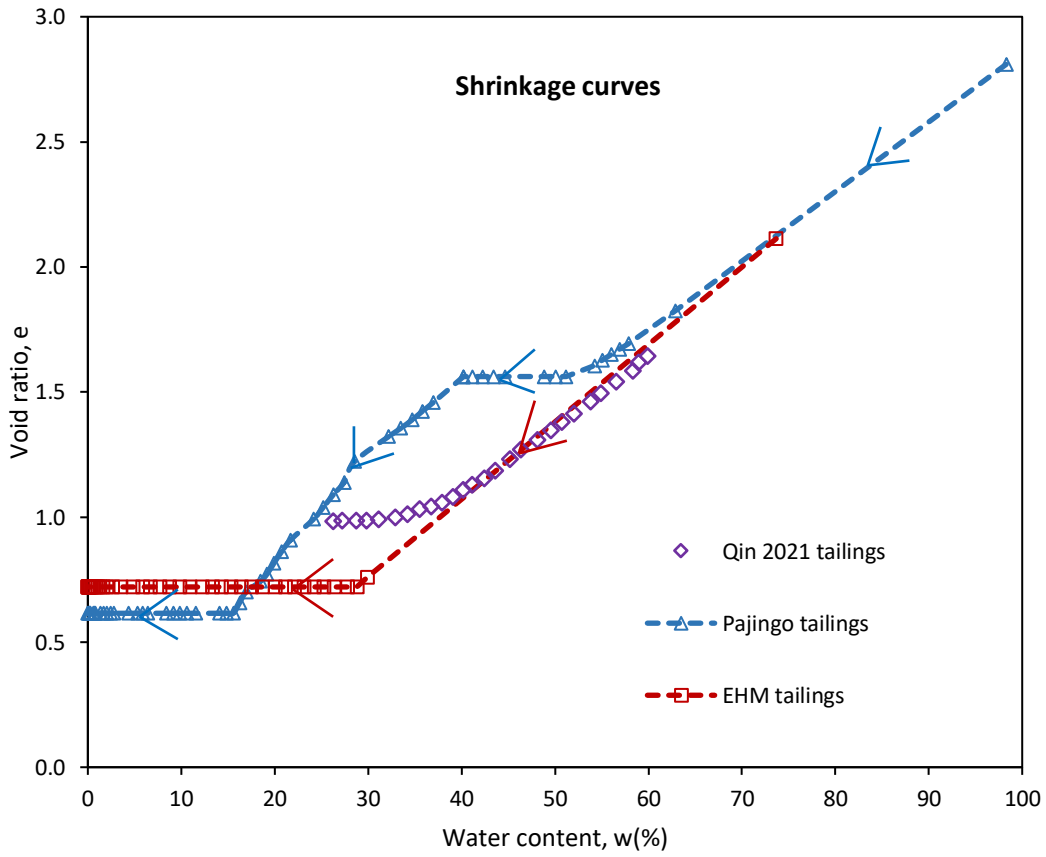

Figure 3.26. Shrinkage curve comparison for different mine tailings

It is important to note that the Pajingo tailings and the tailings used in Qin at al. (2021) study are very similar in characteristics as shown in Table 3.7, with fairly close clay contents. Therefore, with observations made in Pajingo tailing settling behaviour, it can be suggested that if Qin et al. (2021) had continued the shrinkage test over the complete natural drying process, it is highly likely that they would have observed more shrinkage of the specimen, resulting further reduction of void ratio. In settlement calculations for tailings with high amount of clay, to account the lateral strain in vertical settlement, a numerical simulation procedure is required and recommended.

3.9.5 Suitability of tailings for potential stope backfilling

Fine sand

Fine sand sample discussed herein is purely coarse-grained granular material with a very small amount of fines and thus it can be used as an alternative material to the hydraulic fill material in laboratory physical model tests.

EHM tailings

EHM tailings are granular material with significant amount of fines which are predominantly silts and the tailings characteristics are compared well with the typical HF properties given in the literature, as discussed in earlier sections. The settling column test also confirmed the granular nature of the tailings with the fast drainage and settlement of the fill. Hence, it can be concluded that EHM tailings can be used as HF for backfilling of underground stopes.

Pajingo mine tailings

Pajingo tailings are essentially fine-grained soil with a high clay fraction. The settling column test confirmed the lateral shrinkage of the fill induced by the high clay content. This may cause the loss of arching when the fill is settling in a stope, and as a result, it may increase the

lateral pressure on the drive barricade which will exceed the design limits of the barricade wall leading to possible barricade failure. It can be concluded that the Pajingo tailings are not suitable to use as HF due to its large fine content. Moreover, it is recommended that the Pajingo tailings can be used as Paste fill (PF) with its favourable characteristics.

3.10 Summary

The exclusive summary of this Chapter is presented below.

- The granular nature, GSD and other index properties of fine sand suggested that it can be used in laboratory model tests to replicate HF backfilled stopes for research purposes, where the availability and supply of real HF mine tailings are limited or not possible.

- The relationship developed for the variation of friction angle of the tailings with relative density confirmed that the tailing friction angle rapidly increased for larger relative densities of the fill.

- The analysis on the effect of stope wall roughness on interfacial friction angle verified that the interfacial friction angle of rough walls (δ) (e.g., Mine stope) can be equated to the friction angle of the tailing material (ϕ) due to the slip surface being the fill-fill interface.

- The analysis of long-term settling behaviour and determination of fill settling characteristics are considered as the first step in identifying the suitability of tailings for backfill material and in deciding what pre-treatments are required before the tailings can be used as hydraulic fills or paste fills.

- The shrinkage curve of tailing is useful to obtain critical void ratios and thereby to calculate sedimentation and vertical consolidation settlement of backfill slurry of any initial fill height in the stope.

- The lateral shrinkage of fill is not accounted in 1D consolidation equations and hence numerical simulation program is required to analyse the volume variation of fill caused by lateral strain, especially with fills having high clay content.

- The clay content in mine tailings is identified as the influencing factor for lateral contraction of fill during settling thus resulting loss of arching in stope. Therefore, reducing the clay fraction to a suitable level is essential before the tailing can be placed as backfill.

Chapter 4

4 Stresses within Backfilled Mine Stopes

4.1 General

In underground mining, granular backfills such as hydraulic fills (HF) are placed in stopes that are approximately square or rectangular in plan view, where the stress variation with depth is similar to that in a silo. Understanding the vertical as well as horizontal stress distribution, in vertical containments, is necessary for sound geotechnical designs. Proper understanding of vertical stresses will improve design criteria for above mentioned containments and related structures. Terzaghi (1920) mentioned that these earth pressure problems are better solved experimentally than analytically and also the simplifications made in analytical formulations are too unrealistic and therefore might have an impact on the stress estimations. This study aims to identify the vertical stress variation when a container of uniform cross section filled with granular material and how the variation is influenced by the width, shape of the container and wall roughness conditions. The laboratory setup was developed such that filling can be conducted in layers and the average vertical stress at the bottom, and shear stresses and horizontal normal stress on walls could be obtained. Model laboratory tests were undertaken, and test results were compared to what is learned from arching theory and numerical simulations.

Determining the vertical stresses within the HFs is necessary for designing the barricades that block the drives, when underground mine stopes are backfilled. Noting the difficulties associated with the in-situ measurement of stresses within backfills, numerical modelling appears to be an effective tool in understanding the stress conditions within the backfill. Laboratory models have been used in the past for validating the numerical models and analytical equations.

4.2 Analytical solutions

The well-established analytical equations, derived with shear plane method, are introduced by Janssen (1895) for silos and Marston and Anderson (1913) for backfilled narrow trenches. Thereafter, Terzaghi (1943) included cohesion to the arching equation. The equation

has been applied to trap door problem (Ladanyi and Hoyaux, 1969), backfilled narrow trenches (Handy, 1985; Harrop-Williams, 1989), retaining walls (Frydman and Keissar, 1987; Take and Valsangkar, 2001), backfilled narrow mine stopes (Aubertin et al., 2003) and modified for square and rectangular mine stopes (Li et al., 2005; Pirapakaran and Sivakugan, 2007a). The analytical solutions by Marston (1930), Aubertin et al. (2003) and Pirapakaran and Sivakugan (2007a) are directly related to backfilled trenches/stopes and hence discussed in the sections below. The Pirapakaran and Sivakugan (2007a) analytical equation is used in the comparison of stresses within stopes obtained by laboratory model test data and numerical simulations. Schematic diagrams of idealized 3D backfilled narrow trench/stope and its 2D plane strain loading approximation which is used in Marston's theory and Aubertien et al. (2003) analytical solutions, are shown in Figures 4.1(a) and (b), respectively.

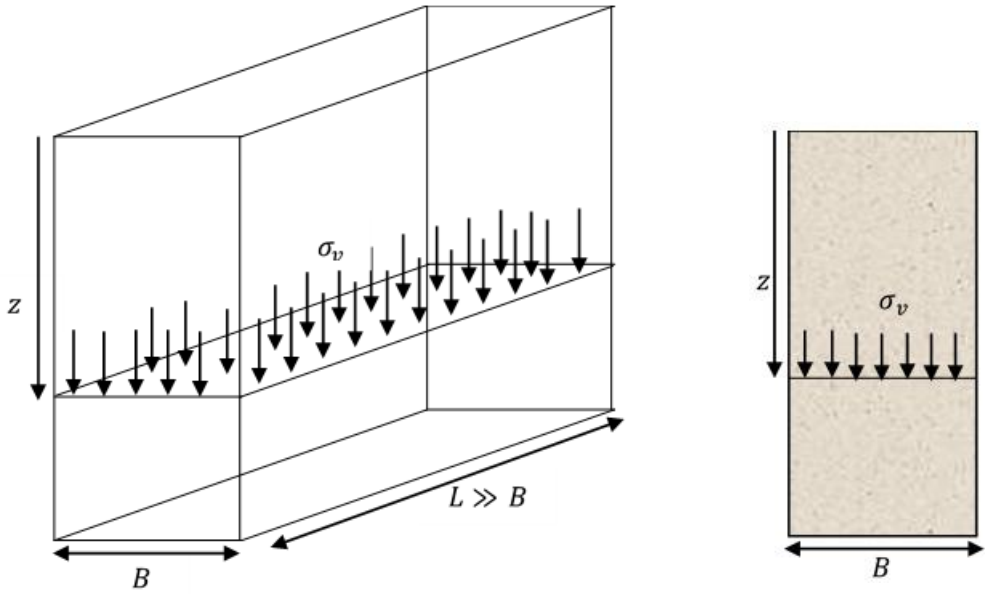

(a) (b)

Figure 4.1. Schematic diagram (a) 3D backfilled trench/stope (b) 2D backfilled stope

4.2.1 Marston's theory

The expression developed by Janssen (1895) using limit equilibrium method was later modified by Marston considering 2D plane strain theory on arching and equations were presented to compute the average vertical and horizontal normal stresses within granular (cohesionless)

backfill stope as given in Equations 4.1 and 4.2, respectively. Here, the stope is considered as a narrow trench where stope length (L) is much greater than stope width (B) and hence it is approximated as 2D plane strain loading.

$$\sigma_v = \frac{\gamma B}{2\mu K_a}\left[1 - exp\left(\frac{-2K_a\mu z}{B}\right)\right] \quad \text{Eq. (4.1)}$$

$$\sigma_h = K_a\sigma_v \quad \text{Eq. (4.2)}$$

σ_v - Average vertical normal stress within the fill

γ - Unit weight of the fill

B - Stope width

z - Fill depth, measured from top of the fill

μ - Coefficient of friction of backfill and rock wall ($\mu = \tan\delta$)

δ - Interfacial friction angle between the fill and the wall

K_a - Rankine's active lateral earth pressure coefficient

Here, δ is taken as ${}^{2\phi}/_{3}$ where ϕ is the friction angle of the backfill.

4.2.2 Modified Marston's theory

In the Marston's equation, the active earth pressure coefficient is used. However, Aubertin et al. (2003) analytical solution suggested that the fill can be in active, passive or at-rest state, depending on the status of the stope wall during filling operation. The modified Marston's equations are given in Equations 4.3 and 4.4.

$$\sigma_v = \frac{\gamma B}{2K\tan\phi}\left[1 - exp\left(\frac{-2Kz\tan\phi}{B}\right)\right] \quad \text{Eq. (4.3)}$$

$$\sigma_h = K\sigma_v \quad \text{Eq. (4.4)}$$

ϕ - Friction angle of backfill

K - Lateral earth pressure coefficient

Here, K can be active earth pressure coefficient (K_a), passive earth pressure coefficient (K_p) or at-rest earth pressure coefficient (K_0), which are determined using the equations discussed in Section 4.2.5.

4.2.3 Extended Marston's theory

The Marston's equation and Aubertin et al. (2003) solutions are mainly applied for backfilled narrow trenches where the fill is subjected to plane strain loading and hence, they can be approximated as 2D stopes. However, the mine stopes are rarely 2D. Therefore, Pirapakaran and Sivakugan (2007a) extended the Marston's theory to 3D stopes. The equations for determining the average vertical and horizontal stresses within a backfilled rectangular shape stope are given in Equations 4.5 and 4.6.

$$\sigma_v = \frac{\gamma B}{2K\tan\delta}\left(\frac{L}{B+L}\right)\left[1 - exp\left\{-2\left(\frac{B+L}{BL}\right)Kz\tan\delta\right\}\right] \qquad \text{Eq. (4.5)}$$

$$\sigma_h = K\sigma_v \qquad \text{Eq. (4.6)}$$

Here, L is the length of the stope and the other symbols stand for standard definitions as mentioned above. For square shape stopes, $L = B$, and hence the arching equation is simplified to Equation 4.7.

$$\sigma_v = \frac{\gamma B}{4K\tan\delta}\left[1 - exp\left(\frac{-4Kz\tan\delta}{B}\right)\right] \qquad \text{Eq. (4.7)}$$

The Equation 4.7 is also valid for stopes and storage vessels/silos with circular cross section (Pirapakaran and Sivakugan, 2007a).

4.2.4 Limitations with analytical solutions

The analytical solutions have been developed based on several approximations and simplifications. Two of the common ones are,

- The vertical normal stress distribution within the backfill, at any depth, is assumed to be uniform. (i.e., both the analytical and laboratory model solutions reflect the average vertical normal stress at any depth of the fill, although laboratory models treat the soil mass as a particulate medium unlike in analytical approach or most numerical models which treat the soil mass as a continuum)
- The lateral earth pressure coefficient is used in the equations as K_0, K_a or K_p, and they are assumed constant throughout the fill depth.

4.2.5 Lateral earth pressure coefficient (K) used in analytical equations

The lateral earth pressure coefficient is an important parameter used in underground structures such as backfilled stopes and drive barricades. For a homogeneous soil mass, K is defined as the ratio between the horizontal effective stress and vertical effective stress acting on the soil mass, as given in Equation 4.8 and thus it is a scalar quantity.

$$K = \frac{\sigma'_h}{\sigma'_v} \qquad \text{Eq. (4.8)}$$

There are three types of lateral earth pressure coefficients as K_0, K_a and K_p defined by different analytical expressions as below. The arching equations for backfill stress determination utilise K value in different ways based on the analytical models developed, considering the stope wall movement during backfilling process. The analytical solutions discussed in this dissertation are for granular soils like hydraulic fills. The granular HF settles in the stope quickly without developing a large pore water pressure due to fast drainage process, and hence, the total stresses within the fill can be considered equal to the effective stresses, as discussed in Chapter 3. Therefore, the lateral earth pressure coefficient expressions are discussed hereafter in terms of

total stresses, considering the dry granular HF used in this study, where the effective stresses and the total stresses are the same.

In Marston's theory, the lateral earth pressure coefficient is taken as Rankine's active earth pressure coefficient (K_a) given by Equation 4.9.

$$K_a = tan^2\left(45 - \frac{\phi}{2}\right) = \frac{1 - \sin\phi}{1 + \sin\phi} \qquad \text{Eq. (4.9)}$$

Terzaghi used the lateral earth pressure coefficient given by Krynine (1945), assuming $\delta = \phi$ for rough vertical walls, as defined in Equation 4.10.

$$K = \frac{1}{1 + 2tan^2\phi} = \frac{1 - sin^2\phi}{1 + sin^2\phi} \qquad \text{Eq. (4.10)}$$

Handy (1985) stated that due to rotation of principal stresses near the wall, K increases from K_a towards K_0, and hence suggested the Jaky's (1944) expression for determining K_0, as given in Equation 4.11.

$$K_0 = 1 - \sin\phi \qquad \text{Eq. (4.11)}$$

The modified Marston's theory by Aubertin et al. (2003) proposed three cases of lateral earth pressure coefficients as the active (K_a), passive (K_p), determined using Rankine's expressions, and at-rest (K_0) earth pressure coefficient by Jaky's (1944) expression. For backfilled underground stopes, the stope wall movement towards the fill in the stope is not possible due to high Young's modulus of the wall rock mass and thus the Rankine's passive earth pressure coefficient (K_p) is not considered for the analytical equations in this dissertation. The extended Marston's theory by Pirapakaran and Sivakugan (2007a) suggested either K_0 or K_a can be used in their analytical equations. It is important to note that all the analytical expressions for lateral earth pressure coefficient depend on the friction angle of the backfill material.

4.2.6 Analytical plots for stress variation within a backfilled stope

Dimensionless plots are presented for the stress variation within a stope filled with granular HF for the fill depth (z) varying from 0 to $6B$ where B is the stope width. The backfill friction angle (ϕ) is taken as 40° corresponding to the 51 % relative density (D_r) of the fill in the stope achieved by pouring the fill under gravity. The analytical solutions discussed above are compared for the variations of lateral earth pressure coefficient (K) and interfacial friction angle (δ), as shown in Figures 4.2, 4.3 and 4.4.

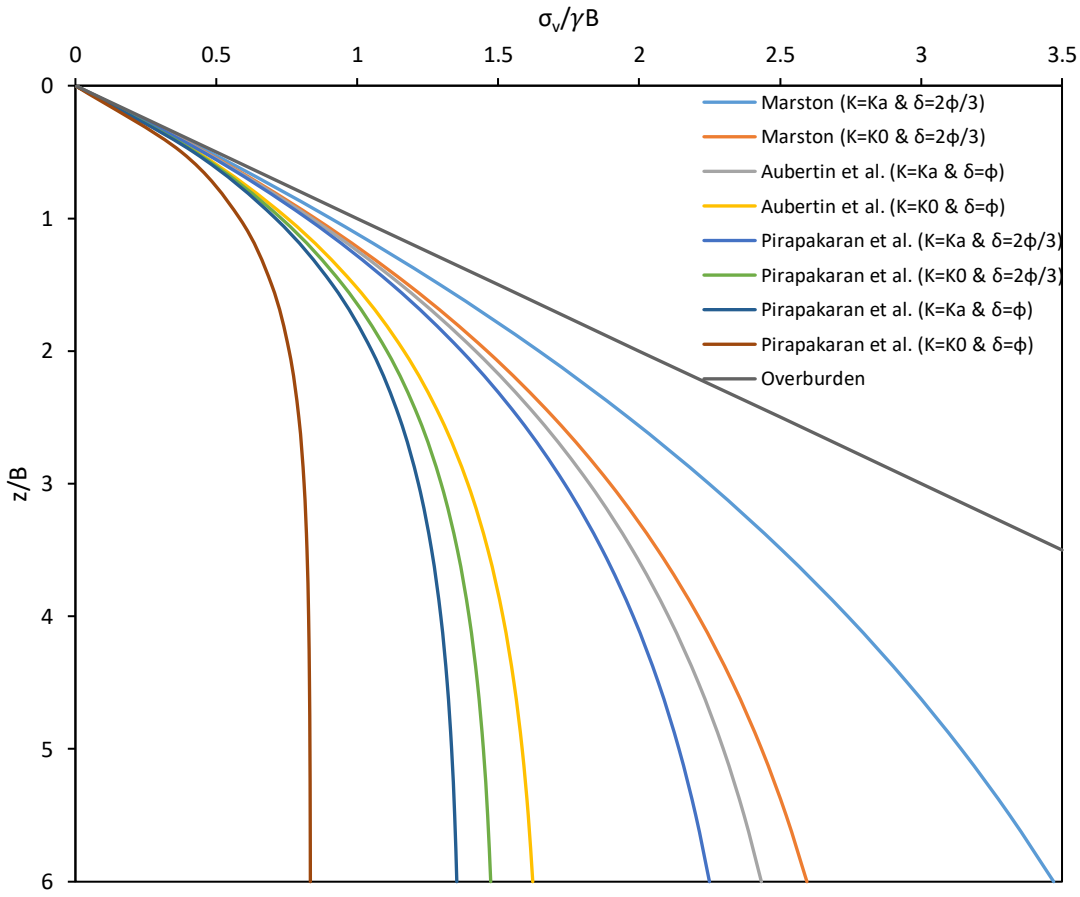

Figure 4.2. Generalised analytical plot for vertical normal stress variation with fill depth

The average vertical normal stress variation with fill depth is shown in Figure 4.2. It can be seen that the vertical stresses are larger for K_a than K_0, as seen from all three equations. Generally, mine stope wall stiffness is 2-3 orders higher than the stiffness of the backfill and thus, the wall movement during backfilling is not expected. Therefore, it is suggested that K_0 can be

reasonably used in the analytical equations, considering the backfill is in at-rest state. This argument is justified further with the stope arching model analysis in Section 4.3. Marston (1930) and Aubertin et al. (2003) equations estimate larger normal stresses within the fill due to stope being considered as a narrow trench. However, Pirapakaran and Sivakugan (2007a) analytical model considers a square stope and hence the normal stresses in the fill are smaller due to higher wall shear stresses generated as a result of arching. Mine stope walls are rough after blasting of the ore and thus the fill-wall interfacial friction angle (δ) is taken as friction angle of the fill (ϕ), as described in Chapter 3. It is also evident that the vertical normal stress within the fill becomes an asymptotic value at $2B$ to $3B$ fill depth with $\delta = \phi$. The horizontal normal stress variation with fill depth as determined using Equations 4.2, 4.4 and 4.6, is presented in Figure 4.3. It is clear that the horizontal stress reaches an asymptotic value at depths of $1B$ to $2B$, relatively faster than the vertical stress.

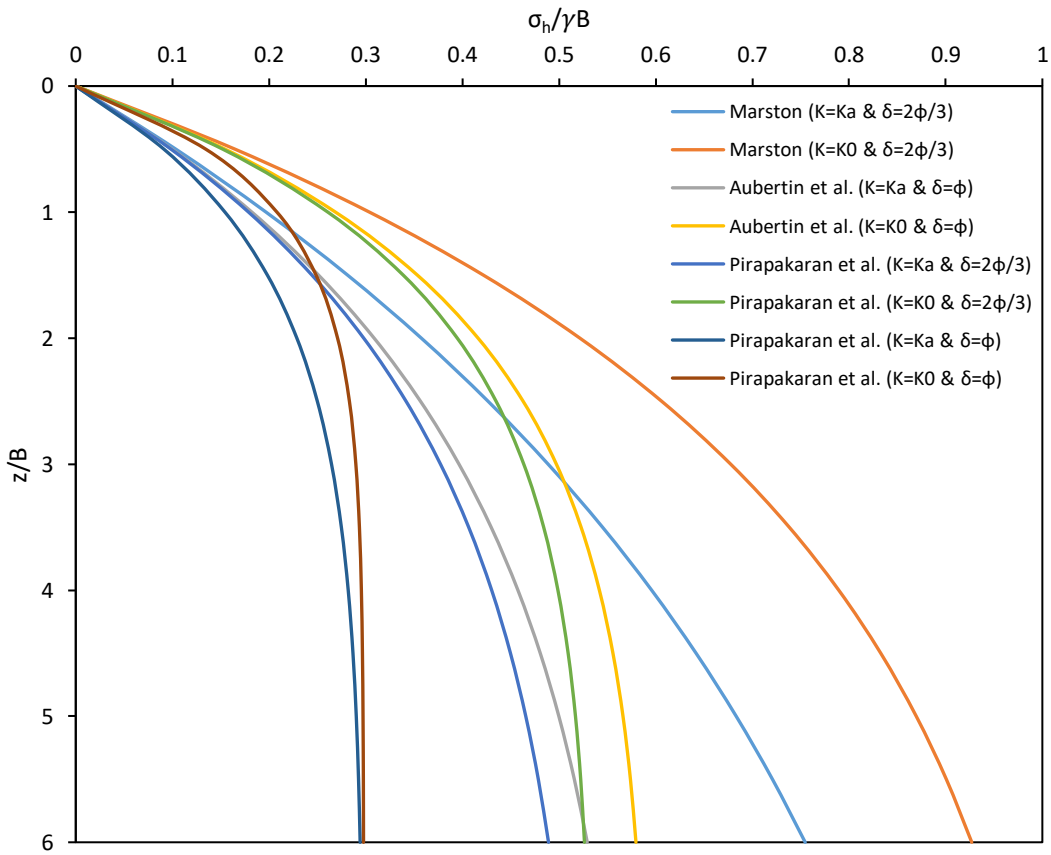

Figure 4.3. Generalised analytical plot for horizontal normal stress variation with fill depth

The wall shear stress (τ) generated with the fully mobilised wall friction due to arching can be determined using Equation 4.12, and the dimensionless plot for shear stress variation with depth is presented in Figure 4.4.

$$\tau = \sigma_h \tan \phi \qquad \text{Eq. (4.12)}$$

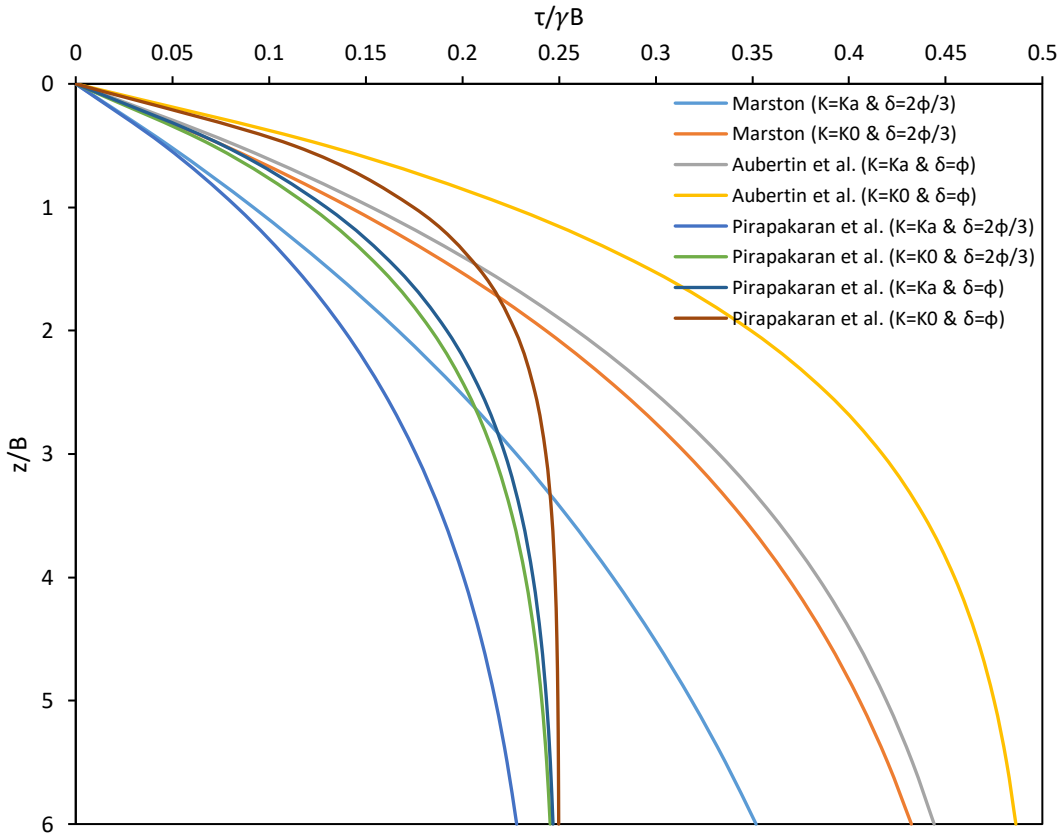

Figure 4.4. Dimensionless analytical plot for wall shear stress variation with fill depth

Marston (1930) and Aubertin et al. (2003) solutions exhibit the shear stress is approaching a constant value, relatively at larger depths like $5B$ to $6B$ due to the fact that only two stope walls in the narrow trench/stope creates less arching. In contrast, the shear stress from Pirapakaran and Sivakugan (2007a) solution becomes asymptotic at $2B$ to $3B$ depth, due to higher degree of arching in square backfilled stopes with wall friction contributing from the four sides.

4.3 Laboratory stope arching model

A laboratory model stope setup was used to study the arching effects on stress developments within the stope while filling with dry hydraulic fill. The model setup called the 'arching apparatus' and its schematic diagram are shown in Figure 4.5. The apparatus was used in determining the average vertical normal stress variation with depth within the fill, shear stress and horizontal normal stress variation along the stope wall, with fill depth. The model stope is suspended from steel wires connected to a load cell (Revere Transducers, type 9363-D3-100kg_20T1; precision 0.001 kg) hanging from the top of the frame. The model stope is positioned vertically until the minimum possible gap between the stope and balance becomes 0.5 mm (less than a grain size), ensuring that there is no load registered on the balance (precision 0.005 kg) and that grains do not flow out through the gap. When the model is filled in layers with a granular material of weight $(m + n)$, the fill load is shared between the balance at the bottom and the top load cell, reflecting the loads carried by the base and the walls, respectively. The load cell records the fill load transferred to the wall (m) and the balance reads the fill load transferred to the bottom (n), given that the balance and load cell readings were zero at the start of the test. Therefore, at any stage of filling, m and n can be measured separately through this setup. The test procedure and preliminary findings are discussed in Jayakodi et al., (2021).

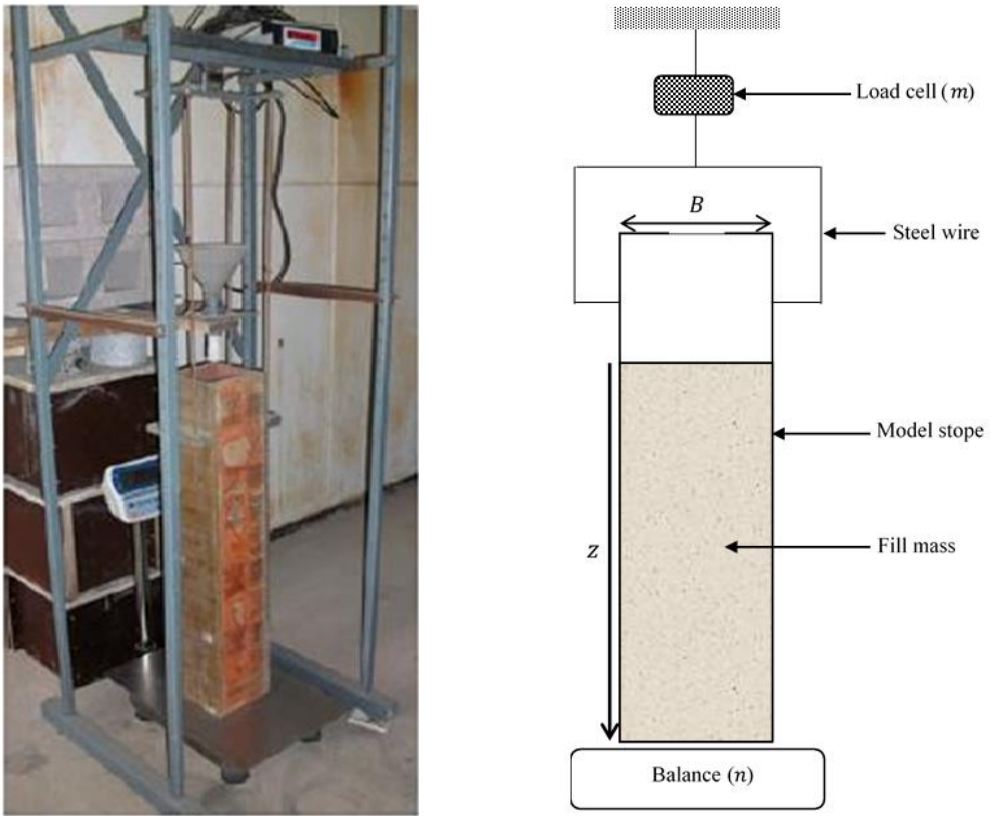

Figure 4.5. Laboratory stope arching model apparatus (a) photo (b) schematic diagram

Square and circular shape stopes with breath/diameter (B) of 150 mm and height (H) of 900 mm with an open bottom, were tested with both smooth and rough walls inside the stope. The rough wall condition was created using P40 coarse sandpaper glued onto the inside wall of the stope to simulate underground mine wall roughness whereas the smooth wall condition was considered with Perspex stope walls, to compare the arching phenomenon. The findings of the smooth wall stope model tests are valid for situations where the stresses within grain silos are of interest. The laboratory stope models used in this study are shown in Figure 4.6(a). Since the stope walls are very rough after blasting, the interfacial friction angle (δ) can be taken as the friction angle of the fill (ϕ) as the failure occurs on the fill-fill interface, not the fill-wall interface. Hence, a similar condition was created using very rough coarse sandpaper attached to the stope walls of the model as shown in Figure 4.6(b).

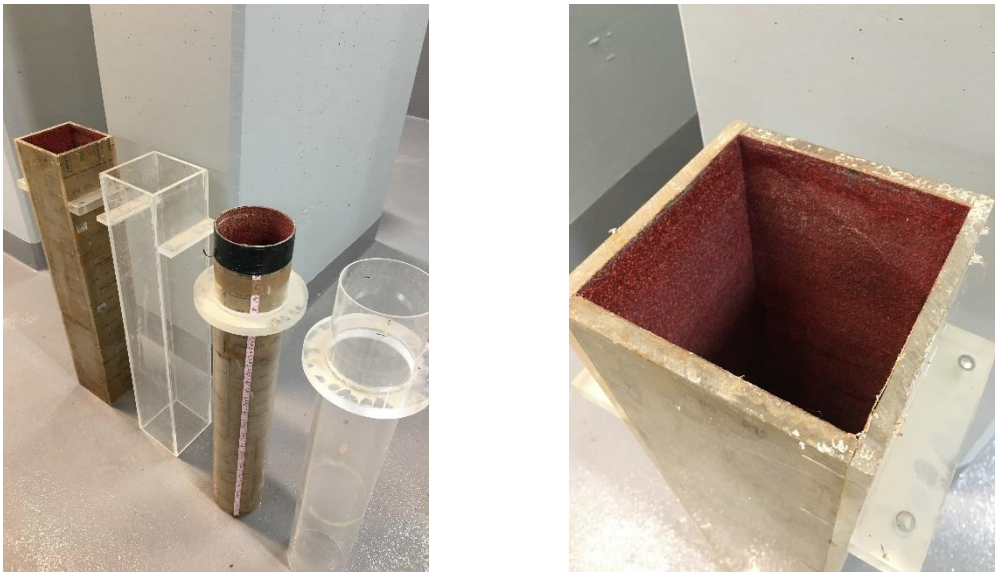

Figure 4.6. (a) Model types used (b) Wall roughness with glued coarse sandpaper

The filling of the stope was carried out with 9 fine sand layers of equal thickness (replicating granular HF), by keeping the funnel at a fixed height as shown in Figure 4.5(a), to maintain uniform relative density and replicate the filling conditions at the mine. After each stage of filling, the readings from the balance and load cell were checked, whether the sum of the load on the load cell and bottom scale, matches the weight of poured sand. As the fill load was shared by the balance and the load cell, this check confirmed the performance of the apparatus after each stage of filling. The geotechnical charaterisation of fine sand and its comparison with HF properties were discussed in detail in Chapter 3. A summary of the geotechnical properties of fine sand used in arching model tests, is tabulated in Table 4.1.

Table 4.1. Properties of fine sand

Property	**Fine sand**
Median grain size, D_{50} (mm)	0.22
Effective grain size, D_{10} (mm)	0.115
Coefficient of uniformity, C_u	2.3
Coefficient of curvature, C_c	1.12
Specific gravity, G_s	2.60

Minimum dry density, $\rho_{d,min}$ (kg/m^3)	1298
Maximum dry density, $\rho_{d,max}$ (kg/m^3)	1591
Friction angle, ϕ (°)	40
Interfacial friction angle, rough walls, δ_{RW} (°)	38.5
Interfacial friction angle, smooth walls, δ_{SW} (°)	25

4.4 Shear stresses within a backfilled stope

During backfilling of a stope, the shear stresses are generated along the rough stope wall which then resulted the reduction of normal stresses within the fill due to the effect of arching. Therefore, establishing the wall shear stress variation in a backfilled stope is essential as the first step of stress analysis within a backfilled mine stope. There is no successful attempt thus far to analyse the shear stress development within a backfilled stope analytically. Therefore, this section proposes a novel method for shear stress interpretation and develops an analytical expression to determine the shear stress at any depth of the fill, and a model for the variation of shear stress with fill depth. This is then extended for the normal stress variations within the fill while validating with stope model test results, as discussed in Section 4.6.3.

A simple version of the laboratory stope arching model filling with 5 equal layers of granular backfill material is used here to explain the concept and interpretation, as shown in Figure 4.7. Adding of each equal layer (i) of ($m + n$) mass into the model will incur the fill load to be transferred to the wall and to the bottom such that the fill mass carried by the wall (m) is reflected on the load cell, and the fill mass transferred to the bottom (n) is reflected on the balance. At any stage of filling, m and n can be measured separately through this setup.

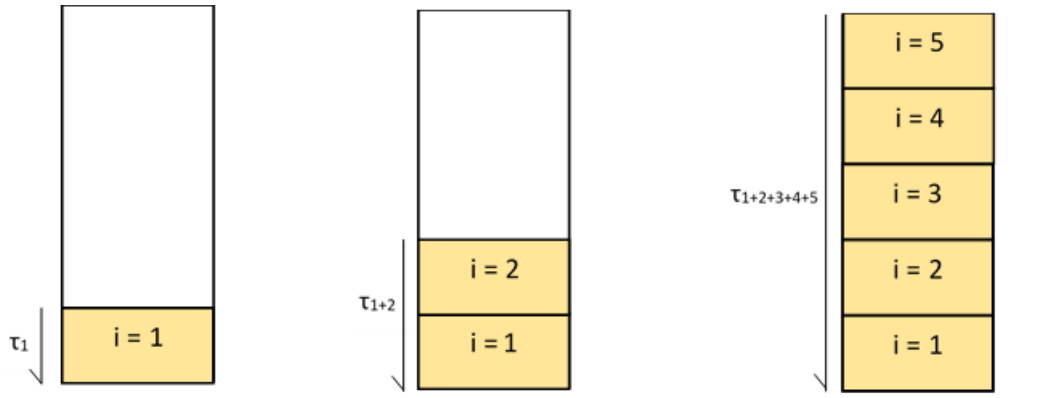

$$\tau_1 = \frac{(m_1)g}{A_w} \qquad \tau_{1+2} = \frac{(m_{1+2})g}{2A_w} \qquad \tau_{1+2+3+4+5} = \frac{(m_{1+2+3+4+5})g}{5A_w}$$

Figure 4.7. Schematic representation of average wall shear stress in the stope arching model

τ_1 – shear stress from layer 1 along layer 1 (average shear stress on wall contributed by layer 1)

τ_{1+2} – shear stress from layer 1 and 2 along both layers (average shear stress on wall contributed by both layers)

$\tau_{1+2+3+4+5}$ – shear stress from layer 1,2,3,4 and 5 along all five layers (average shear stress on wall contributed by all five layers)

m_1 – mass on wall from layer 1 (mass transferred to wall from layer 1)

m_{1+2} – mass on wall from layer 1 and 2 (mass transferred to wall from both layers)

$m_{1+2+3+4+5}$ – mass on wall from layer 1,2,3,4 and 5 (mass transferred to wall from all five layers)

A_w – wall area for one layer, given by the stope perimeter multiplied by the layer thickness

4.4.1 Average shear stress along stope wall up to any depth of the fill

As discussed in Section 4.3, the laboratory stope model setup allows to directly measure the load carried by the wall next to the entire fill height during the layer filling process. Hence, the variation of average shear stress with fill depth is schematically shown in the plots given in Figure 4.8.

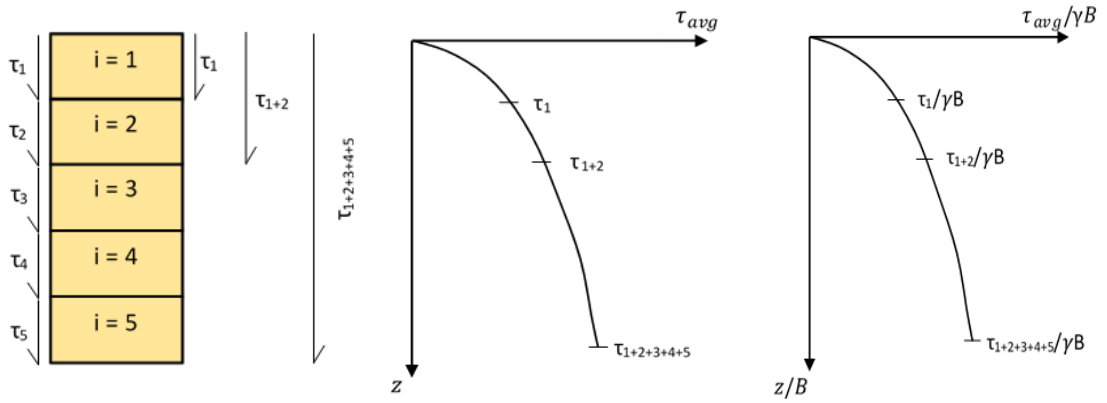

Figure 4.8. Average shear stress variation plot (not to the scale)

τ_i – shear stress on wall next to layer i (i.e. τ_1, τ_2 etc.)

τ_{avg} - average shear stress on wall along fill depth (i.e. τ_{1+2}, τ_{1+2+3} etc.)

z – depth to a point within the fill from the top of the fill

B – stope width

γ – unit weight of the fill

Accordingly, the average shear stress on wall up to any depth of the fill (τ_z) contributed by the fill mass above that level can be determined from the dimensionless plot, for any stope dimensions.

4.4.2 Shear stress on wall next to a fill layer at any depth of the fill from top

An analytical solution is proposed herein for developing a general expression to determine the shear stress on the wall next to the fill strip (layer) of any thickness at any depth of the fill in a backfilled stope.

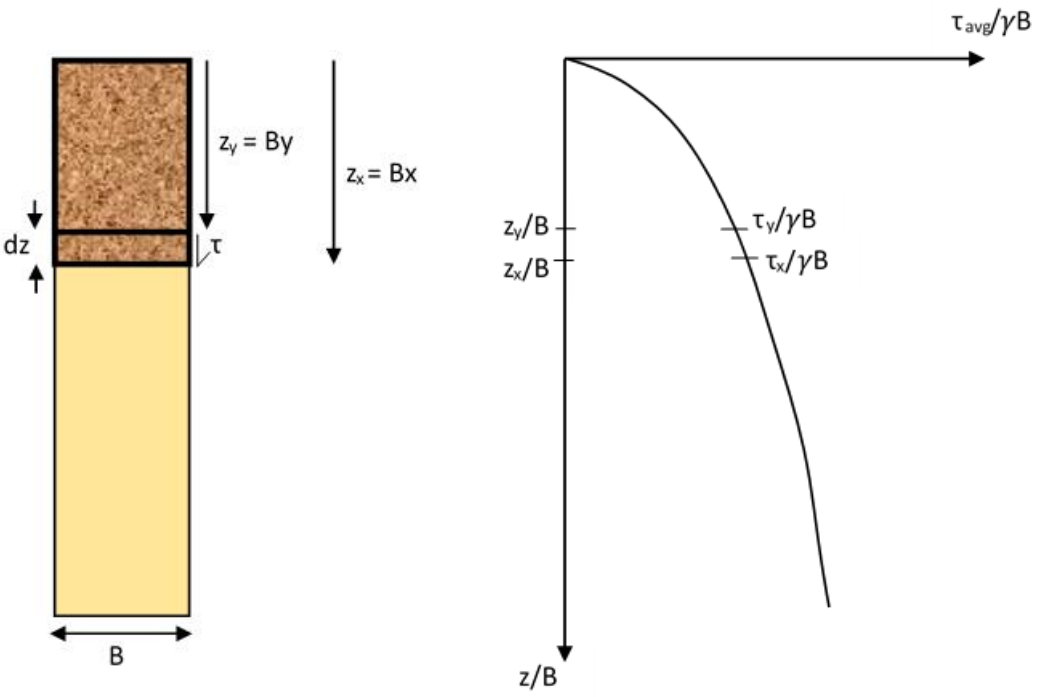

Figure 4.9. Idealised stope with fill layer element and the dimensionless plot of τ_{avg} verses depth z

A fill strip (layer element) of thickness dz bound by depths z_x and z_y within a backfilled stope of width B, length L and fill unit weight of γ, is considered as shown in Figure 4.9.

Stope perimeter, $P = 2(B + L)$

Let's take $\frac{z_x}{B} = x$ and $\frac{z_y}{B} = y$

$z_x = Bx$ and $z_y = By$, then $dz = z_x - z_y = Bx - By = B(x - y)$

$\frac{\tau_x}{\gamma B}$ and $\frac{\tau_y}{\gamma B}$ can be read from the dimensionless plot obtained in Figure 4.9, corresponding to $\frac{z_x}{B}$ and $\frac{z_y}{B}$

With known B and γ, the *average* shear stress values τ_x and τ_y from the top of the fill to depths z_x and z_y respectively, can be calculated.

Then, $\tau_x = \frac{m_x g}{P \times z_x} = \frac{m_x g}{2B(B+L)x}$

Here, m_x is the fill mass transferred to the wall along the fill depth of z_x.

Hence, $m_x = \frac{2B(B+L)x\tau_x}{g}$

Similarly, $\tau_y = \frac{m_y g}{P \times z_y} = \frac{m_y g}{2B(B+L)y}$ where m_y is the fill mass transferred to the wall from the fill depth of z_y

Hence, $m_y = \frac{2B(B+L)y\tau_y}{g}$

Therefore, the load transferred to the portion of the wall in contact with layer dz when the entire fill mass is in place can be written as

$(m_x - m_y)g = 2B(B+L)(x\tau_x - y\tau_y)$

Then, the shear stress on wall at z_x next to layer dz

$\tau_{(z_x,dz)} = \frac{(m_x - m_y)g}{P \times dz} = \frac{2B(B+L)(x\tau_x - y\tau_y)}{2B(B+L)(x-y)}$

Hence,

$$\tau_{(z_x,dz)} = \frac{x\tau_x - y\tau_y}{x-y} = \frac{z_x\tau_x - z_y\tau_y}{z_x - z_y} \qquad \text{Eq. (4.13)}$$

This equation is independent of stope dimensions and is valid for stope with any cross-sectional area (rectangular, square, circular). More importantly, by considering a very thin layer, it is possible to employ the Equation 4.13 to determine the *exact* shear stress at any depth along the wall.

Then, the horizontal normal stress (σ_h) on wall at z_x depth next to layer dz can be calculated for a granular fill having a fill-wall interfacial friction angle (δ) as below.

$$\sigma_{h(z_x)} = \frac{\tau_{(z_x)}}{\tan \delta} \qquad \text{Eq. (4.14)}$$

Interpretation of stope model test data with Eq. (4.13)

The stope model test parameters are as below.

Shape: square cross-section

Width (B): 0.15 m

Maximum filled height (H): 0.9 m

Depth to a point within the fill from the top of the fill (z): 0 to 0.9 m

Fill unit weight (γ): 13.08 kN/m^3

z/B range: 0 to 6

The dimensionless plot for the average wall shear stress variation along the depth of filled stope is shown in Figure 4.10.

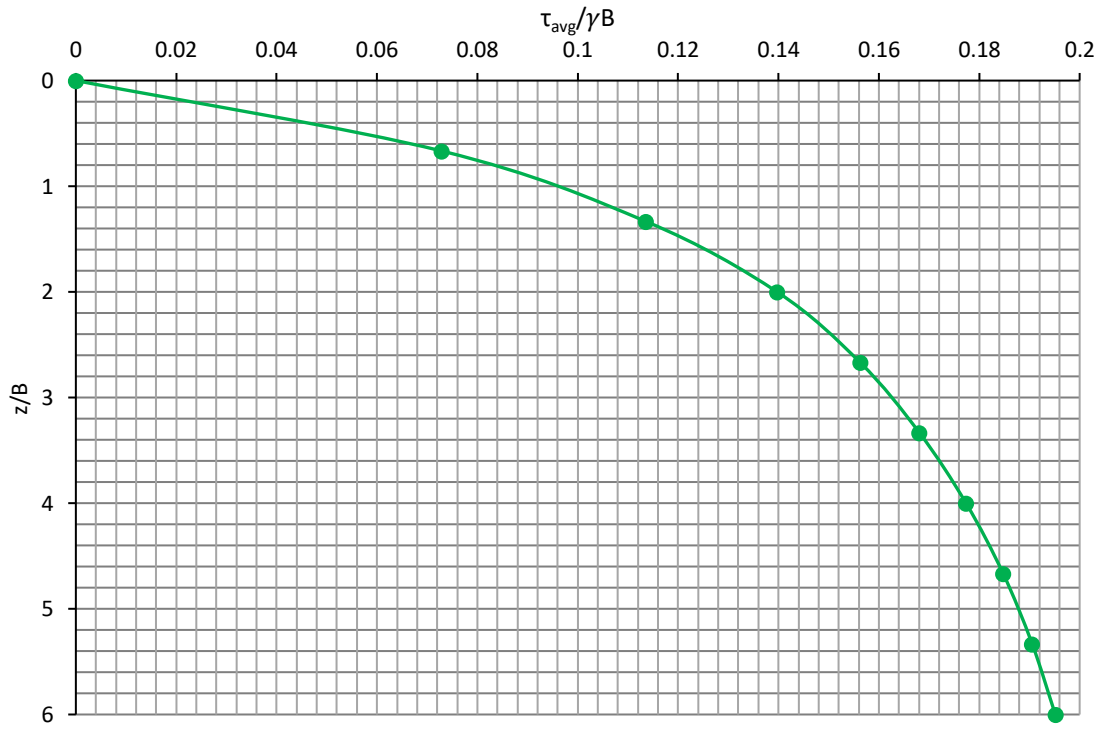

Figure 4.10. Variation of average wall shear stress along the fill depth

x	1.33
y	0.67
$z_x\ (m)$	0.2
$z_y(m)$	0.1
$dz\ (m)$	0.1

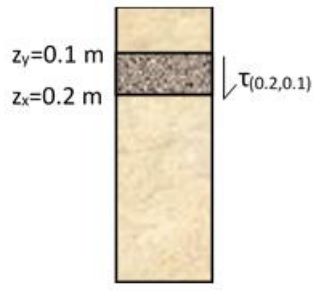

Figure 4.11. Parameters relevant to Eq. (4.13)

Figure 4.11 depicts the parameters required to determine the shear stress on wall next to a layer of 0.1 m thickness, and the example calculation is shown below.

Example calculation:

From plot in Figure 4.10, $\frac{\tau_x}{\gamma B} = \frac{\tau_{1.33}}{\gamma B}$ = 0.1144 Hence, $\tau_{1.33}$ = 0.2245 kPa

Similarly, $\frac{\tau_y}{\gamma B} = \frac{\tau_{0.67}}{\gamma B}$ = 0.0704 Hence, $\tau_{0.67}$ = 0.1382 kPa

From Eq. (4.13),

$$\tau_{(0.2,0.1)} = \frac{1.33\tau_{1.33} - 0.67\tau_{0.67}}{(1.33-0.67)} = \frac{1.33(0.2245) - 0.67(0.1382)}{0.66} = 0.3108 \text{ kPa.}$$

As shown in the example, the exact shear stress on wall next to a layer of 0.1 m in the backfilled laboratory stope arching model can be calculated. Hence, the variation of exact shear stress with fill depth in the stope model can be presented as in Figures 4.12 and 4.13. This is further developed to a general analytical model in Section 4.6.2.

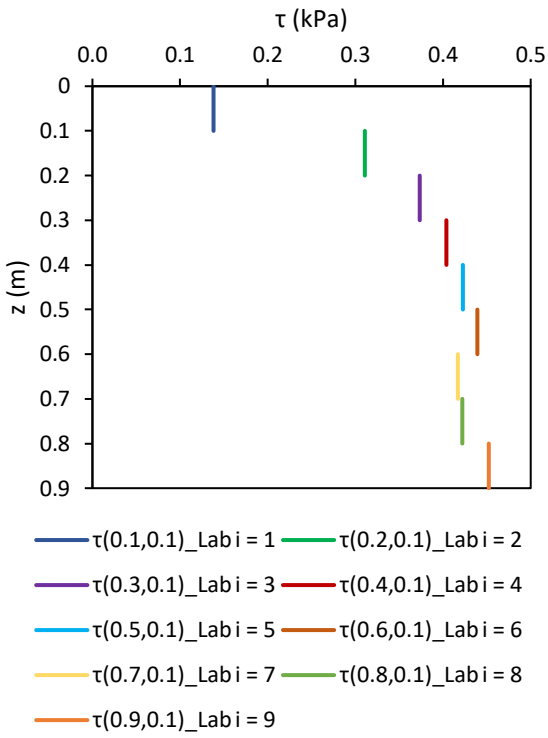

Figure 4.12. Variation of exact wall shear stress with fill depth z, with layer thickness of 0.1 m

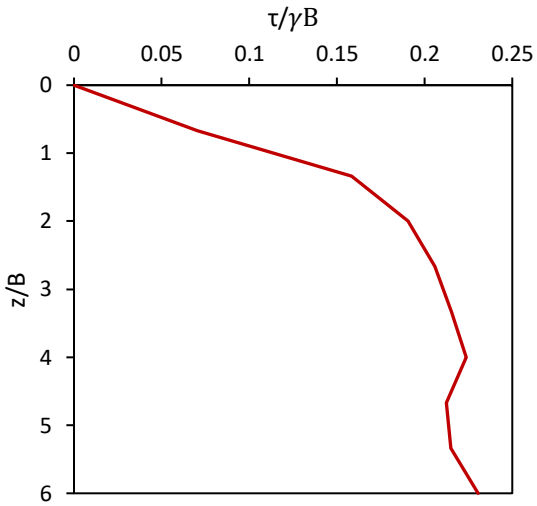

Figure 4.13. Normalised plot for the variation of exact wall shear stress with fill depth

4.5 Normal stresses within a backfilled stope

The normal stresses developed within a backfilled stope can be interpreted using the stope arching model as described below. During equal layer backfilling of the stope, the normal stress developed at the stope bottom is determined using the mass of fill (n) recorded on the balance. Numerical simulations by Sivakugan et al. (2014) have investigated that during backfilling, the normal stress generated from a fill height of z at the fixed stope bottom is larger due to the frictional immobilisation at the fill-bottom interface (Method 1), compared to the normal stress developed from the same fill height from fill top within a backfilled stope where the full frictional mobilisation at the fill-fill interface is occurred (Method 2). The comparison of the two methods is shown in Figure 4.14. Therefore, the arguments and interpretations made herein for normal stress development at the stope bottom, as recorded on the balance during backfilling of the stope can be approximated to the normal stress at any depth of the fill within a backfilled stope on the completion of filling, within conservative margins.

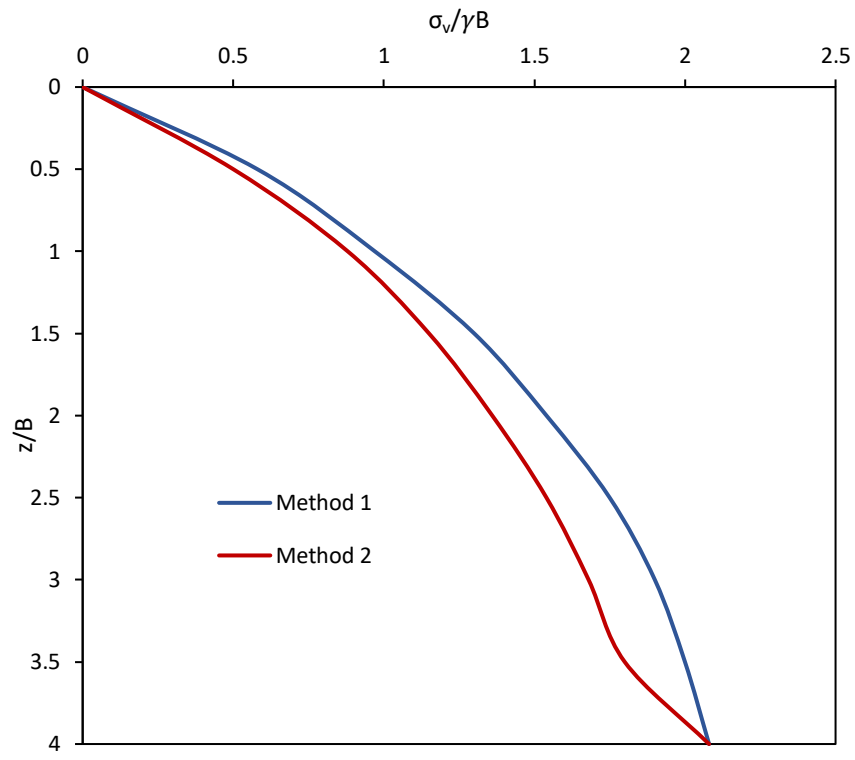

Figure 4.14. Vertical stress variation with depth: During backfilling (Method 1) and on the completion of filling (Method 2)

4.5.1 Stope arching model during backfilling

A simple version of the laboratory stope arching model filling with 5 equal layers of granular backfill material is considered to explain the interpretation, as shown in Figure 4.15.

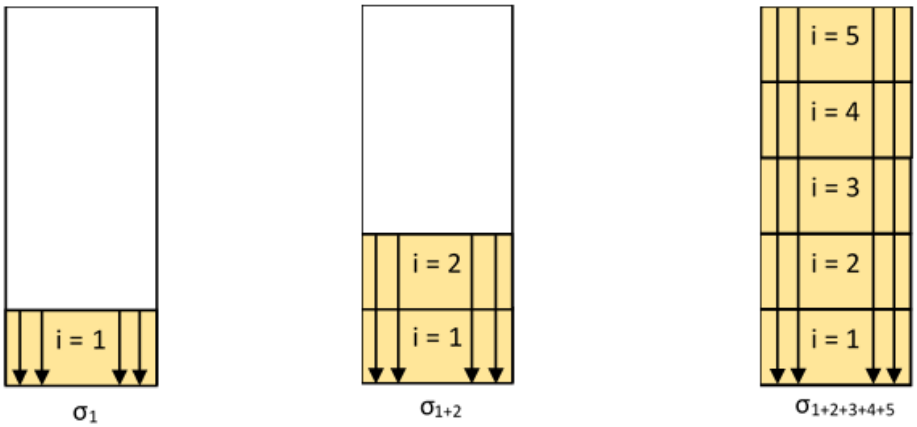

$$\sigma_1 = \frac{(n_1)g}{A_b} \qquad \sigma_{1+2} = \frac{(n_{1+2})g}{A_b} \qquad \sigma_{1+2+3+4+5} = \frac{(n_{1+2+3+4+5})g}{A_b}$$

Figure 4.15. Schematic representation of normal stress in the stope arching model

σ_1 – vertical normal stress from layer 1 at the stope bottom

σ_{1+2} (i.e. σ_2) – vertical normal stress from layer 1 and 2 at the stope bottom

$\sigma_{1+2+3+4+5}$ (i.e. σ_5) – vertical normal stress from all five layers at the stope bottom

n_1 – fill mass from layer 1 on stope bottom

n_{1+2} (i.e. n_2) – fill mass from layer 1 and 2 on stope bottom

$n_{1+2+3+4+5}$ (i.e. n_5) – fill mass from all five layers on stope bottom

A_b – inner cross-sectional area of stope bottom

4.5.2 Normal stresses within the stope on the completion of filling

The average vertical normal stress at any depth of the fill, on the completion of filling can be interpreted as below.

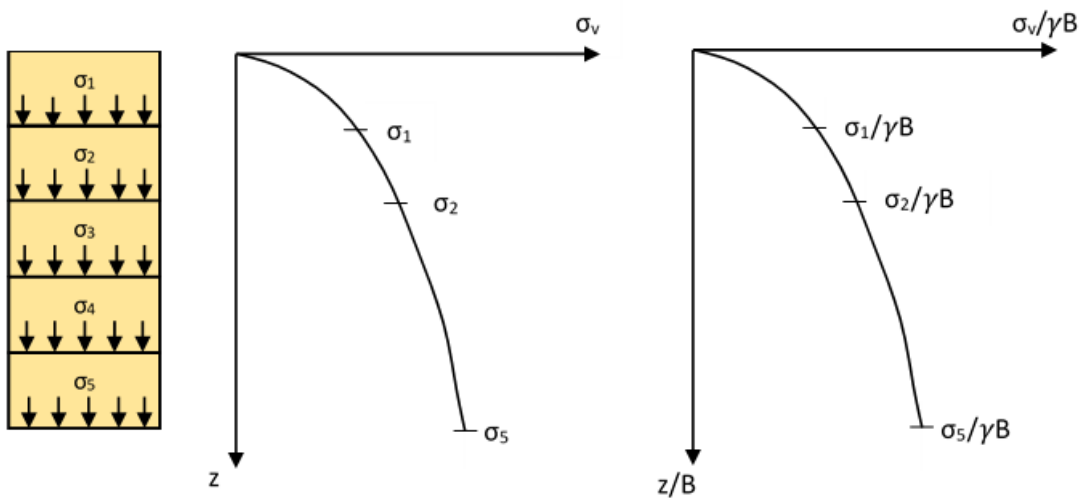

Figure 4.16. Normal stress variation plot (not to the scale)

$\sigma_i (= \sigma_v)$ – average normal stress at the bottom of layer i (i.e. σ_1, σ_2 etc.)

z – fill depth from the top of the fill

B – stope width

γ – unit weight of the fill

Accordingly, the average normal stress at any depth of the fill (σ_v) contributed by the fill mass above that level can be determined from the dimensionless plot presented in Figure 4.17, for any stope dimensions.

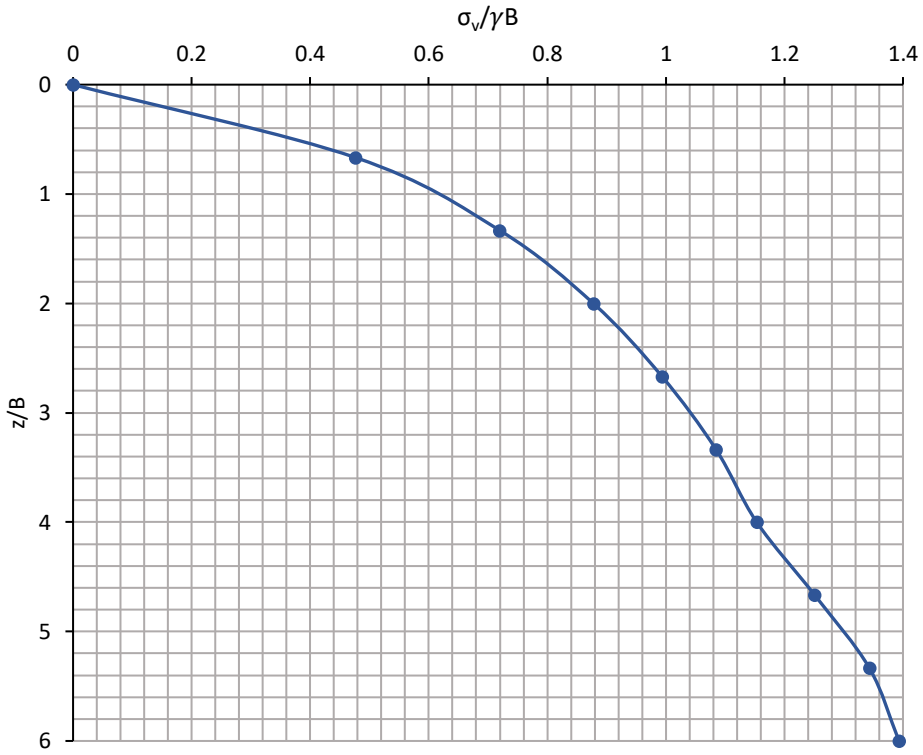

Figure 4.17. Variation of normal stress along the fill depth

4.6 Analytical models for shear and normal stress variation in backfilled stope

The four types of arching model stopes used in laboratory tests are considered herein, reflecting the parameters such as stope shape, size and the wall roughness which affect arching. The model parameters are summarised in Table 4.2.

Table 4.2. Laboratory stope model parameters

Identification	Cross-section	Length L (m)	Width B (m)	Height H (m)	Diameter d (m)	Wall roughness
S150-RW	Square	0.15	0.15	0.9		Rough
S150-SW	Square	0.15	0.15	0.9		Smooth
C150-RW	Circular			0.9	0.15	Rough
C150-SW	Circular			0.9	0.15	Smooth

The equations developed through regression modelling for the variation of shear and normal stresses within all four types of stopes, are discussed below. Some simple analytical solutions developed through curve fitting of the laboratory test data are discussed in Sections 4.6.1, 4.6.2, and 4.6.3, as follows.

- Section 4.6.1 - Average shear stress up to a depth along the wall
- Section 4.6.2 - Exact shear stress at a point on the wall
- Section 4.6.3 - Average normal stress at a depth within the fill

4.6.1 Analytical model for the variation of average shear stress with depth

A general regression equation was considered with two coefficients a and b, as given in Equation 4.15. The two coefficient values for each specific stope were determined by superimposing the stope model test data for the average wall shear stress (τ_{avg}) variation along the depth of filled stope. Here, B is the stope width, γ is the unit weight of the fill and z is the fill depth from top. The appropriate a and b values for all four stopes are tabulated in Table 4.3. The Equation 4.15 is valid only for z/B varying from 0 to 6. The dimensionless plots for average shear stress variation with depth for the four stope types are shown in Figure 4.18.

$$\tau_{avg}/\gamma B = \frac{z/B}{a + b(z/B)} \qquad \text{Eq. (4.15)}$$

Table 4.3. Coefficients for average shear stress equation

Stope ID	Eq. no.	*a*	*b*
S150-RW	4.15.1	6.0125	4.2102
S150-SW	4.15.2	9.5412	4.1196
C150-RW	4.15.3	6.9421	4.2436
C150-SW	4.15.4	14.4256	3.7152

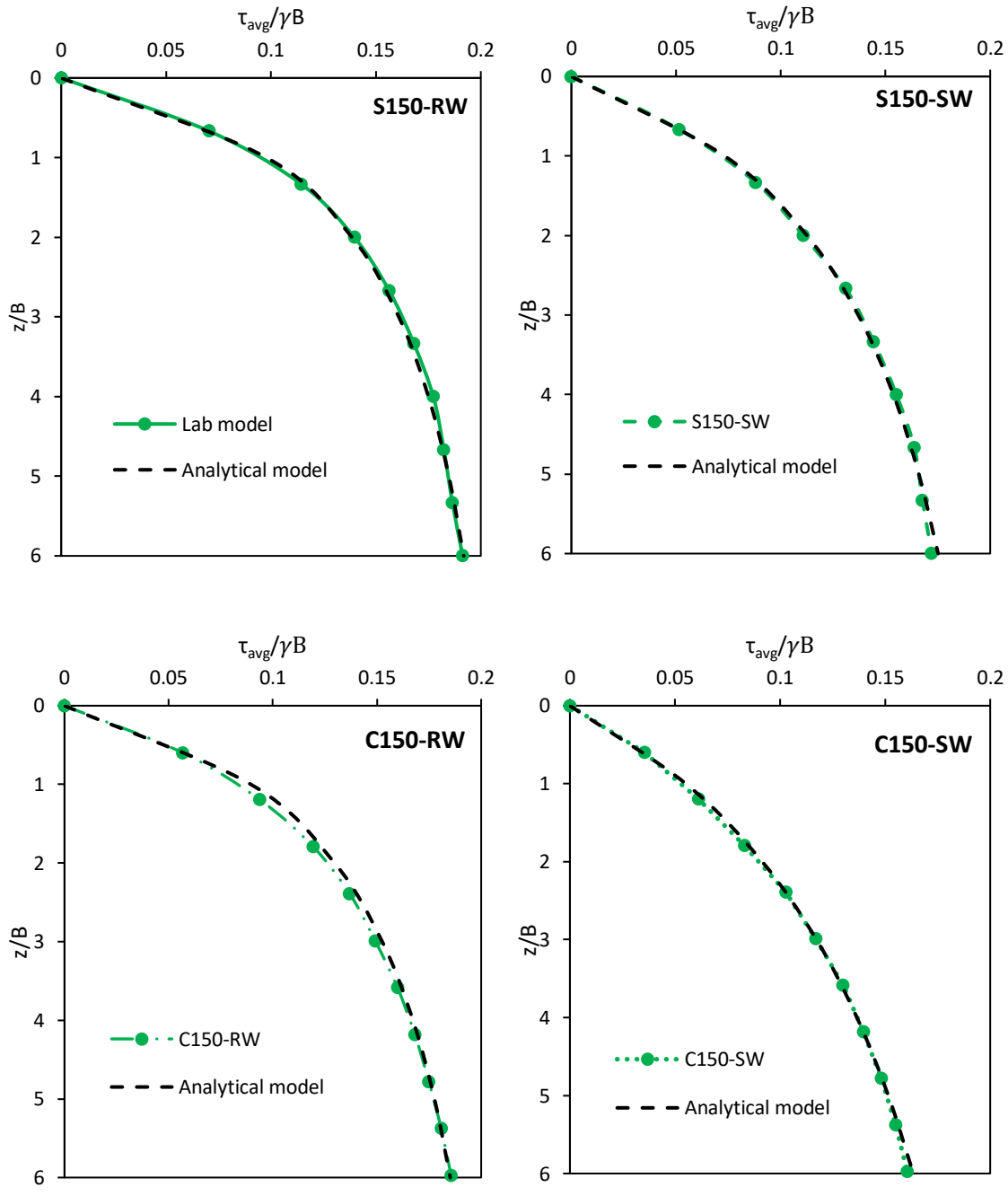

Figure 4.18. Analytical models for average wall shear stress variation with depth

As depicted in Figure 4.18, the average wall shear stress is increased through to $6B$ depth following the Equation 4.15, for both square and circular stopes. Further, the average shear stress is slightly becoming constant at depths of $5B$ to $6B$, with rough wall condition, but the smooth wall stopes do not reflect such plateauing of average shear stress. The hyperbolic form of the Equation 4.15 suggests that the average shear stress reaches an asymptotic value of $1/b$ at very large depths. In the case of rough wall, the asymptotic value is approached at a shallower depth than for smooth walls.

4.6.2 Analytical solutions for the variation of exact wall shear stress with depth

The variation of exact wall shear stress with depth was modelled analytically using the Equations 4.13 and 4.15. The Equations (4.13) and (4.15) allow to determine the exact shear stress on wall next to a very thin layer (dz) of 1 mm, and thus it can be reasonably considered as wall shear stress at a point within the fill. Accordingly, the variation of exact wall shear stress along fill depth (blue curve) is presented in dimensionless plots as shown in Figure 4.19. It can be seen from the four figures that these curves are different to the ones developed for dz = 100 mm (red) and the average (green) ones.

An arching equation is proposed for the exact shear stress variation, with two coefficients α and β accounting the fill properties and wall roughness, as given in Equation 4.16. The two coefficient values for each stope type were determined by superimposing the exact wall shear stress curve (blue curve) using the generalised reduced gradient method. The appropriate α and β values for all four stopes are tabulated in Table 4.4. The Equation 4.16 is valid only for z/B varying from 0 to 6. The dimensionless plots for average and exact wall shear stress variation with depth for all stope types are shown in Figure 4.19.

$$\tau/\gamma B = \alpha\left(1 - e^{-\beta\left(\frac{z}{B}\right)}\right) \qquad \text{Eq. (4.16)}$$

The Equation 4.16 suggests that the exact shear stress (τ) becomes asymptotic at some depth. Considering $\tau/\gamma B = y$ and $z/B = x$, Equation 4.16 can be written as

$$y = \alpha\left(1 - e^{-\beta x}\right)$$

Taking the derivative, $\frac{dy}{dx} = \alpha\beta e^{-\beta x}$

At asymptotic τ, $\frac{dy}{dx}$ is zero. Hence, $e^{-\beta x} = 0$

Therefore, from Equation 4.16, the asymptotic exact shear stress (τ) can be derived as $\alpha\gamma B$.

Table 4.4. Coefficients for the proposed shear and normal stress equations

Stope ID	Eq. no.	α	β
S150-RW	4.16.1	0.2252	1.1356
S150-SW	4.16.2	0.2235	0.7514
C150-RW	4.16.3	0.2214	0.9761
C150-SW	4.16.4	0.2371	0.4951

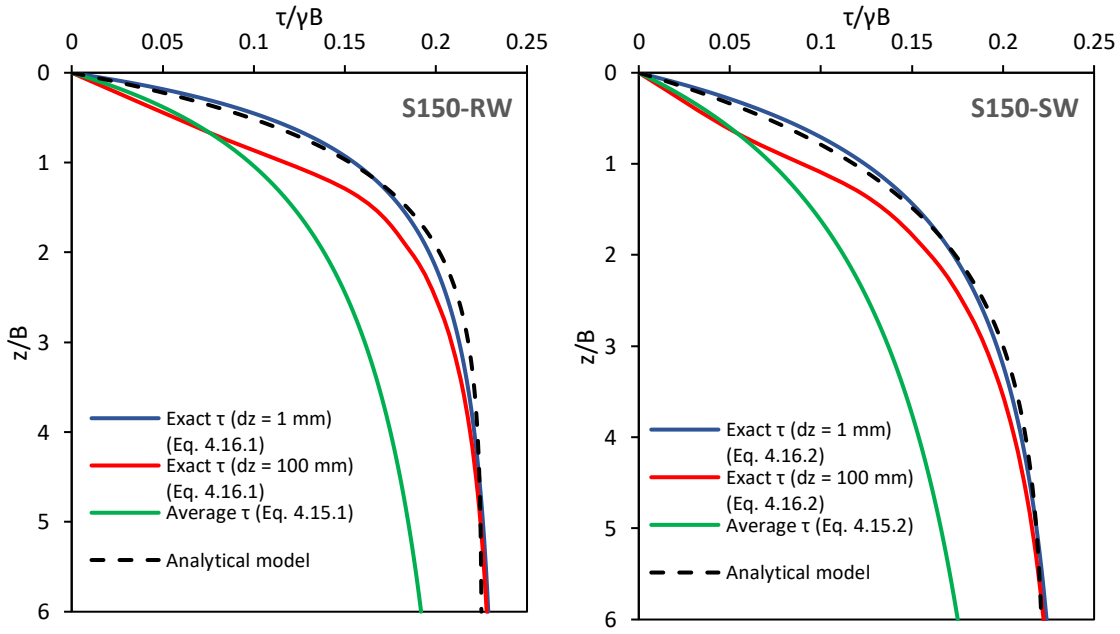

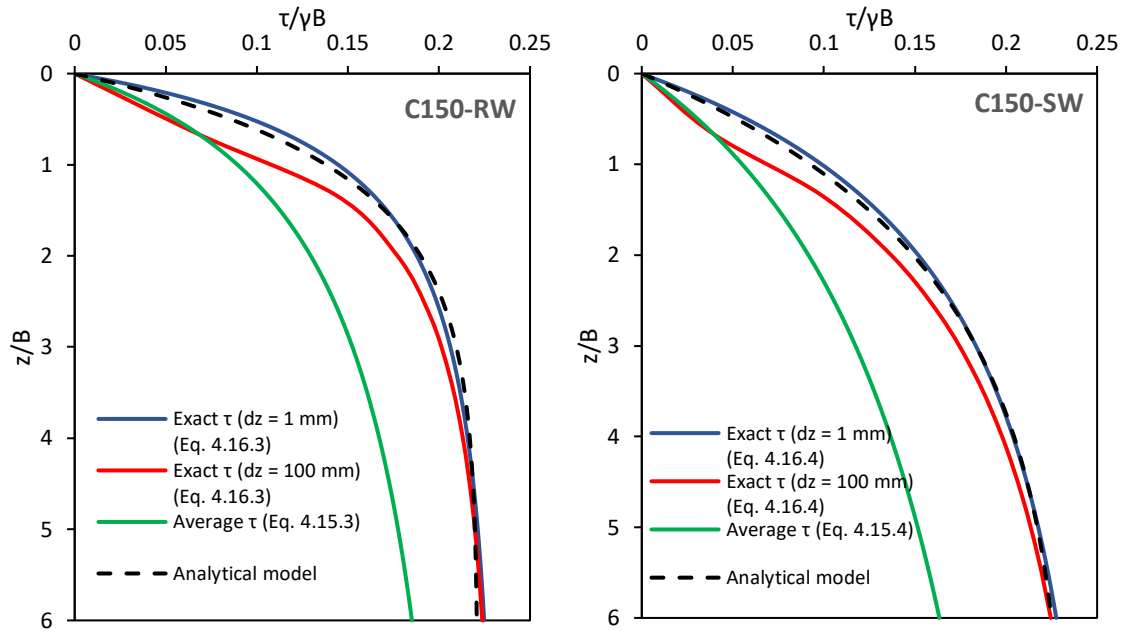

Figure 4.19. Analytical models for the shear stress variation with depth

4.6.3 Analytical model for the average normal stress variation with depth

Expressions for the average normal stresses within a backfilled stope, having rectangular and square cross sections, are derived from the first principles as below. It is considered that the shear stress variation with depth follows Equation 4.16 and no surcharge acting on the top of the granular fill, mimicking the actual mine stopes as well as silos. Considering the force diagram of a fill layer element of dz thickness, perimeter of P and cross-sectional area of A, as shown in Figure 4.20(a), the forces acting on the element can be defined as shown in Figure 4.20(b).

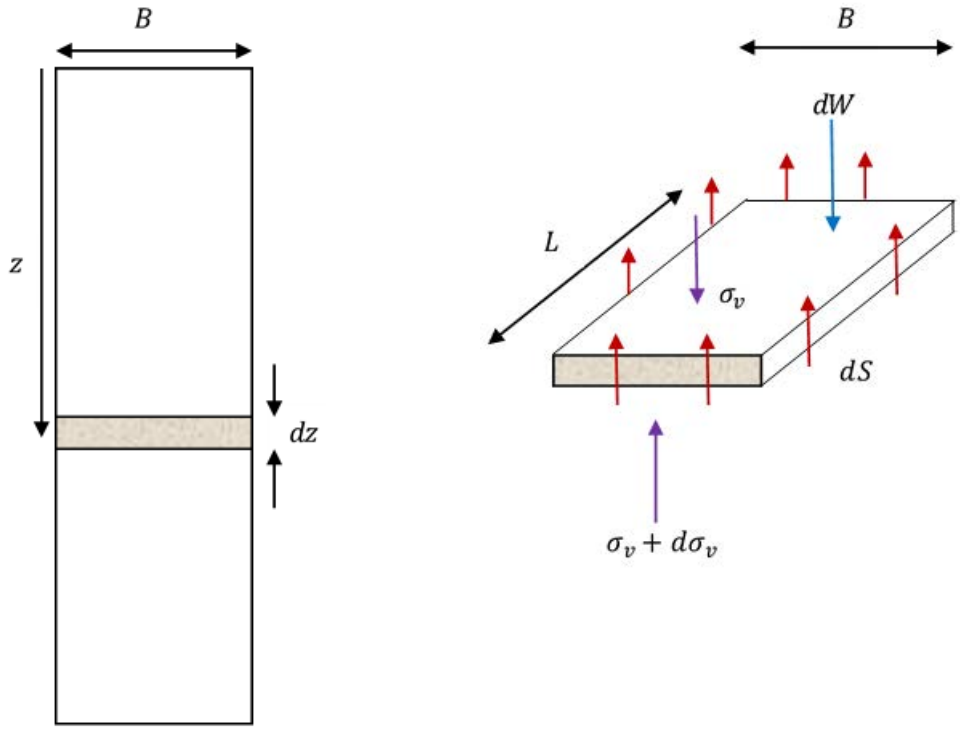

Figure 4.20. (a) Idealised stope (b) Force diagram of fill layer element

Weight of the layer, $dW = \gamma \cdot A \cdot dz$

Shear force acting on the perimeter, $ds = \tau \cdot P \cdot dz$

Considering the force equilibrium in the z direction,

$$(\sigma_v + d\sigma_v)A + \tau P(dz) = \sigma_v A + \gamma A(dz)$$

Simplifying that,

$$(d\sigma_v)A + \tau P(dz) = \gamma A(dz) \qquad \text{Eq. (4.17)}$$

For a rectangular cross section, $A = BL$ and $P = 2(B + L)$, where B is the stope width and L is the stope length. Hence, Equation 4.17 deduces to

$$(d\sigma_v)BL + 2\tau(B + L)(dz) = BL\gamma(dz)$$

Dividing with BL, $d\sigma_v = \left(\gamma - \frac{2\tau(B+L)}{BL}\right) dz$

Substituting Equation 4.16 for τ, $d\sigma_v = \gamma\left[1 - \frac{2\alpha(B+L)}{L}\left(1 - e^{-\beta\left(\frac{z}{B}\right)}\right)\right]dz$

Integrating within the limits from 0 to z,

$$\sigma_v = \gamma z + \frac{2\alpha\gamma(B+L)}{\beta L}\left[B\left(1 - e^{-\beta\frac{z}{B}}\right) - \beta z\right]$$

Simplifying for a square stope where $L = B$,

$$\sigma_v = \gamma z(1 - 4\alpha) + \frac{4B\alpha\gamma}{\beta}\left(1 - e^{-\beta\frac{z}{B}}\right)$$

$$\sigma_v/\gamma B = \frac{z}{B}(1 - 4\alpha) + \frac{4\alpha}{\beta}\left[1 - e^{-\beta\left(\frac{z}{B}\right)}\right] \qquad \text{Eq. (4.18)}$$

It can be proven that the above analytical solution is applicable to circular cross sections after replacing the variable B with diameter. The two coefficients are the same from the shear stress solutions, as given in Table 4.4. The dimensionless plots for average normal stress variation with depth, as obtained from the analytical solution proposed in Equation 4.18, are shown in Figure 4.21 for all four stope cases. The proposed analytical solution was then validated with the average normal stress values obtained from the laboratory stope arching model test data, as shown in Figure 4.21 with discrete data points from laboratory tests. It is evident that the laboratory stope tests data are closely matched with the proposed analytical solutions. These normalised stress-depth plots can be used to determine the average vertical normal stress within any granular backfilled stope, including hydraulic fill stope, and vertical containments comprising granular material (grain silos) of any width B and fill height up to $6B$.

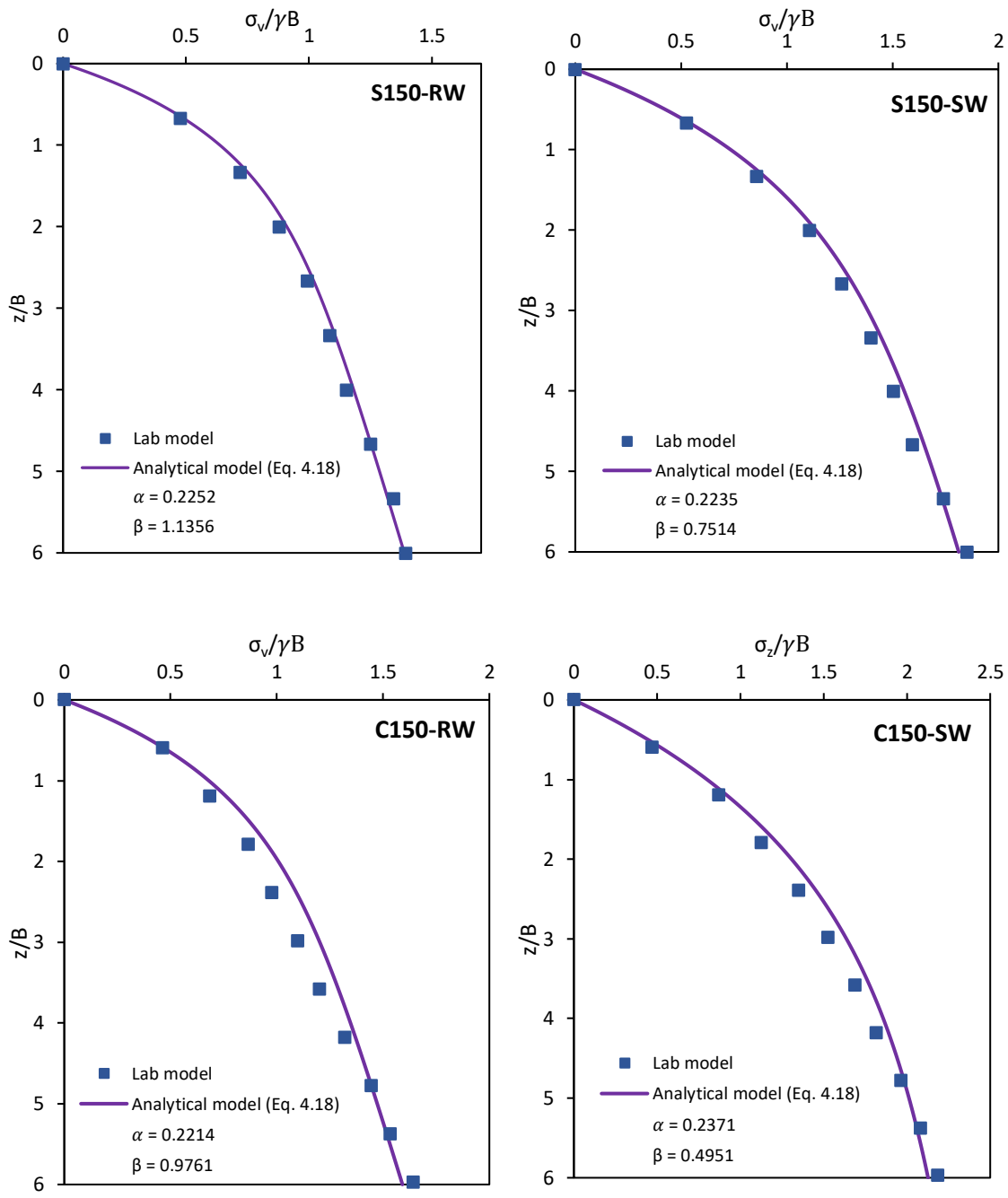

Figure 4.21. Analytical models for the average normal stress variation with depth

4.7 Physical model simulations of backfilled stopes

The four types of laboratory stope arching models mentioned in Table 4.2 are analysed and discussed in this section. The variation of vertical normal stress, horizontal normal stress and wall shear stress along fill depth are compared for both square and circular stopes with rough and smooth wall conditions.

4.7.1 Stress variation within the square and circular backfilled stopes

The dimensionless plots for the normal and shear stress variations in the square and circular stopes are shown in Figures 4.22 and 4.23, respectively.

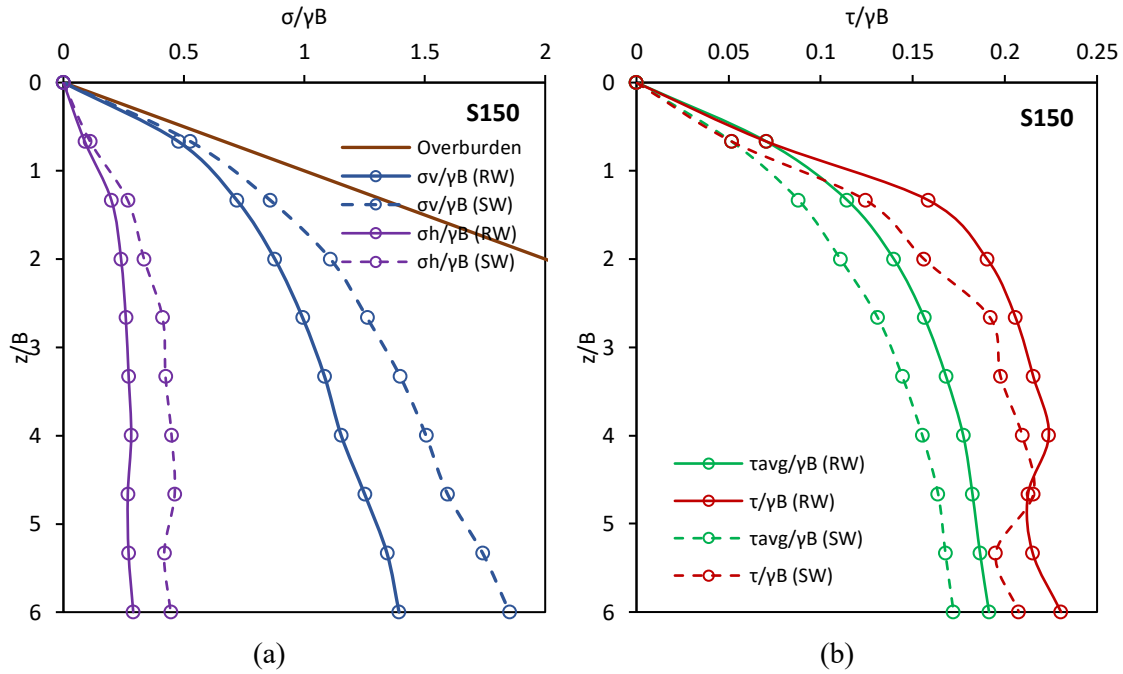

Figure 4.22. Stress variation in 150 mm square stopes (a) Normal stresses (b) Shear stresses

The shear stresses within the square stope are larger with rough walls than the smooth walls, confirming the greater arching effect with rough stope walls and hence the reduction of vertical normal stresses in the fill was evident as shown in Figure 4.22(a). Accordingly, the horizontal normal stresses acting on the wall were smaller with rough walls. Similar variations of stresses were observed with the two circular stopes as well, as depicted in Figure 4.23, except for

the larger normal stresses being generated compared to the square stopes, which can be attributed to the absence of corner effect in circular stopes.

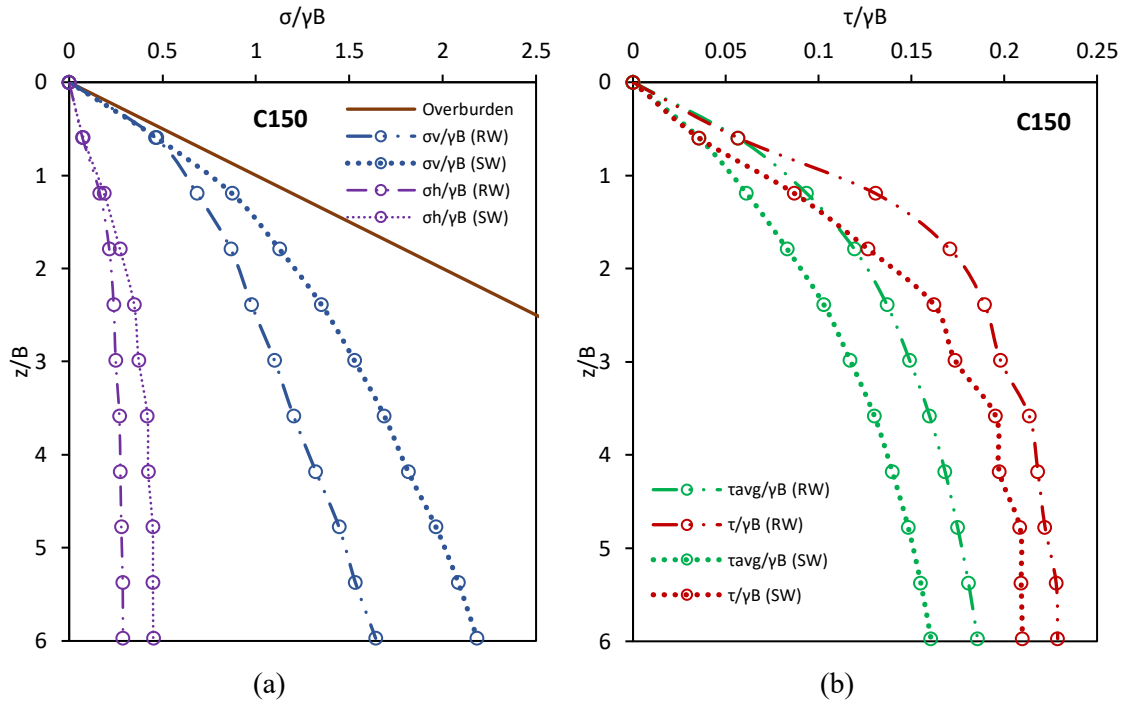

Figure 4.23. Stress variation in 150 mm circular stopes (a) Normal stresses (b) Shear stresses

4.7.2 Experimental and analytical comparison of normal stresses within the fill

4.7.2.1 Vertical normal stress

The analytical equation developed by Pirapakaran and Sivakugan (2007a), given in Equation 4.7, was used for the comparison of average vertical normal stresses generated in the fill, and it is presented in a normalised stress plot as shown in Figure 4.24.

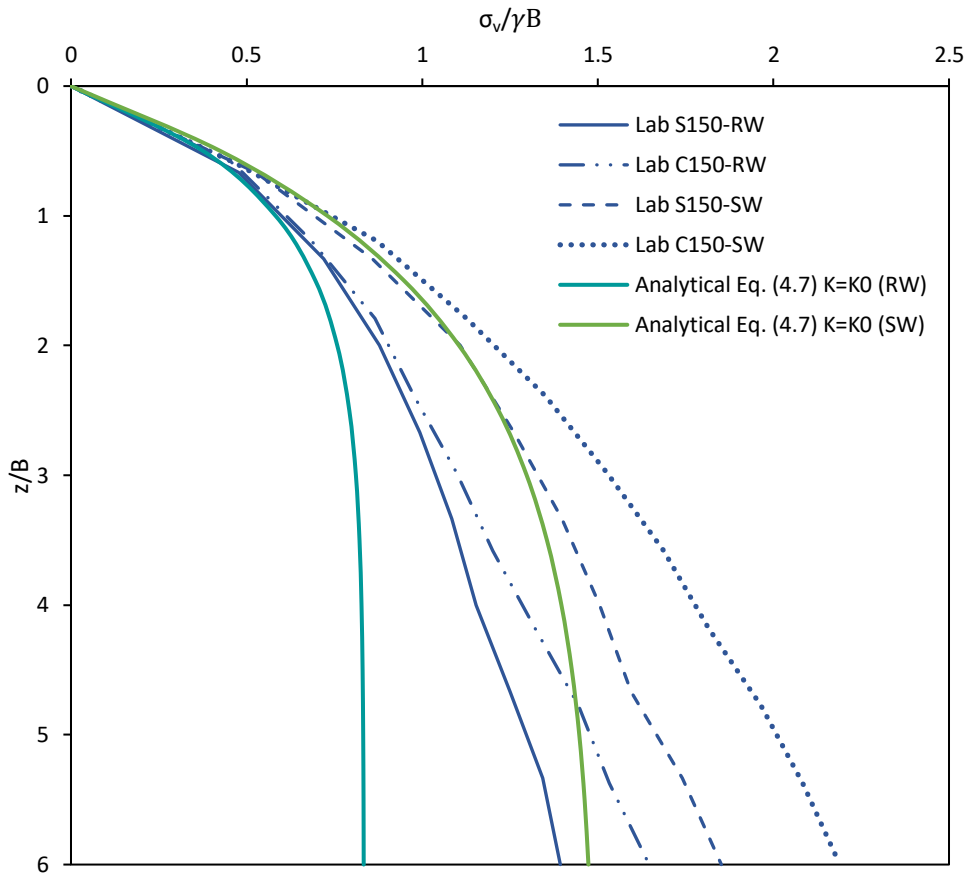

Figure 4.24. Dimensionless plot for vertical normal stress variation with depth

The laboratory stope model tests suggest that the average vertical normal stress within the fill is increased continuously with the fill depth through to $6B$, for both square and circular stopes, whereas the analytical solution suggests that the stress becomes asymptotic after the fill depth of $2B$ to $3B$. The experimental results agreed well with analytical solutions up to depths of $1B$ and $2B$, for rough and smooth wall conditions, respectively.

4.7.2.2 Horizontal normal stress

The dimensionless plot for the variation of horizontal normal stress on wall along fill depth, is presented in Figure 4.25, for both square and circular stopes, and the results were compared with the analytical solutions derived by Pirapkaran and Sivakugan (2007a).

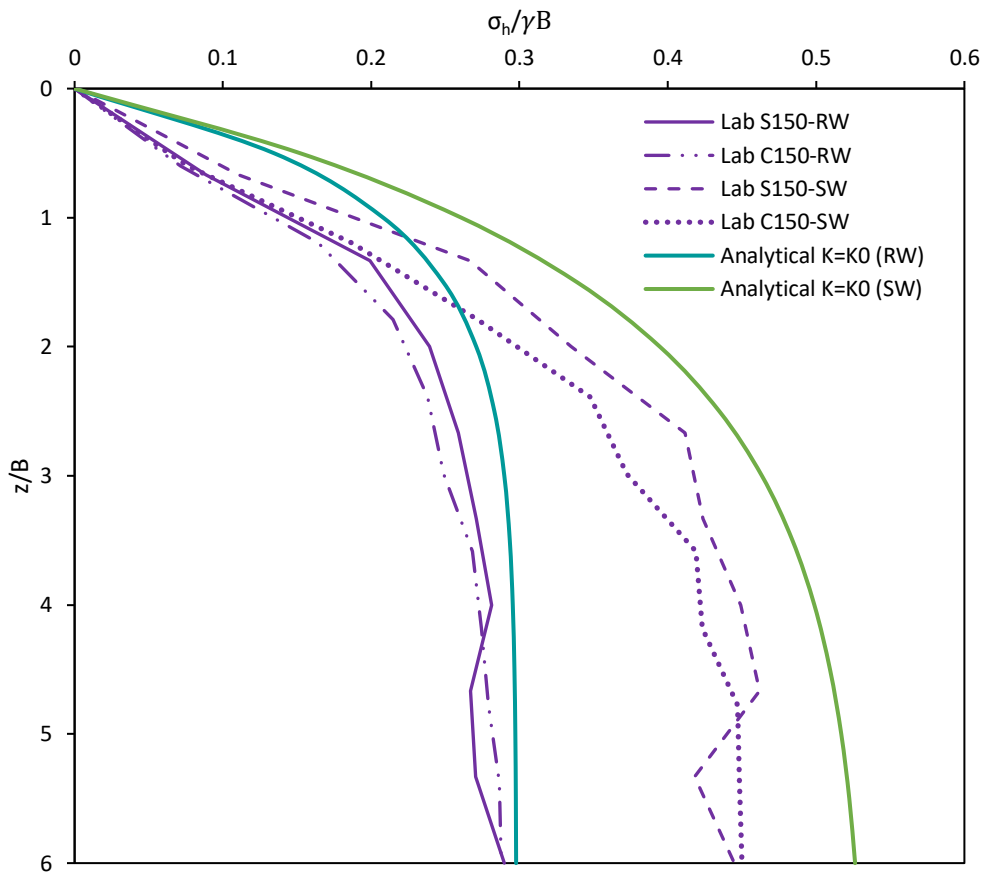

Figure 4.25. Dimensionless plot for horizontal normal stress variation with depth

Unlike vertical normal stress, the horizontal normal stress gradually reaches a constant value at $1B$ to $2B$ depth, as evident with the stope model test data due to asymptotic wall shear stress that occurred at the same depth region, as presented in Section 4.6.2. Further, it is also confirmed that the analytical solution derived with the at-rest earth pressure coefficient (K_0) agrees with the laboratory test results.

4.7.3 Lateral earth pressure coefficient variation with depth

The lateral earth pressure coefficient (K_{calc}) was calculated by taking the ratio between horizontal stress and vertical stress obtained from stope model test data, and its variation with depth is shown in Figure 4.26 (a).

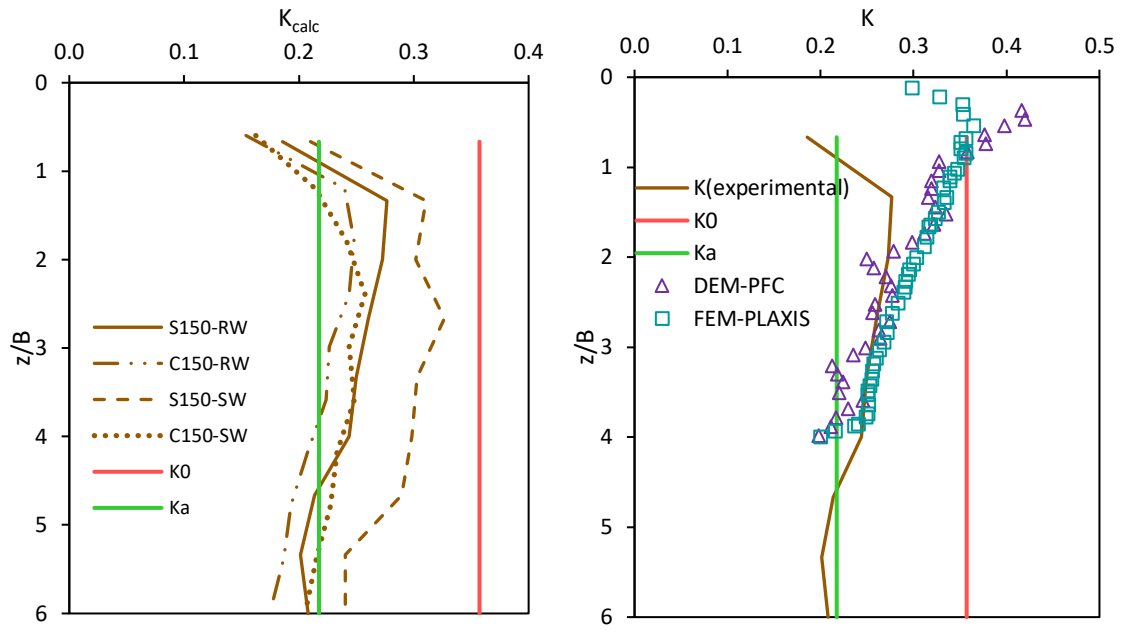

(a) (b)

Figure 4.26. (a) Lateral earth pressure coefficient (K) variation with depth (b) Comparison of existing models for K variation with depth

The active (K_a) and at-rest (K_0) earth pressure coefficients were determined using Rankine's active earth pressure equation and Jaky's (1944) expression, respectively, and they are constant at any depth of the fill. Lenczner (1963) stated that K should be varying with the fill depth instead of maintaining a constant value, to agree with the theoretical vertical stresses. This was confirmed with the K_{calc} values obtained from the stope model test data, such that K_{calc} decreased with the fill depth. It can also be seen that K_a underestimates K_{calc} and thus, it is suggested that K_0 is conservative to use in the analytical equations for stress determination.

Moreover, Figure 4.26 (b) presents a comparison of existing analytical and numerical models for K variation with fill depth along with the experimental results obtained from the laboratory model simulations. According to Yang and Deng (2019), Distinct Element Modelling (DEM) and Finite Element Modelling (FEM) suggest that the lateral earth pressure coefficient is not constant throughout the fill depth instead it gradually decreases as the fill depth increases, agreeing well with the K variation from laboratory model results.

4.8 Numerical simulation of backfilled stope arching model

Geotechnical behaviour related to underground mining are often predicted with numerical simulations. However, due to the level of uncertainty of model predictions and level of simplification, simulations are often questioned (Bloss, 1992). The simulation error can be minimized by the use of appropriate boundary conditions, constitutive models, input parameters, and correct modelling procedures (Pirapakaran and Sivakugan 2007a). Not only laboratory tests, but also numerical simulations can be used to help in understanding the stress transfer mechanisms related to backfilling of mine stopes or granular filling of industrial silos. FLAC (Fast Lagrangian Analysis of Continua), a finite difference numerical package was used in this dissertation to simulate the laboratory scale model filling, in order to compare with model test results. Pirapakaran and Sivakugan (2007a) numerically simulated the in-situ stress measurements on HF backfilled stope by Knutsson (1981). A basic two-dimensional modelling package allows to simulate the plane strain conditions (eg. narrow long stopes) and axisymmetric occurrences, such as circular stopes. However, when the drives and barricades are considered with the stope, the problem becomes three-dimensional, and calculations need to be performed with FLAC^{3D}.

4.8.1 Continuum modelling with FLAC

FLAC is an explicit solution technique, in which the system equilibrium is computed using a time-stepping numerical integration within the model (Itasca, 2021). FLAC uses an explicit, Lagrangian calculation scheme and a mixed-discretization zoning technique, and is well recognised in simulations with mining and geotechnical applications. Coulthard (1999) suggested that FLAC and FLAC^{3D} are the best numerical codes to model mine backfilling, after comparing all the available numerical programmes.

The required geometry is divided into a grid with several zones in FLAC. When the code is executed, the unbalanced forces and displacements, for each grid point, are calculated through a time marching mechanism. An important feature of this numerical software is the built-in

programming language “FISH”, which can be used to include additional variables or properties over time and adjust the external or internal conditions/parameters accordingly. Moreover, stepwise excavations and filling activities can be implemented with codes written in FISH. In explicit calculations, the stress state is determined by considering the previous stress state and time advancements via iterative calculations. A key advantage of finite difference method, over the implicit finite elements method, is that the governing equations for the mechanics are not based on an initial assumption that the system is in equilibrium (Coulthard, 1999). However, the disadvantage of finite difference method is that the time step is tiny and large number of time steps must be taken to reach the equilibrium. Additionally, explicit mechanism (FLAC) is very efficient in modelling non-linear, large strain problems rather than solving linear, small-strain problems (Itasca, 2021).

The stress conditions in backfilled mine stopes have been simulated numerically (Aubertin et al., 2003) and validated with laboratory test data (Pirapakaran and Sivakugan, 2007b; Ting et al., 2012a). Li et al. (2003) used FLAC to simulate narrow stope backfilling but observed an anomalous variation of vertical stress, which exceeds the overburden stress at shallow depths. Later, Pirapakaran and Sivakugan (2007a) suggested a layer wise filling to overcome this vertical stress anomaly. Understanding the stress conditions within the stope is required to simulate the stress conditions within drives. Though the stress state near the barricade is modelled by Li and Aubertin (2009b) and Fahey et al. (2009) with two-dimensional numerical packages, it is difficult to represent the barricade environment under two-dimensional configurations. Because when the drive and barricade are added to the model, the problem becomes three-dimensional. Therefore, the stress distributions in circular and narrow stopes were estimated with FLAC and square stopes with FLAC^{3D} in this dissertation.

In simulations herein, the rock mass was considered as a homogeneous, isotropic material and behaves in a linear elastic manner allowing the use of a ‘linear elastic’ constitutive model. Also, the granular backfill was modelled with Mohr-Coulomb constitutive model (Brinkgreve et al., 2004). Interface elements were used to model the effect of the shearing between stope wall

and backfill. Though previous studies suggested that the interface elements have a negligible effect on the stress state (Li and Aubertin, 2009), there is a need to simulate interface shearing more realistically, especially when replicating the laboratory tests with numerical models. Furthermore, a significant relative movement between the rock mass and the backfill is witnessed in FLAC simulations and this validates the use of interface elements.

4.8.2 Model parameters and FLAC simulation procedure

For simplicity, it is assumed that the HF is granular with no cohesion and is dry. Since the numerical modelling approach discussed herein is for a continuum, which does not consider grain size, the simulation results are applicable to other cohesionless fill types as well. Axisymmetric configuration was used to model cylindrical containments in FLAC. Dimensions of the FLAC models were the same as those of the model containments tested in the laboratory. Height of each model was taken as $6B$. The model consisted of 1 mm × 1 mm grid on a radial plane. Most of the geotechnical properties of HFs were chosen from the literature and the material parameters used for modelling are tabulated in Table 4.5. The model walls were fixed for displacement in both x (radially) and y (vertically) directions. The y-displacement was fixed at the bottom of the model. Smooth Perspex interface and rough sandpaper interface were modelled with appropriate interface parameters (Table 4.5). The interface stiffness parameters k_n and k_s were empirically calculated as suggested by FLAC manual (Itasca, 2021).

Table 4.5. FLAC model parameters

Property	**HF backfill**	**Perspex wall**
Young's modulus, E (MPa)	10	3200
Density, ρ (kg/m^3)	1330	1190
Poisson's ratio, v	0.2	0.3
Friction angle, ϕ	40	-
Interfacial friction angle for rough wall, δ_{RW}	-	38.5
Interfacial friction angle for smooth wall, δ_{SW}	-	25

4.8.3 Particulate modelling with PFC

The Distinct Element Method (DEM) was used in this section for the numerical simulations of backfilled stopes. The Particle Flow Code (PFC2D) software was used for the simulations and the modelling was done considering a 150 mm width and 900 mm height 2D stope similar to the laboratory stope setup dimensions.

Initially, the walls were created replicating the boundary walls of the mine stope. Then, particles were distributed randomly inside the wall without any overlapping between the particles. Afterwards, gravity was activated to enable the particles to fall, fill and self-weight compact. The particles were filled up to around 950 mm height of the stope (5% of extra height) and time-steps were implemented until equilibrium was reached. The convergence criteria used was the average ratio (i.e., total unbalanced force to total force ratio). The value of the average ratio used in this study is 1×10^{-5} and is small enough to achieve a static system. After reaching the equilibrium, the extra amount of material at the top (more than 900 mm height) was removed from the system. Due to the release of force from the top, the compressed material tends to relax. Hence, the time steps were implemented to achieve the new equilibrium state. The same procedure was repeated until the total height is exactly 900 mm. After reaching the equilibrium, user-written (FISH) functions were implemented to calculate the stresses within the system.

DEM parameters were selected using the data available in the literature (Thakur et al., 2016; Cundall et al., 1979; Potyondy et al., 2004), and the equations provided in the PFC software manual (Itasca, 2023). An in-built linear contact model was used to simulate the particle-particle interactions and particle-wall interactions due to the simplicity of calibration. Also, the model is suitable for simulating the frictional and cohesionless granular material similar to the one used in this study (Cundall, 1979). The Poisson's ratio value kept a constant as 0.2 and mono sized particles with 2 mm diameter were used in the simulations where the particles are considered as disks with a unit thickness.

From the parametric study carried out to investigate the effect of stiffness and frictional parameters of the fill and the wall, on stress developments within the backfilled stope, it was confirmed that the particle-particle stiffness and particle-wall stiffness have a lesser influence on the vertical stress variations. It was also verified that the particle-wall friction contributes a lot for the arching and hence a greater influence on the vertical stress generation, while the particle-particle friction showed a smaller effect on stresses. Following the parametric study and model calibration, the selected DEM contact parameters for the simulation are presented in Table 4.6.

Table 4.6. DEM contact model parameters

Contact property	**Particle-Particle contact**	**Particle-Wall contact**
Normal stiffness, k_n (Nm^{-1})	6×10^6	3.7×10^6
Shear stiffness, k_s (Nm^{-1})	5.4×10^6	3.7×10^6
Friction angle, ϕ (°)	40	-
Interface friction angle, δ (°)	-	38.5 (rough wall) 25 (smooth wall)

The laboratory square stope arching model with rough wall condition, as simulated with FLAC and PFC, is shown in Figure 4.27. The fixations for the boundary stope walls and stope bottom are the same for both FLAC and PFC models, as discussed above. FLAC stope consists of blocks with grid zones, mimicking the continuum modelling while the PFC stope comprises particles of 2 mm diameter.

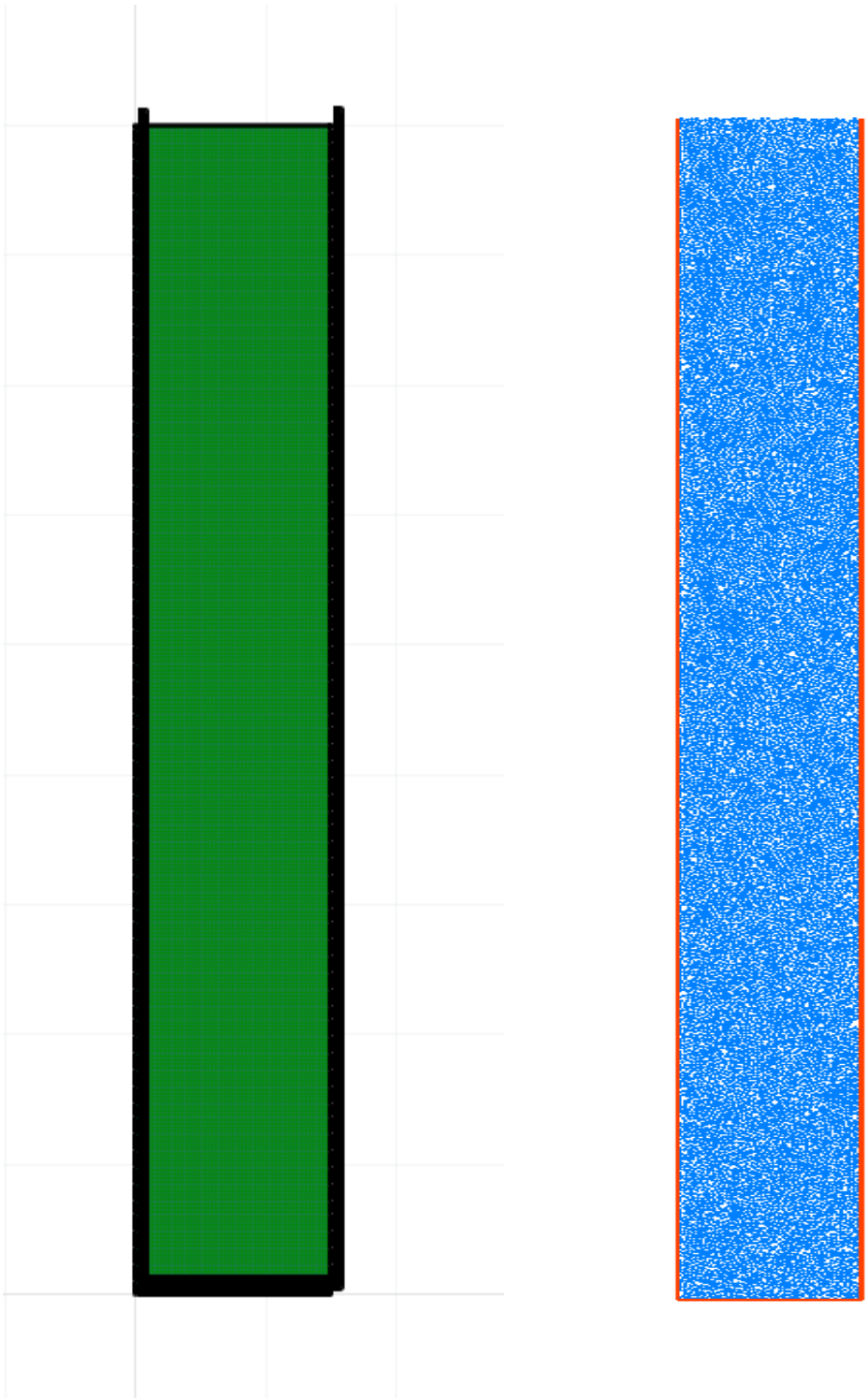

(a) (b)

Figure 4.27. Simulated laboratory square stope (a) FLAC model (b) PFC model

4.8.4 Vertical normal stress variation analysis with analytical, numerical and experimental approaches

Analytical solutions and the numerical simulation of HF backfilled stope are compared with the laboratory stope arching model test data, as presented in normalised plots in Figure 4.28.

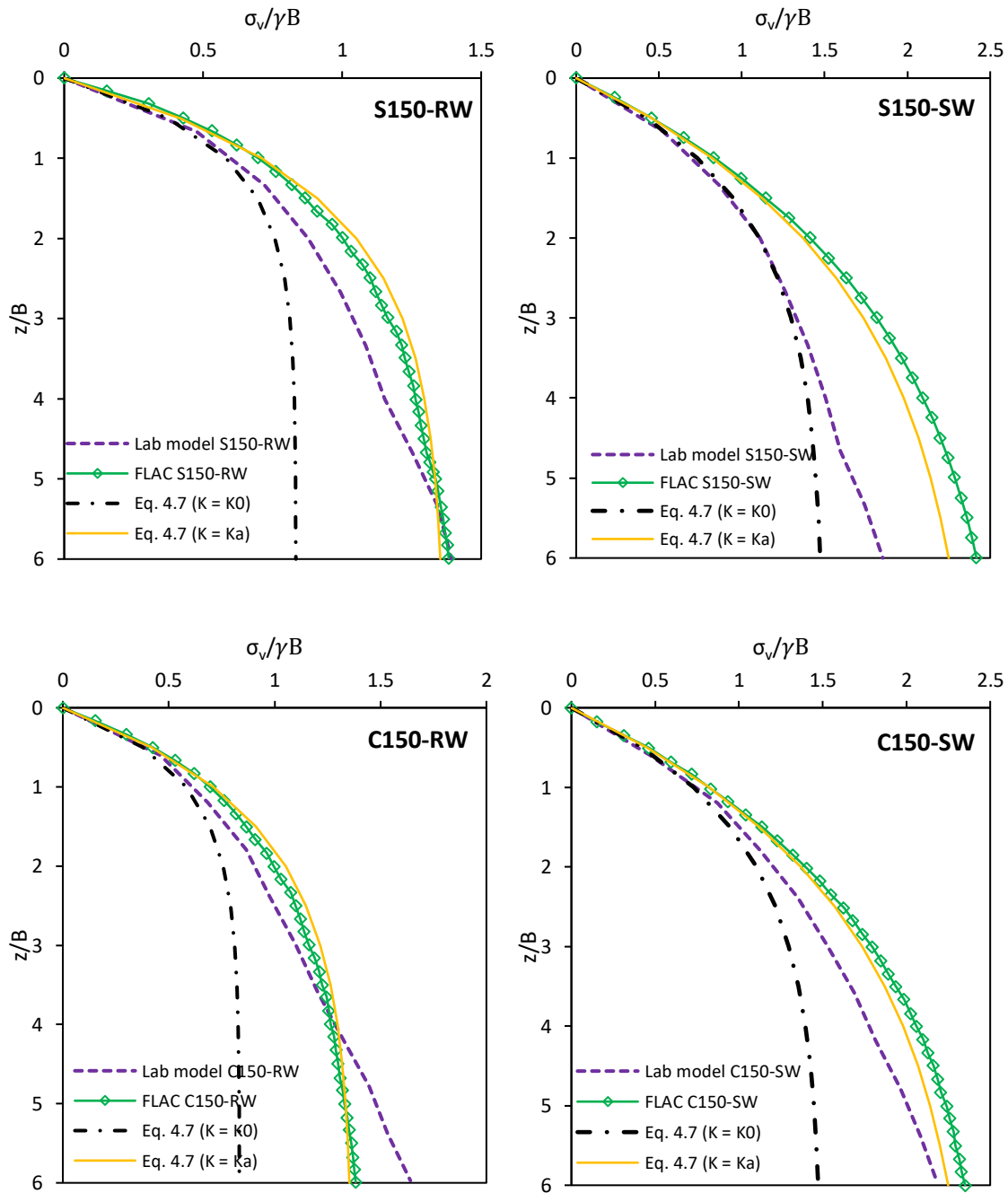

Figure 4.28. Analytical, numerical and experimental comparison of vertical stress variation

It is clear that the vertical normal stress variation with FLAC, reaches an asymptotic value, at depths of $2B$ to $3B$ with rough wall condition and at depths of $3B$ to $4B$ with smooth wall condition, confirming the higher degree of arching in rough wall stope caused the reduction in fill stress relatively quickly. The vertical stresses from the analytical solutions are also reaching constant at depths of $2B$ to $3B$, comparing with the numerical curves. However, the laboratory stope model test results show that the vertical stress is increasing throughout the fill depth $6B$. The difference of vertical stress variation with laboratory stope and FLAC model can be attributed to the particulate nature of the real fill material which is not considered in continuum modelling with FLAC. The vertical stress from FLAC aligns with laboratory model curve up to $1B$ depth, and thereafter FLAC generally overestimates the vertical stress from laboratory model. This overestimation can be due to the less arching effect generated in 2D FLAC model, where only two stope walls are considered (long narrow stope). It can be seen that the analytical solution with active earth pressure coefficient is correlating well with FLAC curves for all four stopes, suggesting the backfill is in active state in the stope. However, the previous analysis of K variation with depth verified that K_0 is reasonably used in backfill stope analysis.

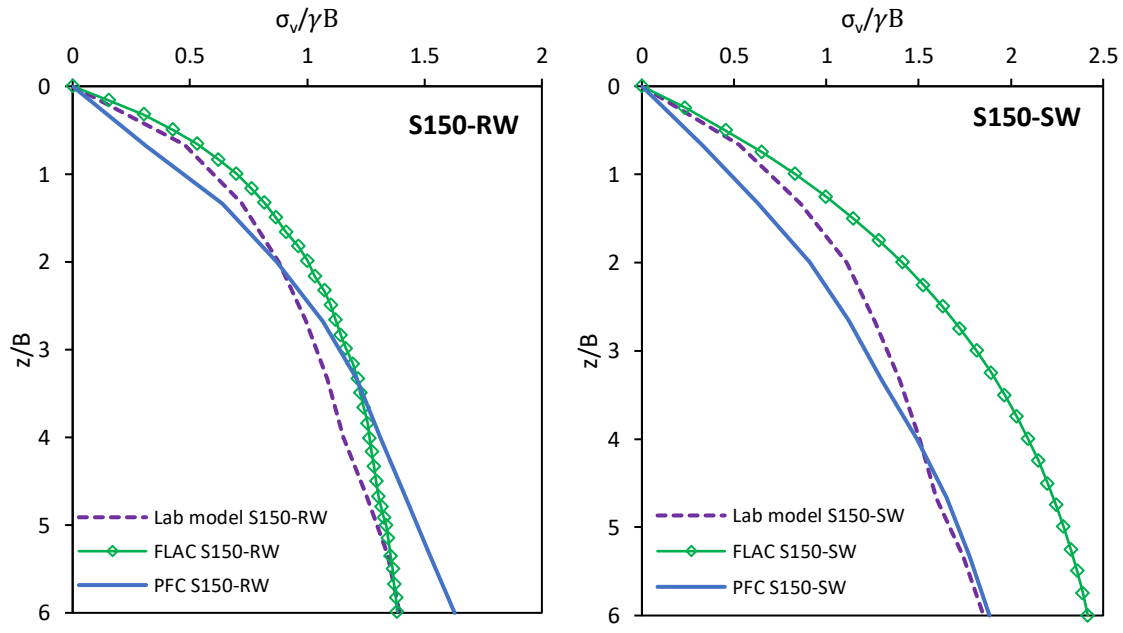

Figure 4.29. FLAC and PFC comparison of vertical normal stress variation with depth

The vertical normal stresses developed within the square backfilled stope, as obtained from FLAC and PFC simulation exercises, are compared with the laboratory stope model test results as shown in Figure 4.29. Two modelling techniques were used here namely continuum approach with FLAC and particulate approach with PFC, which follow FDM and DEM numerical solving methods, respectively. It is evident that vertical stress is increased along the entire fill depth to $6B$, as depicted in PFC plot without reaching an asymptotic value, agreeing well with the laboratory stope model test results. In contrast, FLAC suggests a gradual plateauing of vertical stress with depth. Thus, it is emphasised that for reasonably accurate stress determination within backfilled stopes with numerical simulations, particulate modelling techniques should be considered and employed.

4.9 Summary

The main conclusions drawn from the work reported in this Chapter are summarised below.

- The actual backfilled mine stopes and material silos are replicated satisfactorily with the laboratory stope arching models discussed in this chapter, with different model shapes, sizes and wall roughness, simulating the actual situation.

- Laboratory stope models consisting granular material showed an increase of vertical normal stress in the fill, throughout the fill depth, even at depths as high as $6B$.

- Analytical solutions by Marston (1930), Aubertin et al. (2003) and Pirapakaran and Sivakugan (2007a), etc reach an asymptotic vertical stress after a certain fill depth due to several approximations considered in analytical models.

- It was verified that the lateral earth pressure coefficient (K) variation with fill depth is not constant, which was not considered in above analytical solutions, and it was determined that K_0 is conservative to use in analytical equations than K_a.

- The genaralised plots developed from the proposed analytical models can be used to determine normal and shear stress at any depth of the fill in a backfilled stope or grain silo.

- The continuum numerical modelling approach with FLAC suggested the vertical normal stress in the fill becomes asymptotic at certain depth, similar to the analytical solutions.

- However, the particulate numerical modelling approach with PFC confirmed the increase of vertical normal stress along the fill depth, with good agreements with the laboratory model test results. Therefore, particulate modelling is encouraged to simulate the actual stress developments within backfilled stopes, with greater confidence.

Chapter 5

5 Arching in Backfilled Drives and Lateral Stresses on Barricades

5.1 General

Stress conditions in stopes have been monitored in-situ (Mitchell et al., 1975; Knutsson, 1981; Belem et al., 2004; Helinski et al., 2011; Thompson et al., 2012), as well as studied through laboratory tests (Pirapakaran and Sivakugan, 2007b; Ting et al., 2012a, Widisinghe, 2014). The distance along the drive from the stope brow or the drive entrance is called as the offset distance in backfilling practice. An exponential lateral stress reduction within the backfilled drive is predicted with the offset distance as the major variable in analytical equations, where elastic behaviour with a vertical shear plane method is assumed (Kuganathan, 2002; Li and Aubertin, 2009a). However, the force propagation from the stope to drives, and ultimately the stresses on the barricades are not well understood to-date, showing a gap in research. Understanding the load on the barricade is a concern in the mine backfilling operations. It is expected that the normal stress on the barricade should be kept below 100 kPa to avoid failure (Thompson et al., 2014). However, an evaluation of the stress state along the drive is necessary for designing the barricade with confidence, and also to determine the corresponding filling procedure.

Earth Pressure Cells (EPC) have been successfully used to measure the stresses in the backfills (Take and Valsangkar, 2001; Belem et al., 2004; Thompson et al., 2009; Helinski et al., 2011). For example, Belem et al. (2004) measured the lateral pressure on barricades in paste fill stopes, which included a plug, and a total pressure cell (TPC) attached to the barricade. In Belem et al. (2004) measurements, the barricade stress increased to a maximum and later decreased as the paste fill cures. Yumlu and Guresci (2007) described an in-situ stress monitoring program for paste filled stope at Turkey and concluded that overpressure condition that occurs with tight filling of backfill within the drives, is responsible for most of the failures. Thompson et al. (2009; 2012) presented in-situ stress monitoring results for stopes and barricades in CPB filled mines in Canada and Turkey. Helinski et al. (2011) reported the results of barricade stress measurements in two paste backfilled mines in Australia, and observed very different stress behaviours for different

cemented paste backfill mixtures. Most of the recent in-situ stress monitoring has been carried out for cemented backfills. However, this dissertation focuses on uncemented backfills and, therefore, the studies on uncemented fills are discussed in detail.

Grice (1989) reports a field study of barricade stresses monitoring by loading the barricade in undrained conditions to check the failure. The results showed 4 m × 4 m brick barricade cracked at a pressure of 220 kPa. Later, a discussion by Duffield et al. (2003) on recent barricade failures mentioned that the anticipated stresses can be different if the barricade dimensions are different from Grice's (1989) results. However, in-situ monitoring of backfilling is an expensive process because of the high cost of materials, labour, and monitoring equipment and the instrument is also not retrievable (Dunnicliff, 1988). Therefore, this study aimed to delve into the mechanisms of stress transfer from mine stope to the barricade, where EPCs have been used in the laboratory test setup.

Mitchel et al. (1975) carried out barricade pressure monitoring with rubber 'sandwich' cells and piezometers. Afterwards, model studies on backfill stability (Mitchell et al., 1982) and centrifuge tests have been reported for backfills (Smith and Mitchell, 1982; Mitchell and Roettger, 1984; Mitchell, 1989). Mitchell (1992) studied the lateral stress on temporary barricades for two offset distances. The results showed significant arching development within the drives and an exponential stress reduction, concluding that the anticipated stresses of around 105 kPa for a 3 m × 3 m barricade when placed at the stope entrance (Mitchel 1992). However, Mitchell (1992) has not given details of the stope dimensions for this estimated barricade stress. Even though, the tests conducted by Mitchell (1992) were a good initiative into the study of barricade stress and stress variation, following deficiencies can be identified with the test setup:

- Stope dimensions and the drive dimensions were equal – e.g., 0.2 m.
- Depth of the model stope was only 1.5 times the drive height thus model height is not sufficient to study the barricade load variation when the backfill is subjected to arching.

- Load on the barricade is obtained for 0 and 100 mm distance from stope brow and variation of stress along the drive position has not been analysed.

Reduction of lateral load acting on the barricade with offset distance encourages miners to install the barricade as far as possible from the stope brow (Li and Aubertin, 2009a). However, the drainage decreases with offset distance, leaving the fill to take longer time to develop the effective stresses (Kuganathan, 2002). Therefore, the current industrial practice is to build the barricade one drive height away from stope brow (Kuganathan, 2005). This study also aimed to analyse the effect of offset distance on the loading on the barricade.

5.2 Barricade types and failure mechanisms

In general, underground mining practice, barricade is considered as an impermeable fill retaining structure that allows free drainage of excess pore water. The design and construction of safe, competent drive barricade is the ultimate objective of underground mine backfilling and thus understanding of barricade types and their failure mechanisms are important. The two most common barricade types that are currently used in hydraulic backfilling systems, are given below.

- Brick barricade
- Shotcrete barricade

Although many forms of barricades are encountered in mining, the main features and the loading mechanisms are often the same. However, each design of barricade is applicable to a specific mine environment and may depends on the fill type, cementation of the fill, stope-drive dimensions and time allowed for barricade construction in mining cycle. Loadings on the barricade depend on the shear strength of the fill material and stress transfer with arching (Grice, 1989). Stress redistribution within the backfill and also between backfill and stope walls induces loads on the barricade jeopardising the structural integrity of barricades (Bridges, 2003; Duffield et al., 2003). The strength achieved with design and construction of barricades as well as the operational stresses of barricades is not yet completely comprehended (Berndt et al., 2007).

5.2.1 Brick barricade

Brick masonry barricades are made of specially manufactured porous bricks (Berndt et al., 2007). Brick barricades are mostly used with HF applications and a high duration of time is required before the next filling cycle, when compared with impermeable barricades. The brick barricade should be capable of the following for a successful operation (Grice, 1998).

- Have the strength to withstand initial hydrostatic slurry loading
- Be more permeable than the hydraulic backfill
- Act as an efficient filter to retain all fines

5.2.2 Shotcrete barricade

Over-sprayed concrete was used around reinforcement meshes as barricades and its thickness varied from 20 cm to 50 cm (Archibald et al., 2009). Reinforcements were gabion basket structural supports where sheeting was a welded mesh (Archibald et al., 2009). Horizontal or angle drains with 150 mm diameter perforated PVC pipes are installed towards the fill from the barricade, as the bulkhead is impermeable (Sivakugan, 2008). Installation of drains extending into the stope helps to cease the mobilisation of fill in drives with impermeable bulkheads (Kuganathan, 2001). With the reported failures of aquacrete barricades, barricade quality control (for example, specified thickness, restrict of water pooling at the bottom of the bulkhead) must be maintained when backfilling (Revell and Sainsbury, 2007b).

5.2.3 Barricade failure mechanisms

Barricade stability is one of the main considerations in hydraulic mine backfilling as the stope is filled with hydraulic fill material (Sivakugan, 2008). The following failure mechanisms were identified in the previous studies.

1. Punching failure

Escape of finer particles through the barricade would lead to the formation of erosion pipes (Potvin et al., 2005). The erosion pipes may appear on the fill surface as a sinkhole (Grice, 1989). If water ponds on the fill surface, the erosion pipe may induce hydrostatic loads onto the barricade and leads to a highly concentrated load at the centre of the barricade, like a punching force (Figure 5.1). Cracks can be initiated with bulkhead deflection and further movement leads to barricade failure at the centre, making a circular hole (Kuganathan, 2001). Barricades have been observed failing according to this mechanism. According to a report released by the Resources Safety and Health Queensland, an incident had occurred in an underground mine in Queensland, Australia in 1999 where a large hole was punched through a brick retaining barricade as the hydraulic fill was being placed.

Figure 5.1. Punching failure of a brick barricade

2. Flexural failure

The HF load can be considered as a flexural load applied on the barricade, which is constrained at the walls along the perimeter. The reinforced concrete would fail in flexure when

loaded, while fixed at ends. Similar to those flexural crack lines of reinforced concrete, failed barricades also showed diagonal cracks (Grice, 1989). A cracked barricade that shows the failure profile is shown in Figure 5.2, in which the barricade is subjected to undrained conditions with the cemented aggregate fills (Grice, 1989). The barricade had cracked in tension along the diagonal line as shown in Figure 5.2. This type of barricade failure may occur when the barricade is keyed to host rock and the force from the backfill is larger than the designed load on the barricade.

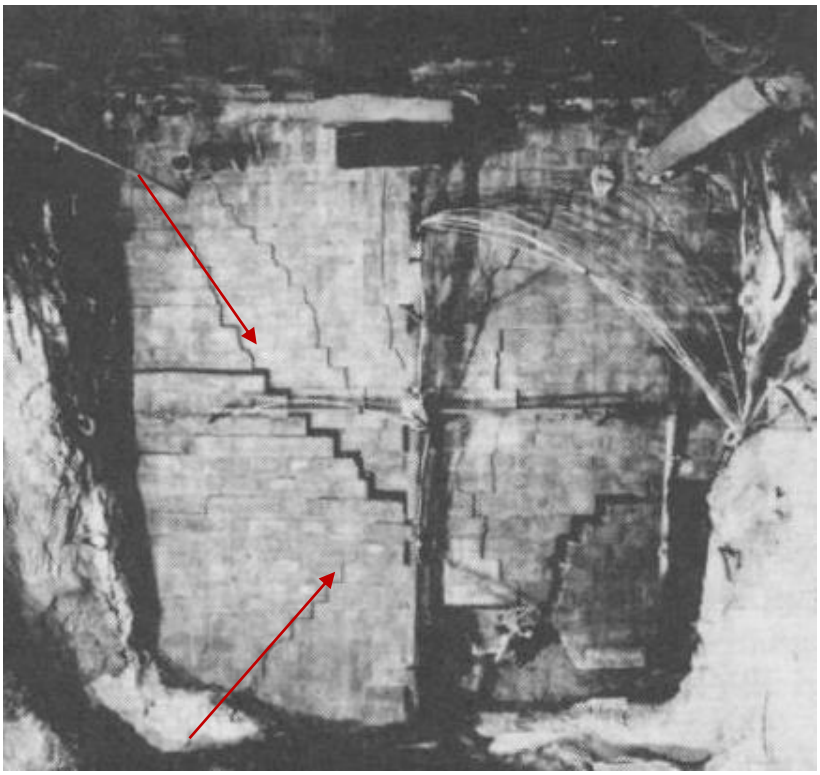

Figure 5.2. Flexural failure crack in brick barricade

3. Shear failure

The insufficient shear strength at the barricade drive interface may lead to removal of the barricade from walls, with the load on the barricade. The shear dislocation of the barricade at a drive was observed with recently reported paste fill bulkhead failures (Revell and Sainsbury, 2007b). Figure 5.3 shows a barricade failure that occurred in Australia. Therefore, additional supports and keying to host rock, such as, rock bolts, rock pins were required to ensure the barricade safety.

Figure 5.3. Shear failure occurred at barricade top

5.3 Analytical solutions

5.3.1 Li and Aubertin (2009) solution

The stope-drive barricade structure backfilled with granular fill is schematically shown in Figure 5.4. The parameters related to barricade stress estimation with the analytical solution (Equation 5.1) proposed by Li and Aubertin (2009) are marked in Figure 5.4. The equation is a function of backfill height (H) in the stope and hence the barricade stress can be directly calculated for any fill height when all other parameters are known.

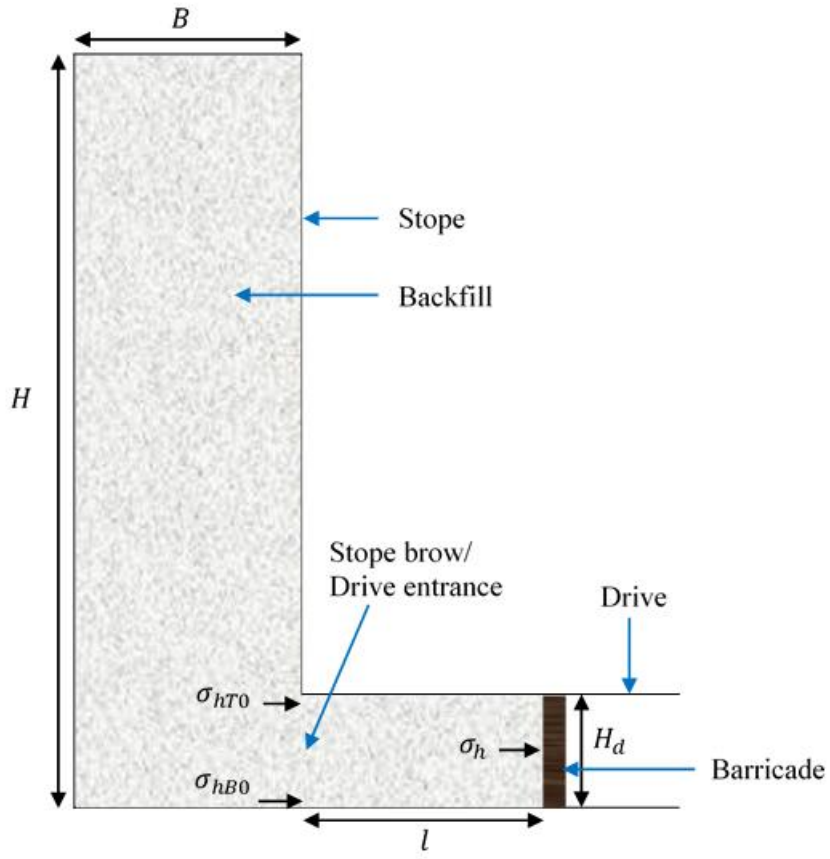

Figure 5.4. Schematic diagram of stope-drive barricade structure

$$\sigma_h = \left[\frac{H}{H_d}\sigma_{hT0} + \left(1 - \frac{H}{H_d}\right)\sigma_{hB0}\right] exp\left[\frac{-2l\tan\delta}{K_{dl}}\left(\frac{1}{H_d} + \frac{K_{dt}}{W_d}\right)\right] \qquad \text{Eq. (5.1)}$$

σ_h - Horizontal stress at barricade (Barricade stress)

H - Backfill height in the stope

H_d - Height of the drive

W_d - Width of the drive

σ_{hT0} - Horizontal stress at the top of the drive entrance

σ_{hB0} - Horizontal stress at the base of drive entrance

K_{dl} - Earth pressure coefficient in longitudinal direction within the drive

K_{dt} - Earth pressure coefficient in transverse direction within the drive

δ - Interfacial friction angle of fill-drive wall interface

l - Barricade setback distance/offset

5.3.2 Kuganathan's barricade stress model

The analytical solution proposed by Kuganathan (2002), for granular fill barricade stress estimation, is presented below. This equation is commonly used by researchers and industry professionals to calculate stress state on drive barricade, as a simplified form of Li and Aubertin (2009) solution. Both Li and Aubertin (2009) and Kuganathan (2002) analytical equations are based on continuum approach, which is similar to analytical solutions proposed by Marston (1930), Aubertin et al. (2003), and Pirapakaran and Sivakugan (2007a) for stress analysis within backfilled stopes. The Kuganathan (2002) analytical solution given in Equation 5.2, is considered for barricade stress comparison with laboratory model results in this dissertation. The load that comes from the backfill in the stope is not directly reflected in the Kuganathan's equation, however, it is embedded in the horizontal stress at drive entrance. The average vertical stress at the stope bottom can be determined using the analytical solutions discussed in Chapter 4. The Kuganathan's barricade stress model is schematically shown in Figure 5.5.

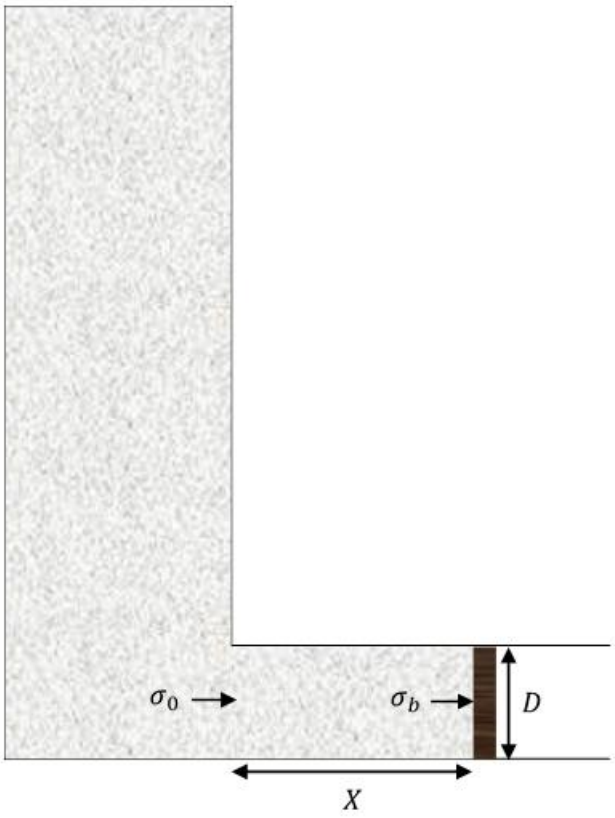

Figure 5.5. Kuganathan's barricade stress model

$$\sigma_b = \sigma_0 \times exp\left(\frac{-PXK_0 \tan\phi}{A}\right) \quad \text{Eq. (5.2)}$$

σ_b - Horizontal stress on barricade (Barricade stress)

σ_0 - Horizontal stress at drive entrance

D - Drive height

X - Barricade offset/setback distance

P - Barricade perimeter

A - Barricade surface area (i.e. cross-sectional area of the drive)

K_0 - At-rest lateral earth pressure coefficient

ϕ - Friction angle of backfill

5.3.3 Modified Marston's equation for backfill stress determination with applied surcharge

Pirapakaran and Sivakugan (2007a) suggested an analytical equation as presented in Equation 5.3, to calculate the average vertical stress at the bottom of the backfilled stope of square cross-section with an applied uniformly distributed load (UDL) at the fill top. This average vertical stress (σ_v) is then used to determine the horizontal stress at the drive entrance (σ_0), using the at-rest lateral earth pressure coefficient (K_0) from Jaky's expression. The Equations 5.2 and 5.3 are employed in the analytical studies of laboratory barricade model, as discussed in Section 5.5. The fill under the surcharge pressure exerted on fill top, assumed by Pirapakaran and Sivakugan (2007a) is depicted in Figure 5.6.

Figure 5.6. Fill in a square stope subjected to surcharge pressure

$$\sigma_v = \frac{\gamma B}{4K \tan \phi}\left[1 - exp\left(\frac{-4Kz \tan \phi}{B}\right)\right] + q \times exp\left(\frac{-4Kz \tan \phi}{B}\right) \qquad \text{Eq. (5.3)}$$

σ_v - Average vertical stress at stope bottom

γ - Unit weight of the backfill

B - Stope width

K - Lateral earth pressure coefficient

z - Backfill height in the stope

q - Surcharge pressure/Uniformly distributed load at the fill top

ϕ - Friction angle of the backfill

5.4 Barricade surface pressure distribution

Similar to the arching condition occurring in backfilled vertical stope as discussed in Chapter 4, the effect of arching within the horizontal drive causes the reduction of fill stress transferring onto the barricade. This has been accounted in analytical solutions discussed above with a continuum approach. However, the backfills are real particulate materials and thus physical model testing were carried out with real HF tailings, to understand and interpret the barricade stress better. The formation of arching in the backfilled drive due to shear resistance occurring along the drive walls and its reflection on barricade surface were evident in the barricade pressure mapping exercise carried out with the laboratory model setup discussed in Section 5.4.4.

5.4.1 Laboratory barricade model setup

A novel square shape stope-drive barricade apparatus was designed and built to simulate the actual conditions of a fill barricade structure. The apparatus consists of vertical square stope of width (B) of 300 mm, height of (H) 500 mm, and several drive-barricade attachments of different sizes as shown in Figure 5.7. The dimensions of the vertical stope were decided considering the space availability in the loading machine from which the surcharge pressure (q) was applied. The square drive sizes (D) used in testing are 75, 100, 125 and 150 mm. The barricade offset (X) was changed within the horizontal drive from 0 mm to 150 mm in 25 mm intervals.

(a) (b)

Figure 5.7. (a) Barricade model setup showing the stope and the drive (b) Drive attachments of different sizes

5.4.2 Barricade pressure mapping

The barricade pressure mapping test was carried out to understand the influence of arching within the drive on stress distribution on the entire barricade surface. Accordingly, the laboratory barricade model having the 75 mm drive attachment, was filled with dry granular HF up to a height of 450 mm in the stope. Then the fill was subjected to surcharge pressures ranging from 30 kPa to 900 kPa applied at the fill top as a uniformly distributed load (UDL) from the universal load testing machine. The UDL was applied in a sequential order with 10 loading steps where each load step was held for 1 minute for stabilisation of the fill under the new load. The surface pressure mapping sensor was fixed on the barricade and the barricade position was set at offsets of 0, 25 and 50 mm in separate tests, to analyse the barricade stress distribution as the offset increases. The apparatus setup and the arrangements are shown in Figures 5.8 and 5.9.

(a) (b)

Figure 5.8. (a) Tactile surface pressure mapping sensor (b) Barricade apparatus in the MTS machine

(a) (b)

Figure 5.9. (a) Tactile sensor fixed barricade placed at 25 mm offset (b) Barricade apparatus

5.4.3 Real-time pressure recording sensor matrix

The knowledge of soil-structure interaction pressure and its associated distribution are of increasing importance in engineering practice. For decades, accurate and reliable measurement of soil-structure interface pressures has been an elusive goal. As a solution, Tactilus technology now delivers, for the first time, the ability to easily, quickly and relatively inexpensively evaluate both pressure magnitude and distribution between soil and structures which is useful in developing reliable load combinations for geotechnical and structural systems.

Tactilus is a matrix-based tactile surface sensor that records and interprets pressure distribution and magnitude between any two contacting or mating surfaces and assimilates the collected data into a powerful Windows™ based software package. Each Tactilus sensor is carefully assembled to exacting tolerances and individually calibrated. The tactile sensor pad and the data logger are shown in Figure 5.10. The specifications of the sensor pad used in this study are shown in Table 5.1.

Figure 5.10. Tactile sensor pad and data logger

Table 5.1. Tactile sensor specifications

Technology	Nano-tube composite
Pressure range	0 to 30 psi (0 to 210 kPa)
Sensing area size	75 mm × 75 mm
Sensor pad thickness	0.4 mm
Matrix/Grid size	32 × 32
Number of sensing points	1024
Accuracy	± 10%
Repeatability	± 2%

5.4.4 Backfill-barricade pressure interaction

The barricade test was carried out with the Tactile sensor as discussed in Section 5.4.2. The pressures generated on the barricade surface for three different offsets (X={0, 25, 50 mm}) under the maximum surcharge pressure (q_{max}= 913 kPa) applied at the fill top, as recorded on the tactile sensor, are presented in 2D and 3D formats as shown in Figure 5.11. The 2D plot shows the pressure distribution on the barricade surface with a spectrum on the left side. The 3D plot exhibits the push on the barricade surface from the pressurised fill in the stope where the third axis (z-axis) is into the barricade. As several combinations of drive barricade size-offset were tested in this study, the following identification code is used hereafter in this dissertation.

Identification: D(#1)-X(#2) where,

#1 - Drive barricade height value (75, 100, 125, 150 mm)

#2 - Barricade offset value (0, 25, 50, 75, 100, 125, 150 mm)

Example: D75-X25 represents the drive barricade size of 75 mm placed at 25 mm offset

Identification	Barricade stress plot (2D view)	Barricade stress plot (3D view)
D75-X0	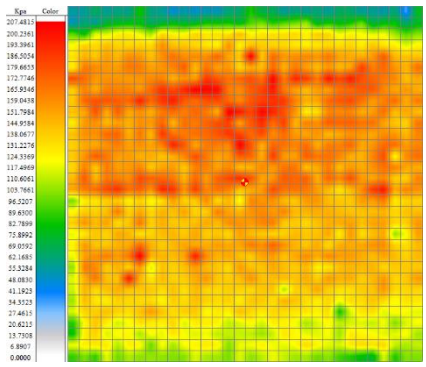	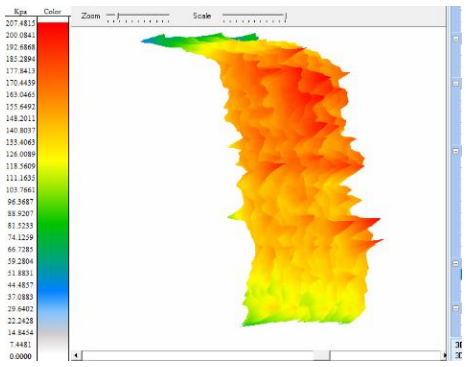
D75-X25	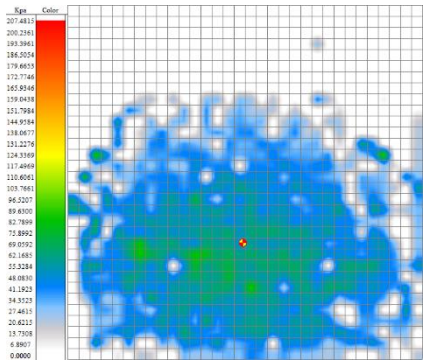	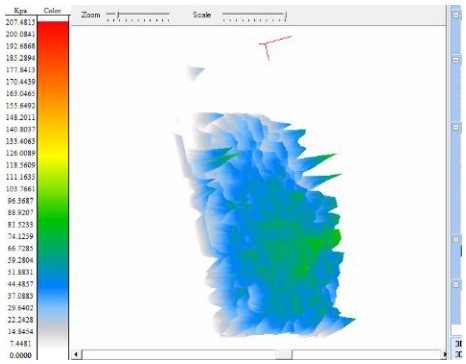
D75-X50	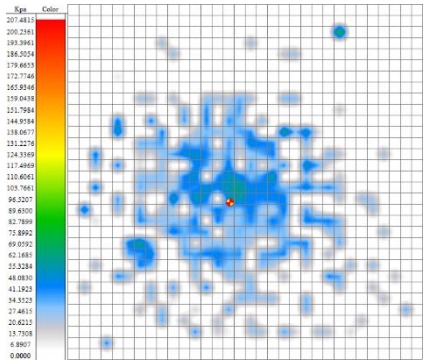	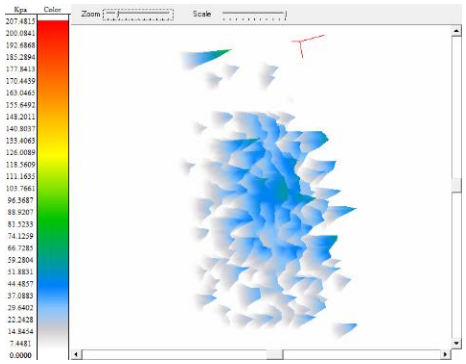

Figure 5.11. Barricade stress mapping plots of 75 mm drive at different offsets

It can be seen that the barricade stress decreased as the offset increases along the drive with highest recorded stress at 0 mm offset where the barricade is at the stope brow and the lowest stress recorded at 50 mm offset, under these test results suggesting that the barricade stress reduces further with the offset. In the 0 mm offset situation, the horizontal pressure acting on the barricade is concentrated more at the drive top-center region whereas the lateral pressure at drive bottom region is low which may have been due to the fixed stope bottom. However, in 25 mm and 50 mm offset situations, the barricade stress distribution is confined to a small area with the highest pressure concentration at the barricade centre region, reflecting the arching condition that

occurred in the drive. The location of the centre of average barricade pressure can be seen with the small circle appearing at the barricade centre region. The shear stresses developed along the drive top, bottom and side walls have caused the reduction of horizontal stress onto the barricade. The barricade stress profiles along the drive height as derived from the Tactile sensor readings are shown in Figure 5.12.

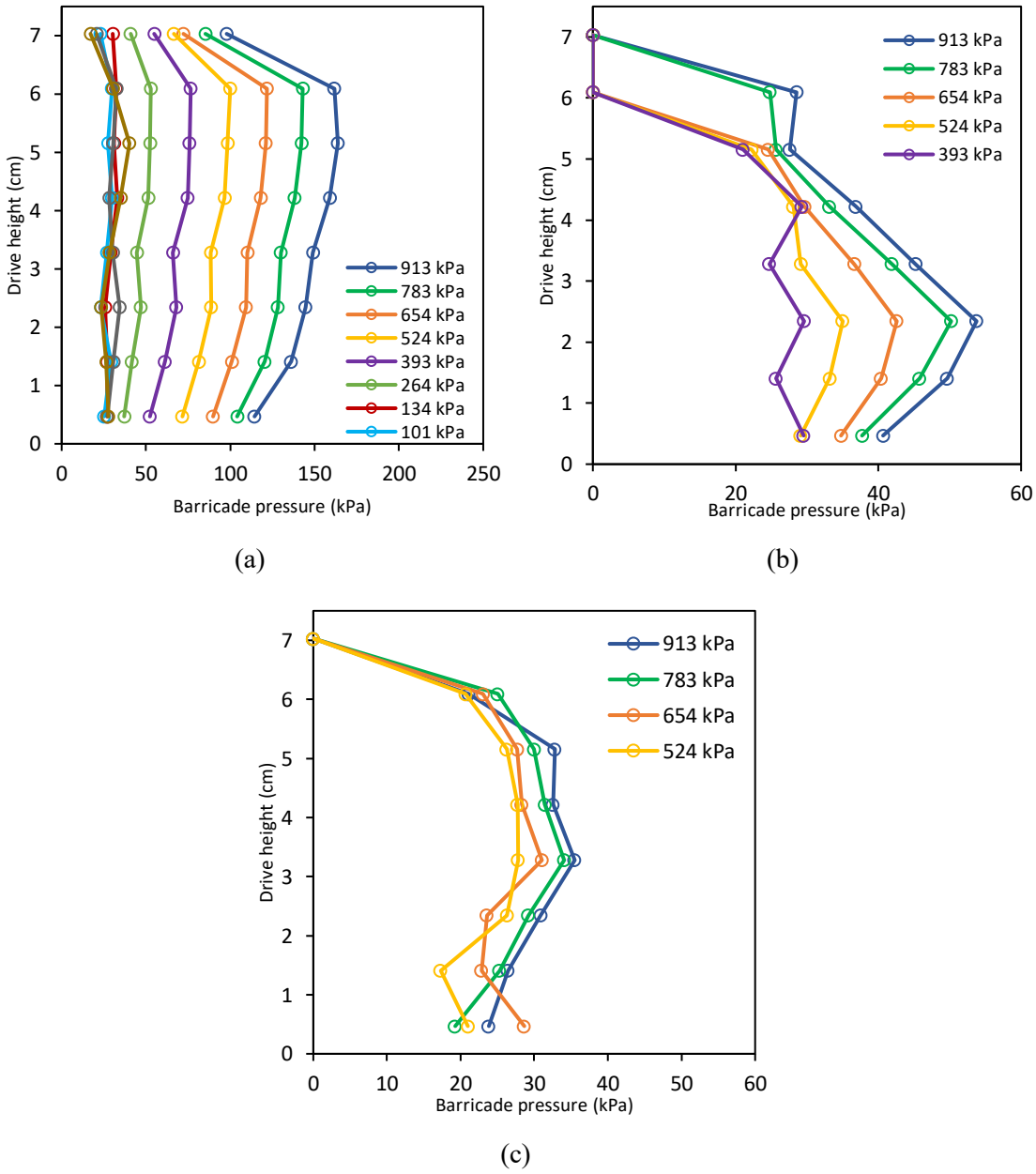

Figure 5.12. Barricade stress profiles (a) 0 mm offset (b) 25 mm offset (c) 50 mm offset

According to Figure 5.12, the recorded maximum barricade stress under the maximum surcharge pressure applied at the top of the fill in the stope are 160 kPa, 55 kPa and 35 kPa, for respective barricade offsets. The detailed quantitative analysis of barricade stress state with the offset, is discussed in Section 5.5.3, presenting dimensionless plots.

5.5 Barricade stress model with earth pressure cells

It was evident that the significant fraction of the stress from the backfill in the stope-drive structure is transferred onto the centre region of the barricade, as discussed in Section 5.4.4. Accordingly, a comprehensive testing program was carried out using the Earth Pressure Cells (EPCs) attached laboratory model, to develop a methodology to estimate the barricade stress for varying drive sizes and barricade offsets. Three different KYOWA BED-A type EPCs that are capable of measuring pressures up to 200 kPa, 500 kPa and 1000 kPa, were used in this study. EPC 1 (200 kPa) was fixed at the barricade centre for recording the barricade pressure which is acting horizontally. Additionally, to quantify the vertical pressure variations within the stope in lateral direction, EPC 2 (500 kPa) and EPC 3 (1 MPa) were installed at the stope edge near the wall and at the stope centre, respectively. The CR1000X data logger manufactured by Campbell Scientific, was used in the data acquisition process during testing. The laboratory model setup with the EPC locations, are schematically shown in Figure 5.13(a) and the photo showing the arrangement of EPCs inside the model stope is presented in Figure 5.13(b).

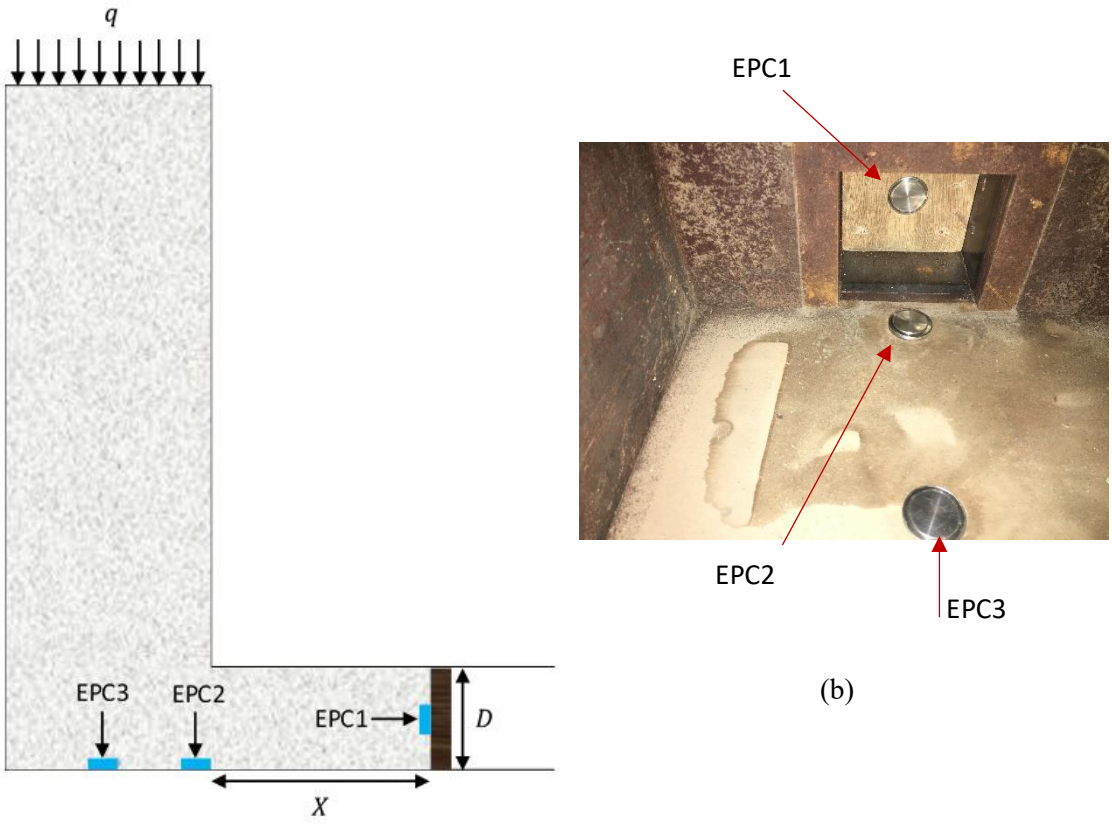

Figure 5.13. (a) EPCs installed in the barricade model apparatus (b) Photo of EPCs arrangement

5.5.1 Arching within backfilled stopes

To understand the lateral variation of vertical normal stress within the backfilled stope, the barricade was placed at the drive entrance at 0 mm offset. Hence, the EPC 1 attached to barricade surface is flushed with the stope wall, allowing to measure the horizontal normal stress acting on the wall near the stope bottom. With this arrangement, the lateral variation of the vertical normal stress can be determined using the soil pressures recorded on EPC2 and EPC3. The fill in the stope was subjected to a sequential loading process as described in Section 5.4.2. The EPC recorded pressures for two drive sizes (100 mm and 150 mm) are shown in Figure 5.14.

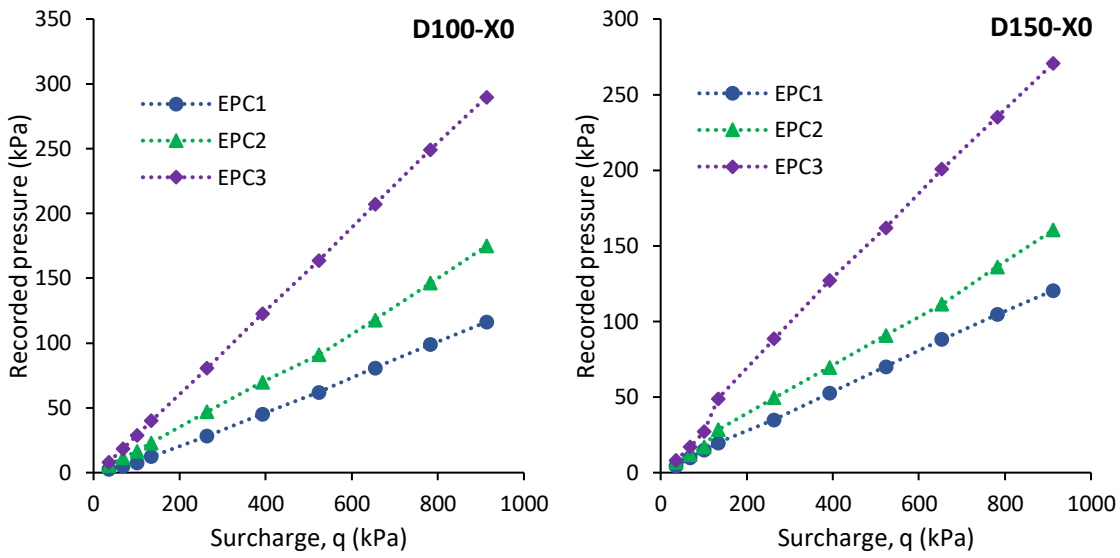

(a) (b)

Figure 5.14. Recorded pressures on EPCs at 0 mm barricade offset (a) 100 mm drive (b) 150 mm drive

It can be seen that, as expected, the EPC 1 has recorded lower pressure values compared to the other two EPCs. The pressure recorded on EPC3 at the stope bottom centre is considerably higher than the pressure values on EPC2, confirming the reduction of vertical normal stress within the fill laterally towards the stope wall, thus exhibiting the arching developments. The vertical stress ratio was calculated using EPC2 and EPC3 values and its variation with the applied surcharge pressures for both drive sizes is shown in Figure 5.15. The vertical stress ratio across half stope width is greater than one, and remains around 1.8 for all applied surcharges.

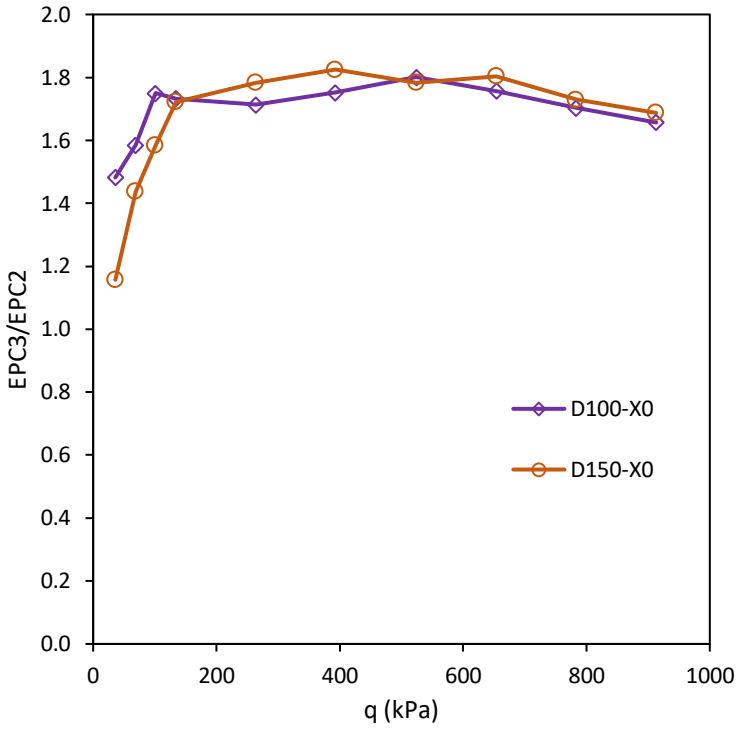

Figure 5.15. Comparison of vertical normal stress at stope bottom centre and edge

5.5.2 Lateral stress ratio comparison

The lateral stress ratio comparison was carried out for the zero offset barricade situation. Three lateral pressure coefficients are defined as below that can be determined using the horizontal and vertical stresses recorded in EPC1, EPC2 and EPC3. The coefficients K_1, K_2 and K_3 were calculated corresponding to all applied surcharges for all four drive sizes but with zero offset, using the laboratory model test results and then the calculated coefficients were compared with the theoretical lateral earth pressure coefficients namely K_0, K_a and $K_{krynine}$ obtained from the relevant analytical equations, as presented in Figure 5.16.

$$K_1 = \frac{EPC1\ (Horizontal\ normal\ stress\ at\ wall)}{EPC3\ (Vertical\ normal\ stress\ at\ stope\ bottom\ center)}$$

$$K_2 = \frac{EPC1\ (Horizontal\ normal\ stress\ at\ wall)}{EPC2\ (Vertical\ normal\ stress\ at\ stope\ bottom\ edge)}$$

$$K_3 = \frac{EPC1\ (Horizontal\ normal\ stress\ at\ wall)}{Avg\ (EPC2{:}\ EPC3)\ (Average\ vertical\ normal\ stress\ at\ stope\ bottom)}$$

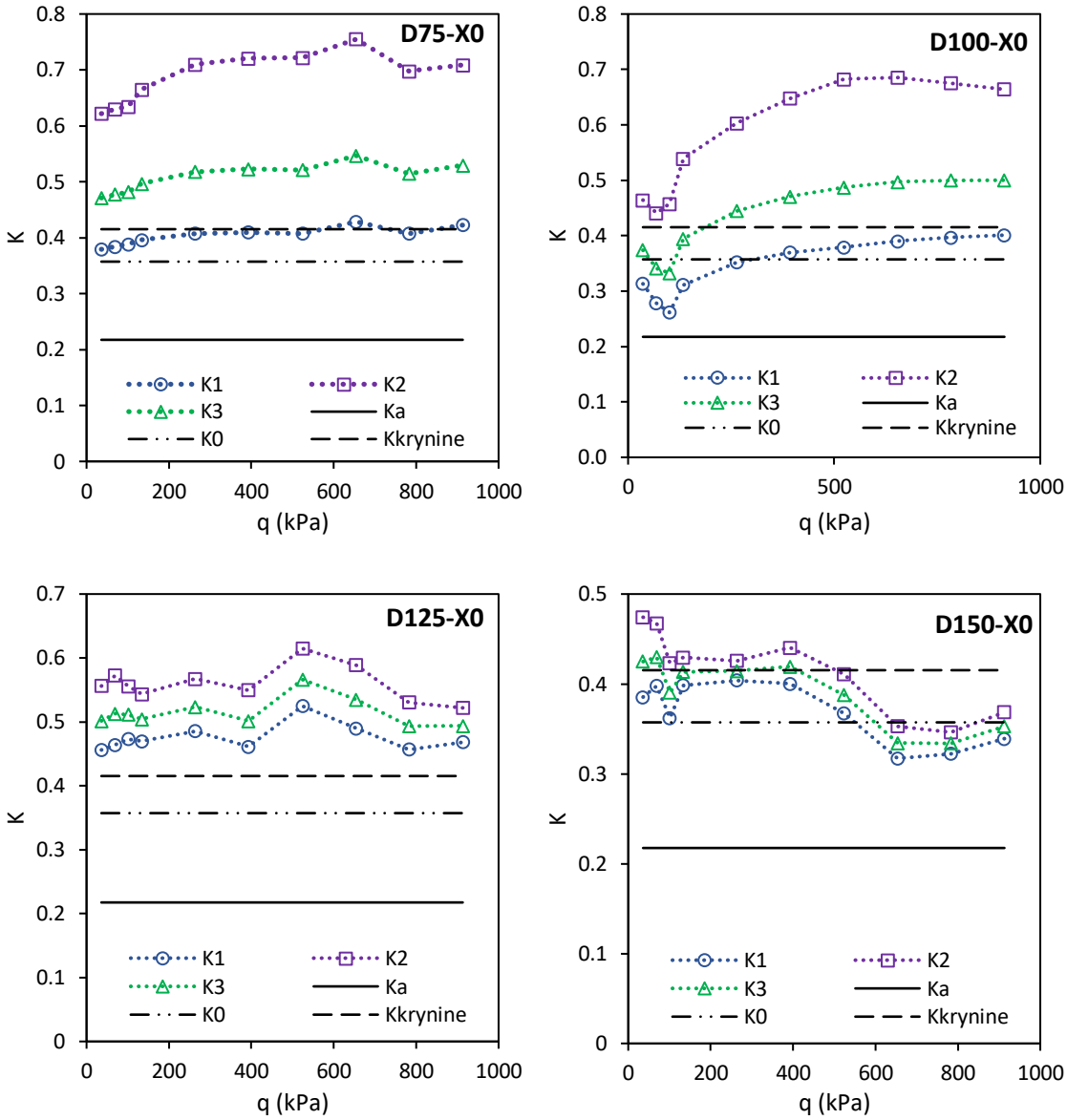

Figure 5.16. Comparison of theoretical and calculated lateral pressure coefficient

It is clear that the calculated lateral pressure coefficient (K_1) is close to K_0 and $K_{krynine}$, where as K_a is well below the calculated K. Therefore, it implies that the active lateral earth pressure coefficient is not appropriate to use in analytical solutions for backfill stress analysis. Furthermore, considering the conclusions made in Chapter 4 with regards to the suitable K for backfill stress analysis, it is reconfirmed that K_0 is the most suitable lateral earth pressure coefficient to use in the analytical equations. Kuganathan (2002) has also suggested K_0 in his barricade stress model.

5.5.3 Barricade stress variation with offset

The analytical solutions suggest that the stress state on the barricade is decreased exponentially with the increasing barricade offset. To investigate the particulate behaviour on arching within the drive and barricade stress development in different drive sizes and barricade offsets, a series of testing was carried out with the EPCs attached laboratory barricade model apparatus. All four drive sizes (D= 75, 100, 125, 150 mm) and seven offsets (X= 0, 25, 50, 75, 100, 125, 150 mm) were tested. The barricade stress equation proposed by Kuganathan (2002) was considered for the comparison of results. The dimensionless plots were developed for each drive size, taking the normalized barricade stress (σ_b/σ_v) on y-axis and normalized offset (X/D) on x-axis, as presented in Figure 5.17. According to Figures 5.2 and 5.3, σ_b and σ_v are the barricade stress and average vertical stress at stope bottom, respectively. The barricade stress depends on the vertical normal stress at the stope bottom that comes from the fill mass in the vertical stope and hence to account this relationship in a dimensionless parameter, (σ_b/σ_v) ratio is considered in the barricade stress – offset plots. From the laboratory model test, the average barricade stress variation curve was obtained considering the stress curves from the surcharge pressures (q) of 36 kPa, 393 kPa and 913 kPa and curve fitting is also given for the average stress.

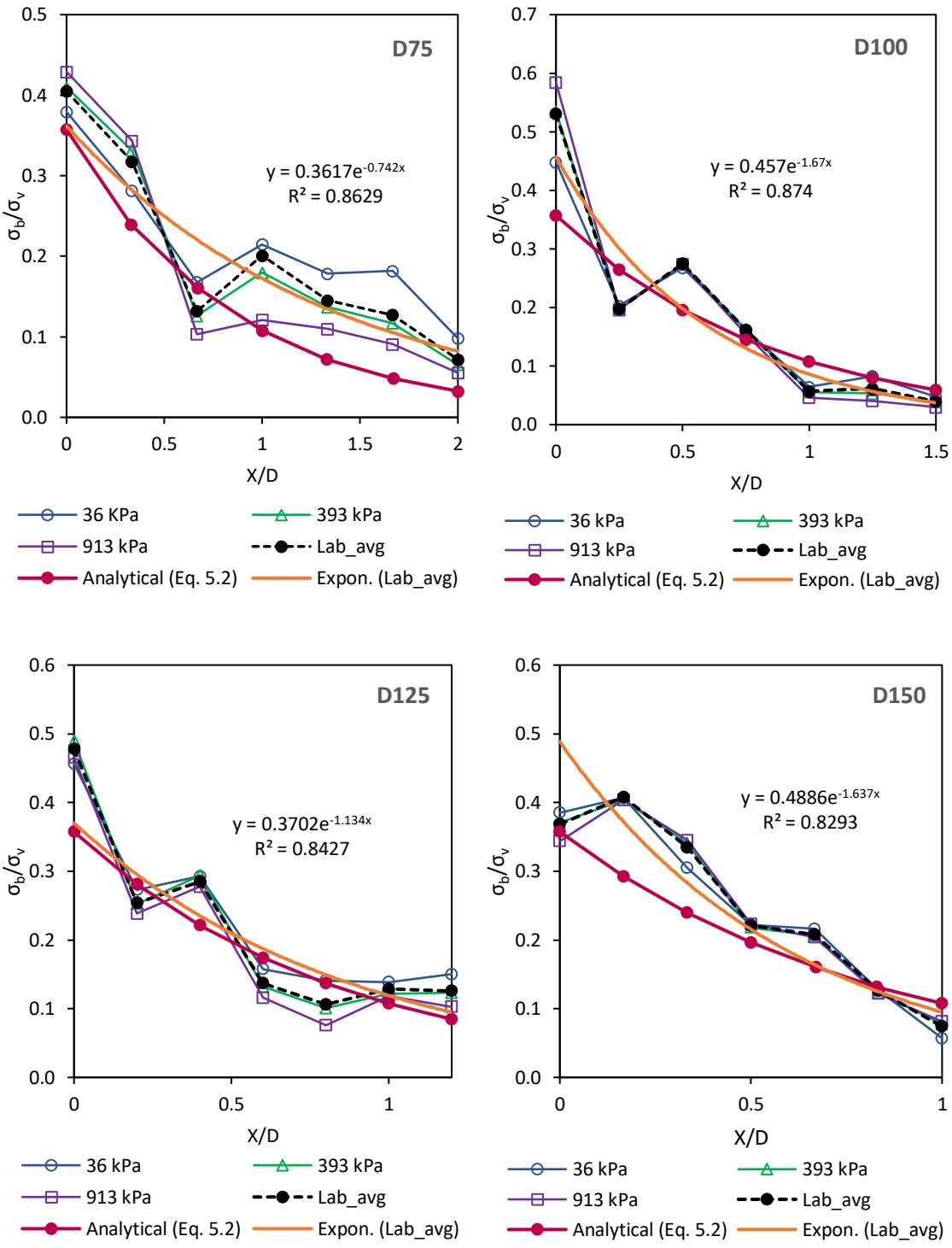

Figure 5.17. Genaralised plots for barricade stress variation with offset

The laboratory barricade model test results from all drive sizes confirmed that the variation of barricade stress with the offset is non-linear and the relationship is described as an exponential decay with high level of confidence. This exponential relationship is comparable well

with the analytical solution suggested by Kuganathan (2002), however, the analytical solution appears underestimating the barricade stress from the laboratory results. Laboratory tests are based on particulate approach with real mine tailings replicating an actual mine backfilled barricade, thus the validity of laboratory model outcomes is high.

5.5.4 Barricade stress variation with drive size

The variation of lateral stress on barricade with the drive size, for an offset of 50 mm is shown in Figure 5.18.

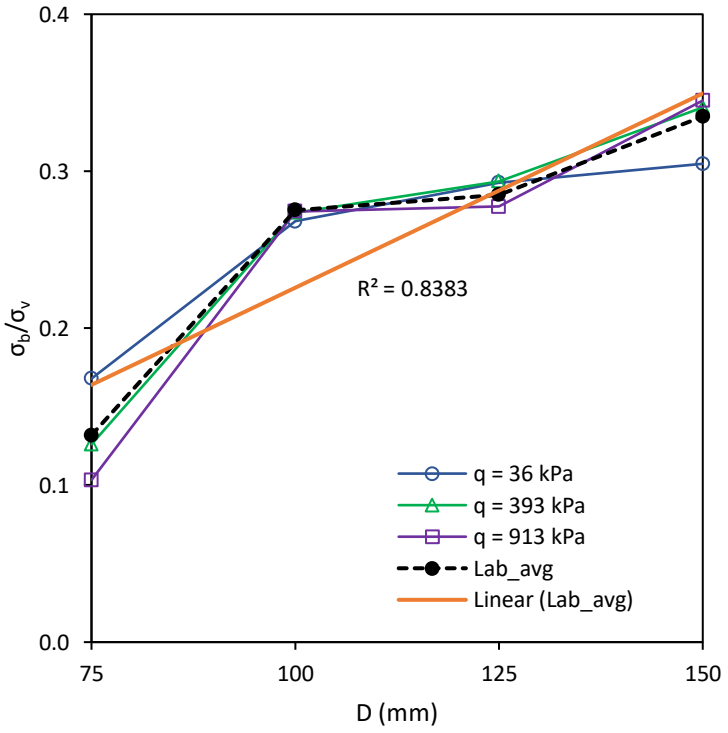

Figure 5.18. Barricade stress variation with drive size for offset of 50 mm

The normalised stress on barricade is increased with the drive size and this implies that a large fill load is transferred to barricade when the drive dimensions are larger. Large drive size provides a path to transfer more load to the barricade, than in the case of confined pathway with the smaller drive size.

5.5.5 Comparison of barricade stress estimated from laboratory, analytical and numerical approaches

The numerical modelling work done by Widisinghe (2014) for replicating the lateral stress onto the barricade using a FLAC code, is considered herein for the comparison of barricade stress estimated from the analytical equation suggested by Kuganathan (2002) and from the laboratory model tests carried out in this study. Accordingly, the normalised barricade stress plots developed for the 125 mm drive size for three different surcharge pressures (Low: 36 kPa, Medium: 393 kPa and High: 913 kPa) applied, are shown in Figure 5.19. The FLAC simulation also suggest that the stress state on the barricade decreases when the barricade is moved away from the stope brow. The overall trend of barricade stress reduction with the offset is agreeing between the laboratory, analytical and numerical estimations.

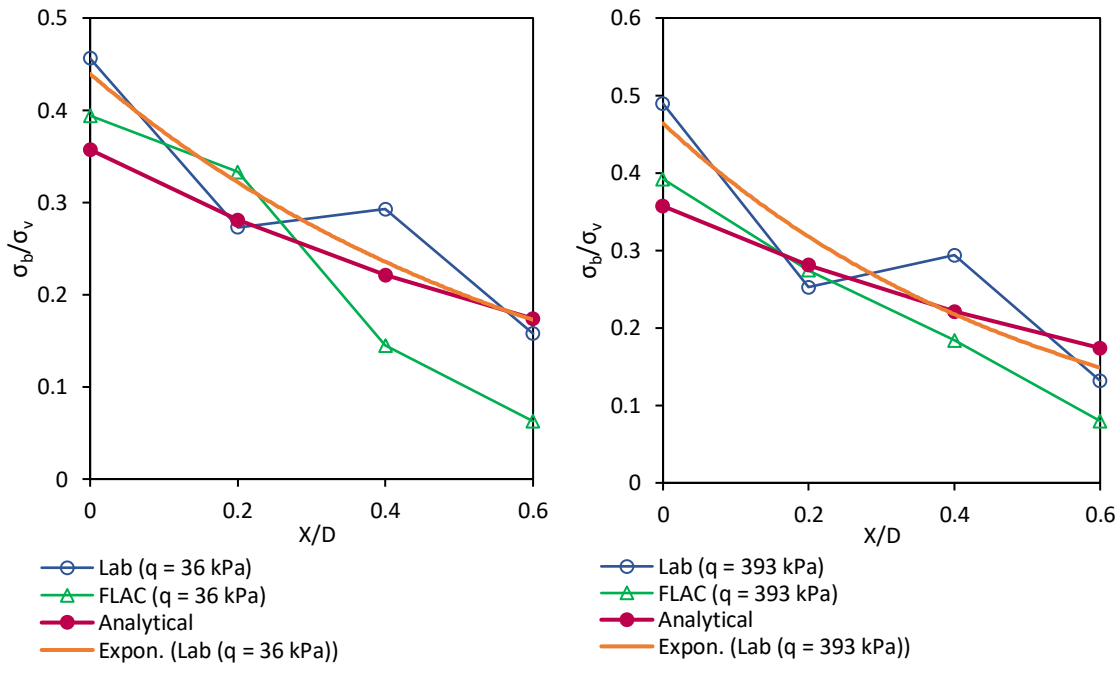

(a) (b)

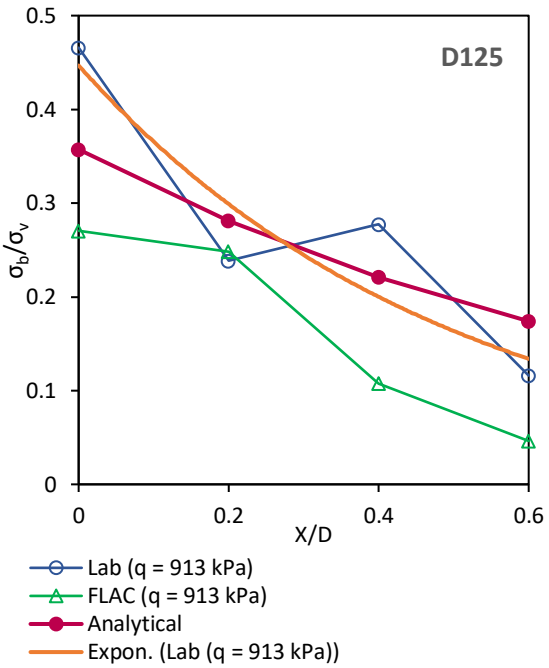

(c)

Figure 5.19. Laboratory, analytical and numerical comparison of barricade stress (a) q = 36 kPa (b) q = 393 kPa (c) q = 913 kPa

5.5.6 An empirical solution for barricade stress estimation

An empirical equation is proposed for barricade stress estimation for any drive size and for any barricade offset, based on laboratory modelling carried out in this study, taking into account the particulate behaviour and replicating the drive arching conditions with granular HF. The normalised plot for barricade stress variation reflecting all three approaches, is presented in Figure 5.20. The drive sizes (D) of 75, 100, 125 and 150 mm, and offsets (X) of 0, 25, 50 and 75 mm were used in developing these plots. It is evident that the analytical and numerical solutions based on continuum approach underestimate the barricade stress compared to the physical model results. This stress behaviour is identical to the stress developments within the backfilled stope as discussed in Chapter 4, where the analytical and continuum modelling solutions underestimate the vertical normal stress within the fill reaching an asymptotic value at shallow fill depths, but the laboratory model simulations give larger vertical stresses with a continuous increase with the fill depth.

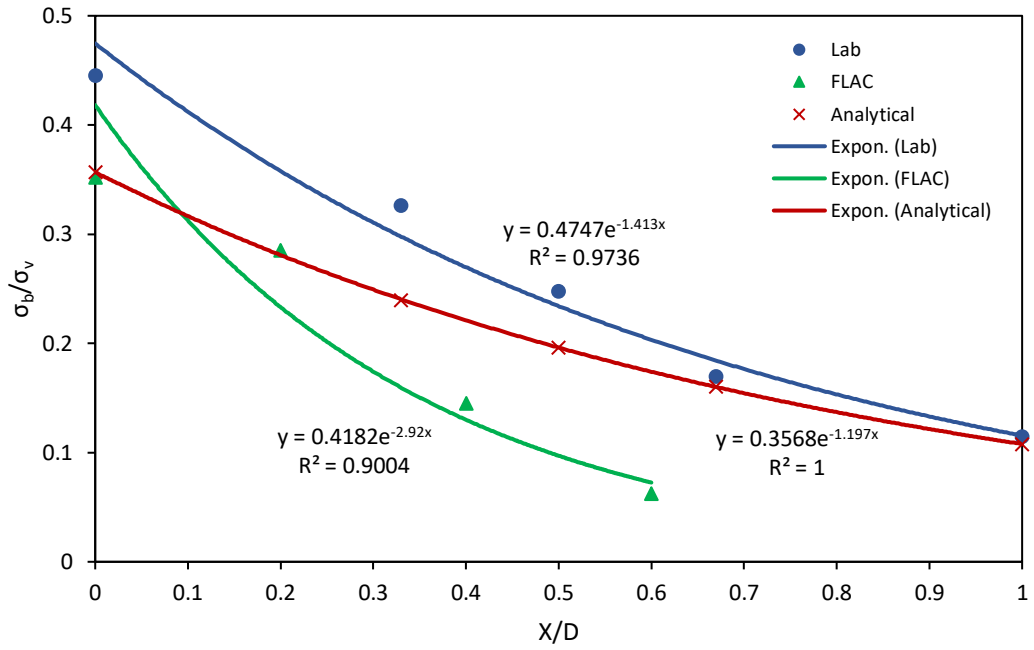

Figure 5.20. Normalised plot for barricade stress estimation

The empirical equation to determine the barricade stress is given in Equation 5.4.

$$\sigma_b = 0.4747\sigma_v \times exp\left[-1.413\left(\frac{X}{D}\right)\right] \qquad \text{Eq. (5.4)}$$

where,

σ_b - Barricade stress

σ_v - Average vertical stress at stope bottom

X - Barricade offset

D - Drive height

Here, the average vertical stress (σ_v) at stope bottom is determined using the analytical equation proposed in Chapter 4. The Equation 5.4 is independent of horizontal normal stresses at the drive entrance, which negates determining them as in the case of Li and Aubertin (2009) and Kuganathan (2002) solutions. Given the small barricade sizes tested with laboratory model, only one EPC was fixed at the centre of the barricade. Therefore, the proposed empirical equation gives the lateral stress at the barricade centre. However, this can be justified using the results of

barricade pressure mapping exercises discussed in Section 5.4.4, where it clearly showed the barricade stress is more concentrated at the centre region than the other areas of the barricade.

5.6 Proposed methodology to estimate barricade stress in a backfilled stope

A methodology to estimate the lateral stress on the barricade in a hydraulic backfilled stope is proposed. The analytical and empirical equations developed in this study are used in calculating the barricade stress as presented in the general example below. Consider a square shape stope having a width (B) of 10 m filled with granular hydraulic backfill up to a height (z) of 50 m at the unit weight (γ) of 16 kN/m3. The drive barricade of size (D) of 5 m is placed at an offset (X) of 2 m from the stope brow.

Calculating the average vertical normal stress at stope bottom using the proposed analytical Equation 4.18 given below. The α and β coefficients were determined as 0.2252 and 1.1356, respectively.

$$\sigma_v/_{\gamma B} = \frac{z}{B}(1-4\alpha) + \frac{4\alpha}{\beta}\left[1 - e^{-\beta\left(\frac{z}{B}\right)}\right]$$

Hence, σ_v is calculated as 205 kPa.

Now the barricade stress is determined using the proposed empirical Equation 5.4.

Hence, σ_b is computed as 55 kPa.

5.7 Summary

The exclusive summary of this Chapter is presented below.

- The barricade stress estimated from Kuganathan (2002) analytical equation and FLAC continuum modelling, is low compared to that of laboratory model testing results, where the difference in stress behaviour can be attributed to the particulate nature of the actual fill material.

- Drive arching significantly contributed to the reduction of stress transferred to the barricade as evident in the barricade pressure mapping with Tactile sensor pad. The barricade stress appeared to be concentrated at the centre region of the barricade surface than the corner areas near to the drive walls.

- It is further confirmed that the backfilled stopes can be considered to be in at-rest state, suggesting from Jacky's expression can be used in the analytical equations.

- The variation of barricade stress with offset is found to be a non-linear relationship based on laboratory model testing, suggesting the barricade stress is decreasing in an exponential trend correlating with the Kuganathan's solution.

- The proposed simple methodology can be used in estimating the lateral stress on the barricade in any hydraulic backfilled stope, irrespective of the stope-drive dimensions.

Chapter 6

6 Summary, Conclusions and Recommendations for Future Research

6.1 Summary

Mine backfilling in an integral part of the underground mining process. It helps to achieve local and regional ground support for the mining progression, to reduce the need and maintenance of conventional surface tailing storage facilities, to dispose waste in an effective, sustainable and environmentally friendly manner, to control surface subsidence while enabling a more complete extraction of the ore body. Given the importance of mine backfilling, there has been research carried out on different aspects of backfilling in an extensive manner since early 1990s. The correct understanding of the stress distribution within backfilled stopes and drives is pivotal for safe and optimised barricade designs. The failure of a barricade could result in severe disruptions to the ongoing mining activities because of the loss of lives and infrastructure damage, which could potentially lead to a temporary or permanent closure of the mine causing a significant financial loss to the company. There has been incidents and accidents of barricade failures and consequences reported worldwide. From the review of literature carried out in this study, it was identified that one of the main reasons for barricade failures is primarily due to underestimation of stress state on the barricade in the barricade design stage. The aim of this research was to comprehensively investigate the effect of soil arching in stress developments within the backfilled stopes, drives and barricades from three independent approaches namely laboratory, analytical and numerical methods.

Three types of materials were used in this study namely fine sand, EHM tailings and Pajingo tailings to determine their suitability for potential backfills. In the first part of Chapter 3, the materials were characterised based on several geotechnical properties. The friction angle of backfill material being an important parameter in stress analysis within backfilled stopes, the variation of friction angle with relative density of the fill was established. The effect of wall roughness on the interfacial friction angle was presented. The later part of this Chapter discussed the long-term settling behaviour of EHM and Pajingo tailing slurries covering the entire natural drying process, mimicking a backfilled stope. The concept of shrinkage curve was brought in for

interpreting the shrinkage behaviour of tailing slurries settling in stopes. Accordingly, the granular EHM fill settled almost instantaneously in the vertical direction. However, interestingly in Pajingo fill, in addition to the vertical strain the lateral shrinkage was observed resulting the loss of fill-wall contact. The characteristics of the settled fill were compared with the typical backfill properties and their suitability to use as Hydraulic fill (HF) or Paste fill (PF) was determined.

The stress developments in the vertical backfilled stopes were extensively analysed and discussed in Chapter 4. Accordingly, the shear stress along the wall, vertical normal stress at the stope bottom and the horizontal normal stress on the wall were examined using analytical, laboratory and numerical modelling methods for a backfilled stope with the normalised fill height (z/B) from 0 to 6. The three main analytical closed form solutions namely Marston (1930), Aubertin et al. (2003) and Pirapakaran and Sivakugan (2007a) were used for comparison with laboratory and numerical results. An extensive laboratory test program was carried out to understand the arching effect on stress developments within backfilled stopes and grain silos by varying the wall roughness. A novel arching equation was developed to determine the shear stress on wall at any depth of the fill which was then applied in formulating analytical models for the variation of vertical normal stress with fill depth. These analytical models were then validated with the laboratory stope model test data successfully. The dimensionless plots developed in this Chapter can be used for stress determination in any granular HF backfilled stope of any dimensions. The lateral earth pressure coefficient (K) variation with fill depth was analysed using laboratory test data and compared with the general analytical expressions suggested by Rankine's active lateral earth pressure coefficient (K_a) and Jacky's expression for at-rest lateral earth pressure coefficient (K_0). Initially, the laboratory scaled backfilled stope was modelled numerically using an explicit finite difference code FLAC which treated the backfill mass as a continuum. However, real mine tailings are particulate materials and thus distinct element method embedded PFC software was used in simulating the arching conditions and stress developments in the laboratory stope model. The particulate modelling with PFC clearly justified how close it

can simulate the backfilled stope agreeing well with the laboratory model test results, compared to the continuum modelling with FLAC.

Similar to the arching conditions developed in the stope, the backfill in the horizontal drive is subjected to the soil arching phenomena, thus a reduction of stress transferred onto the barricade. The accurate estimation of the barricade stress is the ultimate requirement for designing a safe and competent barricade. Accordingly, the Chapter 5 discussed the arching within backfilled drive and lateral stress state on the barricade by means of analytical, laboratory and numerical methods. A novel laboratory barricade model apparatus was designed and fabricated replicating an actual stope-drive-barricade structure. The full barricade surface pressure mapping was carried out with a Tactile sensor pad fixed to the barricade, to understand the arching developments in the drive and the stress distribution on the barricade. Using the Earth Pressure Cells attached in the barricade apparatus, barricade stress variation with offset and drive size was investigated. Accordingly, four drive sizes and seven offsets were tested to obtain the above relationships. The normalised plots developed herein can be used to determine barricade stress at any barricade offset from stope brow. With the barricade placed at zero offset position, the lateral variation of vertical stress was analysed to understand the arching development in the vertical stope. The normalised barricade stress variation with offset was compared with the analytical solution suggested by Kuganathan (2002) and numerical modelling work done by Widisinghe (2014). Finally, an empirical equation was proposed to estimate the barricade stress based on physical model simulations which reflect the actual backfilling of stope with granular backfill material. The simple methodology proposed at the end of Chapter 5 can be adapted to determine the stress that is transferred onto the barricade from the backfill in the mine stope.

The prime motive of this research was to give recommendations to improve mine safety associated with backfills and barricades. In response, methodologies were developed, tested and validated to quantify the stresses within a HF backfilled mine stope. Accordingly, new analytical solutions were proposed in Eq. 4.16 and Eq. 4.18 to determine shear stress on wall and vertical normal stress in fill at a certain fill depth from top, accounting the effect of soil arching. Additionally, corresponding dimensionless charts for stress variation with depth were developed

as shown in Figures 4.19 and 4.21, which would be useful and handy to use by miners for the backfill stress calculations within the stope. Furthermore, some guidelines and equations were proposed for determining the loadings (stresses) on the barricades. The empirical solution proposed in Eq. 5.4 can be used to estimate the barricade stress due to fill mass in vertical stope and horizontal drive, for any drive height (D) and barricade offset (X), where (X/D) ranging from 0 to 1. The application of the proposed equations to estimate barricade stress in an actual HF backfilled stope is presented in Section 5.6. Hence, it is recommended for mines to test similar scaled models with their HF material for verification if necessary or use the stress equations and plots developed in this dissertation as mentioned above.

6.2 Conclusions

The study has been carried out to investigate the arching effect on stress developments within backfilled mine stopes and drives and to develop a methodology to estimate the barricade stress that is transferred from the backfill in the stope. The conclusions that are drawn from this research can be presented as below. The objective 1 of this study is covered in the literature review in Chapter 2 - Appendix A.

Geotechnical characterisation of tailings and alternative materials

The following conclusions address the objective 2 of this study.

- The granular nature, GSD and other index properties of fine sand suggested that it can be used in laboratory model tests to replicate HF backfilled stopes for research purposes, where the availability and supply of real HF mine tailings are limited or not possible.
- The relationship developed for the variation of friction angle of the tailings with relative density confirmed that the tailing friction angle (ϕ) rapidly increased for larger relative densities of the fill, in a range of 37-49 degrees.
- The analysis on the effect of stope wall roughness on interfacial friction angle verified that the interfacial friction angle of rough walls (δ) (e.g., Mine stope) can be equated to

the friction angle of the tailing material (ϕ) due to the slip surface being the fill-fill interface. That is, $\delta = \phi$ was justified for backfilled mine stopes.

- The analysis of long-term settling behaviour and determination of settled fill characteristics are considered as the first step in identifying the suitability of tailings for backfill material and in deciding what pre-treatments are required before the tailings can be used as hydraulic fills or paste fills.
- The shrinkage curve of tailing is useful to obtain critical void ratios and thereby to calculate sedimentation and vertical consolidation settlement of backfill slurry of any initial fill height in the stope.
- The lateral shrinkage of fill is not accounted in 1D consolidation equations and hence numerical simulation program is required to analyse the volume variation of fill caused by lateral strain, especially with fills having high clay content.
- The clay content in mine tailings is identified as the influencing factor for lateral contraction of fill during settling thus resulting loss of arching in stope. Therefore, reducing the clay fraction to a suitable level is essential before the tailing can be placed as backfill.

The following conclusions are linked to the objectives 3, 5 and 6 of this study.

Arching and stress developments within backfilled mine stopes

- Laboratory stope models consisting granular material showed an increase of vertical normal stress in the fill, throughout the fill depth, even at depths as high as $6B$.
- Analytical solutions by Marston (1930), Aubertin et al. (2003) and Pirapakaran and Sivakugan (2007a), etc reach an asymptotic vertical stress after a certain fill depth due to several approximations considered in analytical models.
- The vertical normal stresses within the fill from the laboratory stope model test correlated better with the Pirapakaran and Sivakugan (2007a) analytical solutions for shallow depths

like $1B$ to $2B$, however as the fill depth increased the stress curves from both methods largely diverged.

- It was verified that the lateral earth pressure coefficient (K) variation with fill depth is not constant, which was not considered in above analytical solutions, and it was determined that K_0 is conservative to use in analytical equations than K_a.
- The proposed new arching equation allows to determine the wall shear stress at any depth of the backfilled stope.
- The genaralised plots developed from the proposed analytical models can be used to determine the vertical normal and shear stress at any depth of the fill in a backfilled stope or grain silo.
- The continuum numerical modelling approach with FLAC suggested the vertical normal stress in the fill becomes asymptotic at certain depth, similar to the analytical solutions.
- However, the particulate numerical modelling approach with PFC confirmed the increase of vertical normal stress along the fill depth, with good agreements with the laboratory model test results. Therefore, particulate modelling is encouraged to simulate the actual stress developments within backfilled stopes, with greater confidence.

The following conclusions cover the objectives 4, 5 and 6 of this study.

Arching within backfilled drives and lateral stress on barricades

- The barricade stress estimated from Kuganathan (2002) analytical equation and FLAC continuum modelling, is low compared to that of laboratory model testing results, where the difference in stress behaviour can be attributed to the particulate nature of the actual fill material.
- Drive arching significantly contributed to the reduction of stress transferred to the barricade as evident in the barricade pressure mapping with Tactile sensor pad. The barricade stress appeared to be concentrated at the centre region of the barricade surface than the corner areas near to the drive walls.

- It was further confirmed that the backfilled stopes can be considered to be in at-rest state, suggesting that the Jacky's expression for K_0 can be used in the analytical equations.
- The variation of barricade stress with offset was found to be a non-linear relationship based on laboratory model testing, suggesting that the barricade stress was decreasing in an exponential trend correlating with the Kuganathan's solution.
- The proposed methodology can be used in estimating the lateral stress on the barricade in any hydraulic backfilled stope, irrespective of the stope and drive dimensions.

6.3 Recommendations for future research

Even though this dissertation critically investigated the arching and stress developments within backfilled stopes and drives, and proposed a methodology to estimate the vertical normal stresses within stopes and also the loads on barricades based on analytical, numerical and laboratory modelling approaches, still there are some potential research areas that can be considered in the future as summarised below. These recommendations would help in improving the proposed solutions for an extended scope of applications.

- The proposed empirical equation for the barricade stress estimation is based on square shape drives and barricades. However, there can be instances where irregular shape drives exist in actual mines (e.g., horseshoe shape) thus analysing the stress state on irregular shape barricades would be useful.
- Computational Fluid Dynamics (CFD) coupled numerical modelling is encouraged to replicate better the stress developments associated with the consolidation of the backfill in the stope.
- The mine tailings comprise different size and shape grains which affect the inter particle locking during fill settling process and thus the porosity. As a result, the stress developments in the fill could be influenced by the change of interface properties of the fill. Therefore, incorporating the GSD of the fill and angularity of grains in PFC modelling is recommended to closely simulate the backfilled stope.

- The particle segregation occurs during the slurry sedimentation stage where the backfill slurry settling in the stope under gravity with the coarser and heavier particles settle fast at the bottom while the smaller and finer particles settle slowly on top of the already deposited fill. Therefore, it is important to account the particle segregation phenomena in numerical modelling exercises of backfilled stopes.
- In this dissertation, barricade stress was modelled and analysed considering only one drive located at the stope bottom. However, when there are multiple drives located at intermittent heights along the stope wall, the stress that is transferred onto the barricade in the bottom drive would be less according to an intuitive prediction. Hence, to confirm this, modelling of backfilled stopes with multiple drives is recommended.

References

Archibald, J., De Souza, E. and Beauchamp, L. (2009). Compilation of industry practices for control of hazards associated with backfill in underground mines-Part II underground transport and stope placement. In Diederichs, M. & Grasselli, G. (Ed.), 3rd CANUS Rock Mechanics Symposium. Toronto.

AS 1289.3.2.1 (2009). Soil classification tests - Determination of the plastic limit of a soil - Standard method. *Methods of testing soils for engineering purposes*: Standards Australia.

AS 1289.3.5.1 (2006). Soil classification tests - Determination of the soil particle density of a soil - Standard method. *Methods of testing soils for engineering purposes*: Standards Australia.

AS 1289.3.6.1 (2009). Soil classification tests - Determination of the particle size distribution of a soil - Standard method of analysis by sieving. *Methods of testing soils for engineering purposes*: Standards Australia.

AS 1289.3.6.3 (2020). Soil classification tests - Determination of the particles size distribution of a soil - Standard method of fine analysis using a hydrometer. *Methods of testing soils for engineering purposes*: Standards Australia.

AS 1289.3.9.1 (2015). Soil classification tests - Determination of the cone liquid limit of a soil - Standard method. *Method of testing soils for engineering purposes*: Standards Australia.

AS 1289.5.5.1 (1998). Soil compaction and density tests - Determination of the minimum and maximum dry density of a cohesionless material - Standard method. *Methods of testing soils for engineering purposes*: Standards Australia.

AS 1289.6.2.2 (2020). Soil strength and consolidation tests - Determination of the shear strength of a soil - Direct shear test using a shear box. *Methods of testing soils for engineering purposes*: Standards Australia.

AS 1726 (2017). Geotechnical site investigations. Standards Australia.

ASTM D2487 (2017). Standard Practice for Classification of Soils for Engineering Purposes (Unified Soil Classification System). ASTM - American Society Testing and Materials.

Aubertin, M., Li, L., Arnoldi, S., Belem, T., Bussière, B., Benzaazoua, M. and Simon, R. (2003). Interaction between backfill and rock mass in narrow stopes. In Culligan, P. J. & Whittle, A. J. (Ed.), 12th Pan American Conference on Soil Mechanics and Geotechnical Engineering (pp. 1157-1164). Boston, Massachusetts, USA: MIT.

Belem, T., Harvey, A., Simon, R. and Aubertin, M. (2004). Measurement and prediction of internal stresses in an underground opening during its filling with cemented fill. In Villaescusa, E. & Potvin, Y. (Ed.), Ground support in Mining and Underground construction: Ground Support 2004 (pp. 28–30). Perth, Western Australia: Taylor & Francis group, London.

Berndt, C. C., Rankine, K. J. and Sivakugan, N. (2007). Materials properties of barricade bricks for mining applications. *Geotechnical and Geological Engineering,* 25(4), 449-471. doi: 10.1007/s10706-007-9122-y

Bloss, M. L. (1992). *Prediction of cemented rock fill stability design procedures and modelling techniques.* (PhD Thesis), University of Queensland, Brisbane.

Bridges, M. (2003). A new era in fill-retaining barricades. *AMC's newsletter "Digging Deeper" on current events and modern mining methodology.* Retrieved 05 Sept 2021.

Brinkgreve, R. B. J., Broere, W. and Waterman, D. (2004). PLAXIS finite element code for soil and rock analysis, 2D (Vol. Version 8.6). Delft, Netherlands: Plaxis bv.

Coulthard, M. A. (1999). Applications of numerical modelling in underground mining and construction. *Geotechnical and Geological Engineering,* 17(3), 373-385.

Cundall, P.A., Strack, O.D. (1979). A discrete numerical model for granular assemblies. *Geotechnique* 29(1), 47-65.

Duffield, C., Gad, E. and Bamford, W. (2003). Investigation into the Structural Behaviour of Mine Brick Barricades. AusIMM Bulletin, 2(2,Mar/April), 44-50.

Dunnicliff, J. (1988). *Geotechnical Instrumentation for monitoring field performance*. New York: John Wiley and Sons.

Fahey, M., Helinski, M. and Fourie, A. (2009). Some aspects of the mechanics of arching in backfilled stopes. *Canadian Geotechnical Journal*, 46(11), 1322-1336. doi: 10.1139/T09-063

Frydman, S. and Keissar, I. (1987). Earth Pressure on Retaining Walls Near Rock Faces. *Journal of Geotechnical Engineering,* 113(6), 586-599. doi: 10.1061/(ASCE)0733-9410(1987)113:6(586)

Grice, A. (1989). Fill research at Mount Isa mines limited. In (Ed.), Fourth International symposium on mining with backfill (pp. 15–22). Montreal, Canada.

Grice, T. (2001). Recent minefill developments in Australia. In Stone, D. (Ed.), seventh international symposium on mining with backfill. Seattle, Washington: Society for Mining, Metallurgy and Exploration.

Handy, R. L. (1985). The arch in soil arching. *Journal of Geotechnical Engineering*, 111(3), 302-318. doi: 10.1061/(ASCE)0733-9410(1985)111:3(302)

Harrop-Williams, K. (1989). Arch in Soil Arching. *Journal of Geotechnical Engineering,* 115(3), 415-419. doi: 10.1061/(ASCE)0733-9410(1989)115:3(415)

Helinski, M., Fahey, M. and Fourie, A. (2011). Behavior of Cemented Paste Backfill in Two Mine Stopes: Measurements and Modeling. *Journal of Geotechnical and Geoenvironmental Engineering,* 137(2), 171-182. doi: 10.1061/(ASCE)GT.1943-5606.0000418

Itasca Consulting Group (2021). FLAC-Fast Lagrangian Analysis of Continua (2D), Ver. 7.0. Minneapolis: Itasca

Itasca Consulting Group (2023). PFC - Particle Flow Code (2D), Ver. 6.0. Minneapolis: Itasca

Jaky, J. (1944). The coefficient of earth pressure at rest. *Journal of the Society of Hungarian Architects and Engineers*, 7(2), 355-358.

Janssen, H. (1895). Versuche uber Getreidedruck in Silozellen. *Zeitschrift des Vereines deutscher Ingenieure,* 39, 1045-1049.

Jayakodi, J. D. S. U., Bennett, R. J., Reddicliffe, A. J., Sivakugan, N. and To, P. (2021). Laboratory modelling of stresses within the minefills and loads on barricades. Proceedings of 3rd International Conference in Geotechnical Engineering (pp. 247‑252) Colombo, Sri Lanka.

Jayakodi, S., Sivakugan, N. and To, P. (2024). Geotechnical Considerations of Mine Tailings Management through Mine Backfilling. In: Das, S.K., Reddy, K.R., Nainegali, L., Jain, S. (eds) Geoenvironmental and Geotechnical Issues of Coal Mine Overburden and Mine Tailings. *Springer Transactions in Civil and Environmental Engineering*. Springer, Singapore. https://doi.org/10.1007/978-981-99-6294-5_1

Knutsson, S. (1981). Stresses in the hydraulic backfill from analytical calculations and in situ measurements. In (Ed.), Application of Rock mechanics to Cut and Fill mining (pp. 261-268). Lulea, Sweden: Institution of Mining and Metallurgy, London.

Krynine, D. P. (1945). Discussion of 'stability and stiffness of cellular cofferdams' by K. Terzaghi. *Transactions of American Society of Civil Engineers*, ASCE, 110, 1175-1178.

Kuganathan, K. (2001). Mine backfilling, backfill drainage and bulkhead construction–a safety first approach. *Australian Mining Monthly,* February. 58–64.

Kuganathan, K. (2002). A method to design efficient mine backfill drainage systems to improve safety and stability of backfill bulkheads and fills. In (Ed.), 8th Underground operators' conference, growing our underground operations (pp. 181–188). Townsville: AUSIMM, Carlton, Vic.

Kuganathan, K. (2005). Hydraulic Fills. In Potvin, Y., Thomas, E. D. & Fourie, A. (Eds.), *Handbook on Mine Fill* (pp. 23-47). Perth: Australian Centre for Geomechanics.

Ladanyi, B. and Hoyaux, B. (1969). A study of the trap-door problem in a granular mass. Canadian Geotechnical Journal, 6(1), 1-14. doi: 10.1139/t69-001

Lenczner, D. (1963). An investigation into the behaviour of sand in a model silo. *The Structural Engineer,* 41(12), 389-398.

Li, L. and Aubertin, M. (2009a). Horizontal pressure on barricades for backfilled stopes. Part I: Fully drained conditions. *Canadian Geotechnical Journal,* 46(1), 37-46.

Li, L. and Aubertin, M. (2009b). Numerical investigation of the stress state in inclined backfilled stopes. *International Journal of Geomechanics,* 9(2), 52-62. doi: 10.1061/(ASCE)1532-3641(2009)9:2(52)

Li, L., Aubertin, M. and Belem, T. (2005). Formulation of a three dimensional analytical solution to evaluate stresses in backfilled vertical narrow openings. *Canadian Geotechnical Journal,* 42(6), 1705-1717. doi: 10.1139/t05-084

Li, L., Aubertin, M., Simon, R., Bussière, B. and Belem, T. (2003). Modelling arching effects in narrow backfilled stopes with FLAC. In (Ed.), 3rd International symposium on FLAC and FLAC3D numerical modelling in geomechanics (pp. 211–219). Ontario, Canada.

Marston, A. (1930). The theory of external loads on closed conduits in the light of the latest experiments. Bulletin 96 of the Iowa Engineering Experiment Station, 138-170.

Marston, A. and Anderson, A. O. (1913). The theory of loads in pipes and ditches, and tests of cement and clay drain tile and sewer pipe. In Marston, A. (Ed.), *Bulletin number* 31 (Vol. xi, pp. 30-88). Ames, Iowa.: Engineering Experiment Station, Iowa State College of Agriculture and Mechanic Arts.

Mitchell, R., Smith, J. and Libby, D. (1975). Bulkhead pressures due to cemented hydraulic mine backfills. Canadian Geotechnical Journal, 12(3), 362-371.

Mitchell, R., Olsen, R. and Smith, J. (1982). Model studies on cemented tailings used in mine backfill. *Canadian Geotechnical Journal,* 19(1), 14-28. doi: 10.1139/t82-002

Mitchell, R. and Roettger, J. (1984). Bulkhead pressure measurements in model fill pours. CIM Bulletin, 77(888), 50-55.

Mitchell, R. J. (1989). Model studies on the stability of confined fills. Canadian Geotechnical Journal, 26(2), 210-216. doi: 10.1139/t89-030

Mitchell, R. (1992). Centrifuge model studies of fill pressures on temporary bulkheads. *CIM Bulletin,* 85,(960) 48-54

Pirapakaran, K. and Sivakugan, N. (2007a). Arching within hydraulic fill stopes. *Geotechnical and Geological Engineering*, 25(1), 25-35. doi: 10.1007/s10706-006-0003-6

Pirapakaran, K. and Sivakugan, N. (2007b). A laboratory model to study arching within a hydraulic fill stope. Geotechnical Testing Journal ASTM, 30(6), 496-503. doi: 10.1520/GTJ103693

Potvin, Y., Thomas, E. and Fourie, A. (2005). *Handbook on mine fill*: Australian Centre of Geomechanics, The University of Western Australia.

Potyondy, D.O., Cundall, P. (2004). A bonded-particle model for rock. *International journal of rock mechanics and mining sciences* 41 (8):1329-1364.

Qin, J., Zheng, J., & Li, L. (2021). An analytical solution to estimate the settlement of tailings or backfill slurry by considering the sedimentation and consolidation. *International Journal of Mining Science and Technology*, 31(3), 463-471. doi: 10.1016/j.ijmst.2021.02.004

Rankine, K., Sivakugan, N. and Cowling, R. (2006). Emplaced geotechnical characteristics of hydraulic fills in a number of Australian mines. *Geotechnical and Geological Engineering*, 24(1), 1-14.

Rankine, R., Pacheco, M. and Sivakugan, N. (2007). Underground mining with backfills. *Soils and Rocks*, 30(2), 93-101.

Revell, M. and Sainsbury, D. (2007b). Paste bulkhead failures. In Hassani, F., Archibald, J. & Nantel, J. (Ed.), Minefill 2007: 9th international symposium on mining with backfill. Montreal: Canadian Institute of Mining, Metallurgy and Petroleum.

Sivakugan, N. (2021). *Soil Mechanics and Foundation Engineering*: McGraw Hill, New York.

Sivakugan, N. (2008). Drainage issues and stress developments within hydraulic fill mine stopes. Australian Journal of Civil Engineering, 5(1), 61(11).

Sivakugan, N. and Widisinghe, S. (2013). Stresses Within Granular Materials Contained Between Vertical Walls. Indian Geotechnical Journal, 43(1), 30-38. doi: 10.1007/s40098-012-0029-z

Sivakugan, N., Widisinghe, S. and Wang, V. (2014). Vertical Stress Determination within Backfilled Mine Stopes. *International Journal of Geomechanics,* 14(5), 06014011. doi: 10.1061/(ASCE)GM.1943-5622.0000367

Smith, J. and Mitchell, R. (1982). Design and control of large hydraulic backfill pours. CIM Bulletin, 75,(838) 102-111.

Take, W. A. and Valsangkar, A. J. (2001). Earth pressures on unyielding retaining walls of narrow backfill width. *Canadian Geotechnical Journal,* 38(6), 1220-1230. doi: 10.1139/cgj-38-6-1220

Terzaghi, K. (1920). Old earth-pressure theories and new test results. Engineering News-Record, 85(13), 632-637.

Terzaghi, K. (1943). *Theoretical soil mechanics*: John Wiley & Sons, New York. Pages 66-99.

Thakur, S.C., Ooi, J.Y., Ahmadian, H. (2016). Scaling of discrete element model parameters for cohesionless and cohesive solid. Powder Technology 293:130-137

Thompson, B. D., Bawden, W. F. and Grabinsky, M. W. (2012). In situ measurements of cemented paste backfill at the Cayeli Mine. *Canadian Geotechnical Journal,* 49(7), 755-772. doi: 10.1139/t2012-040

Thompson, B. D., Grabinsky, M. W., Bawden, W. F. and Counter, D. B. (2009). In situ measurements of cemented paste backfill in long-hole stopes. In Diederichs, M. & Grasselli, G. (Ed.), ROCKENG09; 3rd CANUS Rock Mechanics Symposium. Toronto.

Thompson, B. D., Hunt, T., Malek, F., Grabinsky, M. W. and Bawden, W. F. (2014). In situ behaviour of cemented hydraulic and paste backfills and the use of instrumentation in optimising efficiency. In Potvin, Y. & Grice, A. G. (Ed.), Minefill 2014: 11th International Symposium on Mining with Backfill (pp. 337-350). Perth: Australian Centre for Geomechanics.

Ting, C. H., Sivakugan, N. and Shukla, S. K. (2012a). Laboratory simulation of the stresses within Inclined stopes. *Geotechnical Testing Journal* ASTM, 35(2), 1-15. doi: 10.1520/GTJ103693

Widisinghe, S.D. (2014). Stress developments within a backfilled mine stope and the lateral loading on the barricade. (PhD thesis), James Cook University, Queensland.

Yang, M. and Deng, B. (2019). Simplified Method for Calculating the Active Earth Pressure on Retaining Walls of Narrow Backfill Width Based on DEM Analysis. *Journal of Advances in Civil Engineering*. doi: 10.1155/2019/1507825

Yumlu, M. and Guresci, M. (2007). Paste backfill bulkhead failures and pressure monitoring at Cayeli mine. CIM Bulletin, 1001-10.

Appendix A

The Chapter 2 of this dissertation is covered by the published research article, attached below.

Chapter 1
Geotechnical Considerations of Mine Tailings Management through Mine Backfilling

Seneth Jayakodi, Nagaratnam Sivakugan, and Peter To

1.1 Mining and Mine Backfilling

Mining is a complex but systematic process of extracting valuable minerals from ore deposits. Currently, almost every continent in the world except Antarctica is undergoing mining activities extensively and the major contributing countries include Australia, Brazil, Canada, China, India, Poland, South Africa and USA. Nature has bestowed Australia generously with valuable minerals and the amount the country has mined out thus far is considerably less compared to the amount it reserves. Main Australian mining commodities are Gold, Zinc, Copper, Lead, Coal, Silver, Diamonds, Mineral Sands and Bauxite for which Australia is known as the world's largest producer. Mining contributes a substantial proportion to the country's Gross Domestic Product (GDP) and is the backbone of the Australian economy. Mining of all resources contributes about 10% to Australia's GDP and around 60% of total export revenue [1]. The BHP Group, Rio Tinto, Glencore, Fortescue Metals, Newcrest Mining, South32, Northern Star Resources and Evolution Mining are some major mining companies operating in Australia. Figure 1.1 shows the locations of major mines and mineral deposits in Australia.

Mining can be categorised as open pit mining and underground mining based on the orientation and location of the deposit. When the ore deposit is at shallow depth and spreading more longitudinally, it can be mined out by removing the overburden as the open pit mining method. In contrast, when the ore body is located deep inside the ground, underground mining techniques are adopted to reach the ore body through shafts and cross-cut tunnels, and to extract the valuable ore where the removal of ore generates large voids, known as stopes. These stopes are accessed through horizontal drives located along the ore body, allowing access to machinery

S. Jayakodi (✉) · N. Sivakugan · P. To
College of Science and Engineering, James Cook University, Townsville, Queensland, Australia
e-mail: seneth.jayakodi@my.jcu.edu.au

S. K. Das et al. (eds.), *Geoenvironmental and Geotechnical Issues of Coal Mine Overburden and Mine Tailings*, Springer Transactions in Civil and Environmental Engineering, https://doi.org/10.1007/978-981-99-6294-5_1

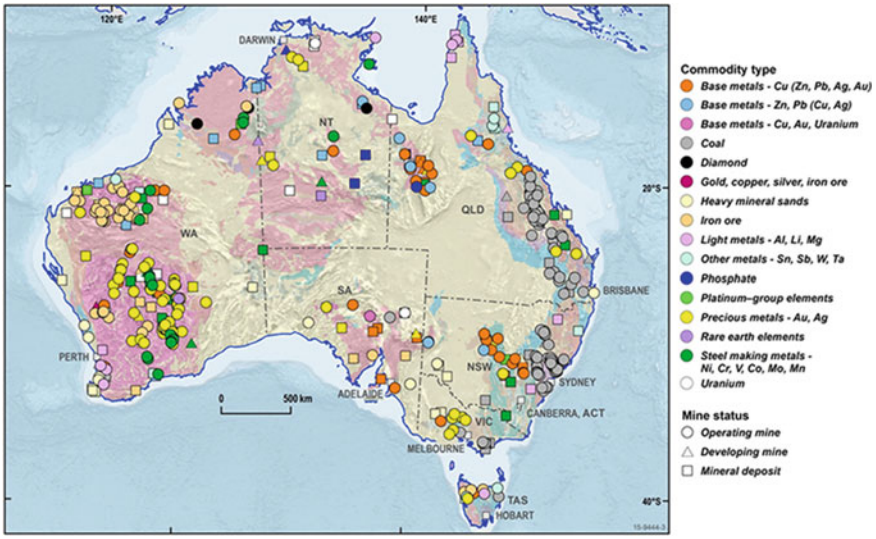

Fig. 1.1 Major mining and mineral deposits in Australia, 2016 (*Source* Major mining and mineral deposits in Australia, 2016 https://www.ga.gov.au/education/classroomresources/minerals-energy/australian-mineral-facts by Geoscience Australia which is © Commonwealth of Australia and is provided under a Creative Commons Attribution 4.0 International Licence and is subject to the disclaimer of warranties in section 5 of that licence)

and other underground services. Underground mine stopes have base dimensions of 10–15 m or more and heights as high as 100 m or more, and they are assumed rectangular in cross section for analytical purposes [2]. Once the ore has been removed and processed, the stope requires backfill for surrounding stability and continued production. The backfilling of stopes can represent up to 20% of underground mining costs [3]. The horizontal drives need to be barricaded or capped to allow for the backfill process to take place. The construction and performance of these barricades is a major topic in the mining industry today. The correct calculation of the stress state in the backfill and the associated pressures exerted on the barricade is a critical engineering challenge [4].

Mine backfilling is an essential step in the mining cycle for artificially supported underground mines [5]. An efficient backfill system provides several operational and economic benefits such as maximum ore extraction, minimum ore dilution, improvement of regional stability around the ore body, avoid the risk of land subsidence of mined out premises, ensure the safety of miners, etc. In addition, backfilling plays a vital role in the disposal of mine tailings with a minimum impact to the environment, thus ensuring sustainable mining practice. The mining industry in Australia is also the largest generator of solid wastes [6], making the backfilling of voids and the disposal of tailings an integral part of the mining process [7]. The mine tailings are waste material generated during the mining process which should be carefully disposed to Tailing Storage Facilities (TSF) surrounded by tailing dams [8], and/

or used to backfill the underground voids. The underground voids created annually in Australia can reach 10 million cubic metres [3]. Though the backfill system is often expensive, typically covering about 30% of total mining costs, reliability and flexibility of the backfill system greatly support the mining operation [9]. Backfilling gives an extra advantage over tailing dams as it rules out the cost for constructing tailing dams, negates the acquisition of massive land surface for TSFs, and reduces the negative environmental impacts.

1.2 Types of Mine Backfills

Backfills are generally processed mine tailings and are in the form of Hydraulic fills, Paste fills, Aggregate fills, Rock fills, Sand fills, etc. The choice of materials that are utilized for backfill operation depends on the location of backfilling, availability of materials for a particular fill, physicochemical properties of the materials, and prevailing ground conditions. Backfills are of two types according to cohesiveness namely Granular backfills (no cohesion) and Cohesive backfills. Further, backfills fall into two main categories based on the backfilling strategy being used as Cemented and Uncemented.

1.2.1 Uncemented Backfills

Uncemented backfills have no binding agents mixed thus mechanical behaviour and performance can be studied using soil mechanics theories. This includes Sand fills (SF), Rock fills (RF), Aggregate fills (AF), and Hydraulic fills (HF).

Hydraulic Fills (HF)

Hydraulic fills are sandy silts (ML) or silty sands (SM) with no clay fraction where the fine fraction is removed by the desliming process using hydrocyclones. Physicochemical properties of the fill material are among the first few important aspects, to understand the suitability of the material for a particular backfilling process. Particle size distribution, specific gravity, bulk density, Atterberg limits, relative density, permeability, angularity of grains, friction angle, etc. are the main physical characteristics of the fill material while the chemical properties include the presence of mineral phases, elemental composition, acidity/alkalinity, total organic compounds, heavy metal concentration, etc. [10, 11]. According to Rankine et al. [12] and Sivakugan et al. [13], based on the analysis of more than 25 HFs from different major mines in Australia, it has been found that all fills fall within a narrow particle size distribution band and the specific gravity of the grains are in the range of 2.8–4.5 due to presence of heavy metals. HFs have very sharp, angular grains, giving higher friction angles (ϕ) than those for natural soils. All HF slurries settling only under self-weight, manage to settle at high relative densities (D_r) of 40–70%. According to Pettibone

and Kealy [14], the in-situ measurements showed D_r values ranging from 44 to 66% at four different mines in the United States and that confirms the above laboratory test results by Rankine et al. [12] and Sivakugan et al. [13]. Further, HF has void ratio (e) of 0.67, and porosities (n) of 37–49% and dry unit weight (γ_d) in kN/m^3 of 5.7 times specific gravity [$\gamma_d\left(\text{kN/m}^3\right) = 5.7G_s$]. Typical γ_d of HF is in the range of 16–25 kN/m^3 [12]. The lower cost for production and transportation through pipelines, and the simplicity in handling are the main advantages of hydraulic fills.

Behaviour of Hydraulic Fill during Backfilling Operation

Hydraulic fills are initially transported to the stope in the form of a slurry through pipelines, at solid contents of 65–75% [12, 13]. The horizontal drives blocked by a barricade wall, made of special porous bricks with permeability (k) 2 or 3 orders of magnitude greater than that of HF [12], retains the fill and allows the water to drain through. The horizontal access drives are often located at more than one level. Initially, the drives located at upper levels of the vertical stope act as exit points for the decanted water, and also serve as drains when the HF rises in the stope [13]. Filling the stope does not occur instantaneously or continuously at one stretch instead it is carried out as layer filling with breaks/laps at certain filling intervals, allowing for drainage (e.g., 12 h filling and 12 h resting).

Drainage Considerations

One of the primary causes of barricade failures is liquefaction which is often referred as 'mud rush' by miners. This scenario occurs when the pore water pressure builds up and reduces the effective stresses and hence the shear strength within the stope as a result of poor drainage in the hydraulic fill system.

Herget and De Korompay [15] have suggested that the minimum hydraulic conductivity/permeability (k) of HF should be 100 mm/h in order for the fill to perform satisfactorily. When the permeability is high, faster removal of water from the stope helps to increase the stability of the mine fill stope. Grice [16] has suggested that the effective grain size $D_{10} > 10$ μm will ensure adequate drainage.

Sivakugan et al. [13] observed that when $k = 7$–35 mm/h, HF systems in the mine stopes performed well, suggesting that Herget and De Korompay [15] threshold value is too conservative. D_{10} for adequate drainage was found to be 10–40 μm, satisfying Grice's [16] recommendation. However, the anecdotal evidence and back calculations using the measured flow in the mine stopes suggest that the permeability of the HF in the mine is often larger than what is measured in the laboratory under controlled conditions [7]. Brady and Brown [17] and Kuganathan [18] proposed permeability values in the range of 30–50 mm/h, which are significantly larger than those measured in the laboratory for similar fills but still their values are much less than the threshold limit prescribed by Herget and De Korompay [15], which is 100 mm/h. Figure 1.2 shows drainage pipes fixed to the reinforced concrete barricade wall to release water out from the HF slurry and to avoid building up the pore water pressure within the fill.

Fig. 1.2 Drainage pipes fixed to the reinforced concrete barricade to drain the water from hydraulic fill slurry

Stability Considerations

The stability of the HF stope depends on several parameters that govern the strength and stiffness of the fill which are directly related to the relative density of the fill. When the HF is denser, the relative density (D_r) and friction angle (ϕ) are higher, and thus the fill is more stable. Oedometer tests on HF showed significant creep settlements that took place on the completion of consolidation settlements [13].

1.2.2 Cemented Backfills

Cemented backfills include a small amount of binding agent such as cement, fly ash, gypsum, blast furnace slag to improve strength. Following fill types are some examples for cemented backfills.

Cemented hydraulic fills (CHF) have grain size < 420 μm and are more similar to paste fill but the significant difference is larger particle size distribution (PSD) compared to paste fill.

Cemented rock fill (CRF) is a mixture of RF with CHF (RF:CHF = 1:1 to 3:1 by weight) and the properties vary within the stope as the two fills segregate during placement.

Cemented aggregate fill (CAF) is a mixture of AF with CHF (AF:CHF = 1:3 by weight) and it suffers from segregation thus properties vary within the stope like in CRF.

Paste Fills (PF)

Paste fills use a very fine fraction of the tailings. A rule of thumb is that 15% of particles should be less than 20 μm, with a typical effective particle size (D_{10}) of 5 μm [19]. PF is a mixture of tailing material with a small percentage of binder, in the order of 3–6% by weight, and water [13]. The PSD is finer than HF and CHF, but have negligible colloidal fraction finer than 2 μm, and the maximum particle size is around 350–400 μm [13]. However, during transport, Pullum [19] has shown stratification of paste during pipe flow with all paste fills with a maximum particle size of over 20 μm. Paste fills with the maximum particle size D_{max} < 20 μm tend to form homogeneous paste fills during both transportation and deposition.

Paste fills fall into the broad category of thickened tailings which was introduced by Dr Ely Robinsky in the mid 1970s [20]. It is the densest form of backfill in the spectrum of thickened tailings placed underground as a backfill material [20, 21]. Thickened tailings are a special case of slurry tailings and tend to show many similar characteristics to paste, but paste fills are not same as thickened tailings. The primary difference is that the thickened tailings will segregate or settle out once a minimum velocity is reached. Hydraulic fills fall into the thickened tailings profile. However, a significant difference with the PF in terms of drainage is that the water content in paste fill is retained on placement, through the large surface area of the particles, eliminating the need for the design of drainage of the fill or barricades. Hence, the static and dynamic stability requirements should only be considered when designing paste filled stope systems. The static stability requirement is addressed by designing the PF system with an adequate strength to ensure that the vertical walls of the backfilled stopes remain stable throughout the mining of neighbouring stopes. If the paste becomes unstable, the adjacent walls may relax and displace into the open stope, causing high level of dilution and loss of mining economics. The dynamic stability of the PF system is achieved by designing the backfill mass to resist liquefaction or other seismic activities. There is a high risk of liquefaction in a PF system due to increased residual moisture content in the PF. According to Clough et al. [22], cemented sand with an Unconfined Compressive Strength (UCS) of 100 kPa was capable of resisting a seismic activity measuring 7.5 on the Richter scale and this value has been used by the mining industry as the minimum design strength of fill for any fill mass. The strength of PF satisfying static stability requirements is generally in excess of dynamic strength requirements. Because of no drainage requirement in PF system, the barricades are designed as temporary structures in PF stopes. Nevertheless, barricades must be designed with sufficient strength to retain the liquid mass of fill, until such time as it has cured properly to act as a plug at the base of

the stope, thus preventing the additional deposited paste from entering the mine workings.

1.3 Stress Developments within Backfilled Mine Stopes

1.3.1 General

Mine stopes which have been generated by the ore removal during mining, are backfilled with processed mine tailings called backfills. A stope can be approximated as a cuboid with the cross-section dimensions of 10–15 m and vertical wall heights exceeding 100 m and thus the aspect ratio falls between 6 and 10. Backfilled or non-backfilled stopes are interconnected by horizontal access drives with a typical cross section of 5 m $\times$ 5 m or 6 m $\times$ 6 m, located at different sublevels of the stope, which allow access to mine machinery and other underground services.

1.3.2 Theory of Soil Arching

Arching phenomenon occurs when the frictional material moves against stable strata where the relative movement generates shear stresses along the interface that tend to hold the frictional material at its initial position. As result, the vertical stresses within the yielding material will be lower than the actual overburden stress, and that is known as arching [23].

Arching plays a significant role in many geotechnical and mining applications such as earth pressure on retaining walls [24–26], underground situations such as backfilled trenches and underground mine stopes [23, 27–32], pressures on piles and piled embankments [33–35], loadings on ditch conduits and pressures on buried structures [25, 36–40], designing storage silos (e.g., vessels storing granular materials such as chemical powders, capsules in pharmaceutical industry, flour, cement) [41, 42].

Arching Effect in Backfilled Mine Stopes

During filling, the vertical shear stresses acting on the stope walls can be significant. As a result, the vertical normal stress anywhere within the fill can be significantly less than the actual overburden pressure (γz) where γ is the unit weight of the fill and z is the fill height from top. Therefore, a substantial amount of the fill load is carried by the rock walls in the form of shear stresses [23].

1.3.3 Analytical Methods to Investigate Arching Effect

Some of the analytical solutions for arching and stresses within backfills include the 3D sliding wedge failure method [43], Simple arching theory and its modifications [29, 36, 40, 44], etc.

Mitchell et al. [43]:

In reality, backfilled stopes are surrounded by adjacent rock mass thus the backfill material is subjected to lateral confinement. The confined block mechanism (3D Sliding Wedge Failure) explained how the rock walls' support to reduce the fill stress due to arching effect in a confined environment like mine stope. The design strength required for stability is given by

$$UCS = \left(\gamma - 2\frac{c}{l}\right)\left[h - \frac{w}{2}\tan\alpha\right](\sin\alpha)(F) \tag{1.1}$$

γ Bulk unit weight of the fill (kN/m^3)
c Cement bond strength of the fill/Cohesion (kPa)
l Length of the block (m)
h Height of the block (m)
w Width of the block (m)
α Angle of failure plane from horizontal ($= 45° + \phi/2$)
ϕ Friction angle of the fill
F Safety factor

In the long term, the UCS of the fill is mainly due to binding agents, and strength contributed by friction can be neglected (i.e., $\phi = 0$). For frictionless material, $c = UCS/2$ ($q_u = 2c_u$). Then Eq. (1.1) becomes

$$UCS = \left(\gamma - \frac{UCS}{l}\right)\left(h - \frac{w}{2}\right)\frac{F}{\sqrt{2}} \tag{1.2}$$

Equation (1.2) can be simplified further as below by assuming $F = \sqrt{2}$ and $h \gg l$

$$UCS = \frac{\gamma h}{h/l + 1} \tag{1.3}$$

Marston's theory [36]:

Janssen [41] observed a significant vertical stress reduction in a corn-filled silo, compared to overburden stress (γz). Attributing this reduction to arching, an expression was developed using the limit equilibrium method to determine the average vertical stress at any given depth of the fill (z). This was later modified by Marston considering a 2D plane strain theory (for a trench) on arching and equations were

developed to compute the vertical (σ_v) and horizontal (σ_h) normal stresses within cohesionless ($c = 0$) mine fill stope as below.

$$\sigma_v = \frac{\gamma w}{2\mu K_a}\left[1 - exp\left(-\frac{2K_a \mu z}{w}\right)\right] \tag{1.4}$$

$$\sigma_h = K_a \sigma_v \tag{1.5}$$

$$K_a = \tan^2(45^\circ - \phi/2) \tag{1.6}$$

γ Unit weight of the fill
w Stope width
z Fill depth from top of the fill
ϕ Friction angle of backfill
μ Coefficient of friction of backfill and wall (rock) ($\mu = \tan\ \delta$)
δ Interfacial friction angle between the wall and the fill (between $1/3\ \phi$ and $2/3\ \phi$)
K_a Rankine's active earth pressure coefficient

Terzaghi's theory [40]:

This includes the effect of cohesion into the Marston's equation enabling it to be used for any soil.

$$\sigma_v = \frac{(\gamma w - 2c)}{2K\ \tan\ \phi}\left[1 - exp\left(-\frac{2Kz\ \tan\ \phi}{w}\right)\right] \tag{1.7}$$

$$\sigma_h = K\sigma_v \tag{1.8}$$

$$K = \frac{1}{1 + 2\tan^2\ \phi} \tag{1.9}$$

c Cohesion of the fill
$\tan\ \phi$ Coefficient of internal friction of fill (same as μ, but with $\delta = \phi$)
K Lateral earth pressure coefficient

Aubertin et al. [44]: Modified Marston's theory

Marston's theory uses the active earth pressure coefficient (K_a) in the equation. However, the Aubertin et al. [44] solution (Eq. 1.10) is based on status of the stope wall during filling operation assuming the fill to be in active, passive or at-rest state.

$$\sigma_v = \frac{\gamma w}{2K\tan\ \phi}\left[1 - exp\left(-\frac{2Kz\tan\ \phi}{w}\right)\right] \tag{1.10}$$

$$\sigma_h = K\sigma_v \tag{1.11}$$

Active Earth Pressure Coefficient $K_a = \tan^2(45^\circ - \phi/2)$

Passive Earth Pressure Coefficient $K_p = \tan^2(45^\circ + \phi/2)$

At-rest Earth Pressure Coefficient $K_0 = 1 - \sin\ \phi$

Extended Marston's theory [23]:

Analytical solutions provided by Aubertin et al. [44], Marston [36] and Terzaghi [40] are for the 2D stope where the fill is subjected to plane strain loading (e.g., a trench). In reality, mine stopes are rarely 2D. Therefore, it is useful to extend these theories to 3D. Therefore, equations were developed for square and circular stopes as well.

Circular stopes are uncommon, but they are quite easy to model using finite element or finite difference methods as axisymmetric problems. Square stopes can only be approximated as axisymmetric problems.

Vertical and horizontal stresses which are acting within the backfilled rectangular stope can be found as follows.

$$\sigma_v = \frac{\gamma w}{2K\tan\ \delta}\left(\frac{l}{l+w}\right)\left[1 - exp\left\{-2\left(\frac{l+w}{lw}\right)Kz\tan\ \delta\right\}\right] \tag{1.12}$$

$$\sigma_h = K\sigma_v \tag{1.13}$$

$$\sigma_h = \frac{\gamma w}{2\tan\ \delta}\left(\frac{l}{l+w}\right)\left[1 - exp\left\{-2\left(\frac{l+w}{lw}\right)Kz\tan\ \delta\right\}\right] \tag{1.14}$$

For square stopes ($w = l$),

$$\sigma_v = \frac{\gamma w}{4K\tan\ \delta}\left[1 - exp\left(-\frac{4Kz\tan\ \delta}{w}\right)\right] \tag{1.15}$$

$$\sigma_h = \frac{\gamma w}{4\tan\ \delta}\left[1 - exp\left(-\frac{4Kz\tan\ \delta}{w}\right)\right] \tag{1.16}$$

These equations are also valid for circular stopes and storage silos/vessels with circular cross section.

For a very long stope (i.e. $w/l = 0$), Eqs. (1.12) and (1.14) reduce to Eqs. (1.10) and (1.11), given by Aubertin et al. [44].

[Note: Here the backfill material is approximated as dry granular soils (Natural moisture content $w_n = 0$ and cohesion $c = 0$). No pore water pressure is present and hence effective stresses are equal to total stresses].

The reason for using K as K_0 is that typically rock is around two orders of magnitude larger in stiffness than backfill materials, and therefore wall movement is very small and once the backfill is put in place, it would be at rest condition confirming no lateral deformation of the wall due to the fill.

Pirapakaran and Sivakugan [23] have suggested that during loose backfilling, it is suitable to use the wall friction angle (δ) as 2/3 of the backfill friction angle

(ϕ). Numerical solutions have also shown that $K = K_0$ and $\delta = 0.67\ \phi$ in the analytical equations give predictions that compare better with the results from the Fast Lagrangian Analysis of Continua (FLAC) simulation program.

Arching theories [36, 40] have suggested that when arching occurs the vertical stress at the bottom of the filled stope is significantly less than that from the self-weight pressure/overburden pressure ($= \gamma z$).

Sivakugan and Widisinghe [32] have developed a general expression for the average vertical normal stress (σ_z) within the mine fill at a depth of 'z' from the top of the fill. For generality, the fill is assumed to have both cohesive and frictional properties, and a uniform surcharge of 'q' is applied at the top of the fill. The fill-wall interface has a friction angle of δ and adhesion of c_a. The lateral earth pressure coefficient is 'K'. The stope cross section has an area 'A' and perimeter 'P'.

$$\sigma_z = \frac{\left(\gamma - \frac{P}{A}c_a\right)}{K(\tan\ \delta)\frac{P}{A}}\left(1 - e^{-K(\tan\ \delta)\frac{P}{A}z}\right) + qe^{-K(\tan\ \delta)\frac{P}{A}z} \tag{1.17}$$

The first component in Eq. (1.17) comes from the fill weight and the second component is from surcharge at the top of the fill.

This Eq. (1.17) can be simplified to Eq. (1.12) by assuming the stope cross section to be rectangular (width $= w$, length $= l$), fill is granular ($c = 0$) and no surcharge is applied ($q = 0$).

The Eq. (1.17) can be simplified to Eq. (1.15) by assuming the stope cross section to be square (width = length $= w$), fill is granular ($c = 0$) and no surcharge is applied ($q = 0$).

The Eq. (1.17) can be simplified to Eq. (1.4) which was originally developed by Marston [36] for plane strain loading situation by assuming a narrow trench where, $l \gg w$, $A = lw$, $P = 2(l + w)$ and $P/A \cong 2/w$ and the backfill is granular ($c = 0$) and no surcharge is applied ($q = 0$).

The Eq. (1.17) can be simplified to Eq. (1.7) which is an extension of the Marston's theory by Terzaghi [40] by assuming a narrow trench situation with plane strain loading, incorporating cohesion to the backfill and no surcharge is applied ($q = 0$).

Concerns with Analytical Equations

Analytical solutions are based on several approximations and simplifications. Two of the common ones are:

(1) The vertical normal stress distribution within the backfill, at any depth, is assumed to be uniform. (i.e., both the analytical and laboratory test solutions reflect the average vertical normal stress at any depth of the fill, although laboratory models treat the soil mass as a particulate medium unlike in analytical approach, and also most numerical models treat the soil mass as a continuum)
(2) Assume an earth pressure coefficient as K_0, K_a or K_p.

1.3.4 *Lateral Earth Pressure Coefficient (K) used in Analytical Equations*

In a homogeneous fill, the lateral earth pressure coefficient (K) at any given point is defined as the ratio between effective horizontal stress and the effective vertical stress acting on the soil mass.

Marston [36] suggested that the lateral earth pressure coefficient (K) is given by the Rankine's active earth pressure coefficient (K_a) [45].

$$K_a = \tan^2\left(45 - \frac{\phi}{2}\right) = \frac{1 - \sin\ \phi}{1 + \sin\ \phi} \tag{1.18}$$

Terzaghi [40] used the lateral earth pressure coefficient given by Krynine [46]. For rough vertical walls, assuming $\delta = \phi$.

$$K = \frac{1}{1 + 2\tan^2\ \phi} = \frac{1 - \sin^2\ \phi}{1 + \sin^2\ \phi} \tag{1.19}$$

Handy [25] suggested that due to rotation of principal stresses near the wall, K increases from K_a towards K_0, and hence suggested the Jaky's [47] expression (Eq. 1.20) for K. Aubertin et al. [44]—modified Marston's theory suggested three cases of lateral earth pressure coefficients as the active (K_a), passive (K_p) (given by Rankine's expressions) and at-rest earth pressure coefficient (K_0-from Jaky's expression).

$$K_0 = 1 - \sin\ \phi \tag{1.20}$$

Relationship between Fill-Wall Interfacial Friction Angle (δ) and Friction Angle of the Fill (ϕ) [32, 48]

The fill-wall interfacial friction angle (δ) can be in the range of $0 - \phi$, depending on the roughness of the wall. In underground mine stopes that are backfilled, the walls formed by blasting and excavation can be very rough (Fig. 1.3). Hence, the slip of the fill takes place along a vertical plane at a few grain sizes away from the rock wall, on a fill-fill interface, where $\delta = \phi$. But in the case of grain silos or storage vessels, walls may not be very rough, and δ may be taken as 0.5–0.7 times ϕ as in the case of pile foundations and retaining walls.

Variation of $K \tan\ \delta$ against the Friction Angle of the Fill (ϕ) [32]

For very rough fill-wall interface ($\delta = \phi$), $K \tan \delta$ is insensitive to the friction angle of the fill. Here, with the increasing friction angle, $\tan \delta$ increases, and K decreases such that $K \tan \delta$ remains approximately the same. Hence, even an estimated friction angle would be adequate when applying analytical equations for a very rough fill-wall interface. Assuming at-rest conditions (i.e., K_0 from Jaky's [47] expression) and

Fig. 1.3 Roughness of mine stope walls

a very rough fill-wall interface (i.e., $\delta = \phi$, underground backfilled mine stopes), $K \tan \delta$ can be approximated as 0.3 for all friction angles ranging from 30° to 49°. For moderately rough fill-wall interface ($\delta = 0.5\,\phi$), $K \tan \delta$ increases slightly with the increase in friction angle of the fill.

1.3.5 The Essence of Numerical Modelling

Numerical modelling for mine backfilling is extremely valuable for large underground mines, where field measurements and monitoring of stresses, pore pressures, etc. is usually very challenging, costly or impractical at all. Moreover, software simulations are necessary as a validating tool for laboratory models and also to solve more complex scenarios that cannot be addressed analytically.

Numerical models embedded with correct input parameters, appropriate constitutive models and sensible boundary conditions can give more realistic predictions of stress behaviour within backfilled stopes. Examples are Bloss [49]-CHF TVIS model at Mount Isa mines, Pierce [50]-PF FLAC^{3D} at Brunswick mine, Canada; Rankine et al. [51]-PF FLAC^{3D} at BHP Cannington mine, Australia; Aubertin et al. [44]-HF 2D models using PHASE2, Li et al. [29]-HF 2D models using FLAC which is an explicit finite difference software being used in solving mining and geotechnical problems. It is worthwhile to note that a very long (length is significantly larger) narrow (height is much greater than width) rectangular trench can be modelled as a 2D plane strain problem in FLAC. A circular stope can be modelled representing an axisymmetric problem (symmetric around the center axis). For stopes with square and rectangular cross sections, modelling is in 3D.

Aubertin et al. [44] and Li et al. [29] models:

These models have demonstrated that the vertical normal stress at the bottom of the stope is lower than the actual overburden pressure (=γz). Further, the vertical stress reaches a peak value at the mid height of the stope which exceeds the overburden

pressure unrealistically. This may be due to the way they placed the fill in the stope during model construction. They assumed that the entire fill is placed instantaneously as one whole body of soil mass which is not the reality. Modelling with layer filling is more sensible and it mimics the actual backfilling process in the mine.

Pirapakaran and Sivakugan [23]:

Through FLAC modelling, it has been investigated that the vertical stress does not exceed the overburden pressure when the stope is filled layer by layer.

FLAC results for the fill stresses from both rectangular and circular stopes compare better with the results from the Marston's analytical equation with $K = K_0$ and $\delta = 0.67\ \phi$. Stress values from Modified Marston's equation [44] with $K = K_0$, $\delta = \phi$ and $K = K_a$, $\delta = \phi$ give lesser equality with the stresses from FLAC results.

Through the analysis of both rectangular and circular stopes, it has been evident that the lateral variation of the vertical normal stress across the stope width is non-uniform and the values are lower near to walls compared to that at the middle region. Also, the reduction of vertical normal stresses along the stope height is significantly increased when compared to the overburden pressures at locations along the stope height. This effect on vertical stresses is known as the arching effect.

It has been shown that the friction angle of the backfill material (ϕ) is increased with the increasing relative density (D_r) of soil mass. In general, the friction angle of any backfill type varies from 30 to 49 degrees, and depends on different packing densities. The influence of friction angles of hydraulic fills on vertical stresses has been studied for narrow stope and circular stope using FLAC simulations. The vertical stresses are approximately the same for all the friction angles within the upper region of the stope and the stresses are nearly equal for friction angles of 30 and 35 degrees in the middle region of the stope, but these are slightly reduced for 40 and 45 degrees. However, vertical stresses differ significantly for all angles closer to the stope floor region and it has showed completely different variations for vertical stresses when compared to analytical solutions. Further research is recommended to understand the stress developments within the stope for various friction angles at stope floor and closer regions.

1.3.6 Stress Variation within Mine Stopes Backfilled with Granular Soils

In-situ stress measurements within backfilled mine stopes have been reported in a few studies from past research [52–55]. Because of limited availability of field data, laboratory and numerical modelling of backfill systems has been carrying out for past few decades [4, 23, 29, 31, 32, 43, 44, 56–62].

Stress developments within backfilled mine stopes should be investigated considering the arching effect. There are three main independent approaches used extensively in geotechnical studies namely analytical equations, laboratory modelling, and numerical/statistical modelling simulations.

Analytical and numerical models based on continuum modelling approach, suggest that vertical normal stress within the fill reaches a maximum value at a certain depth beyond which the stress remains constant, whereas laboratory model tests show that the vertical normal stresses increase continuously even at very large depths without reaching any asymptotic value indicating that the behaviour of the soil mass should be analysed in particulate level.

Given the significance to the particulate modelling in geotechnical engineering, To and Sivakugan [63, 64] has analysed the stress distribution of granular material settling in silos using the Discrete Element Method (DEM). According to To and Sivakugan [64], it concluded that the experimental results for the stresses in the granular fill correlate better with DEM simulation results compared to other analytical and continuum modelling methods as shown in the dimensionless plot in Fig. 1.4. Fill stresses from DEM show a similar trend to that of lab model results where the stresses are increasing with the fill depth without reaching an asymptotic value in the case of analytical and Finite Difference Method (FDM) modelling. DEM results overestimate the vertical stress from the lab model results although the rates are similar. The difference is assumed to be attributed to the use of uniform spherical particles in DEM simulations where the friction is underestimated due to less number of contacts and contact areas, and hence higher stress generation within the fill. Therefore, further research on DEM simulations of stopes/silos filled with granular material considering the angularity of grains with more number of particles is highly recommended.

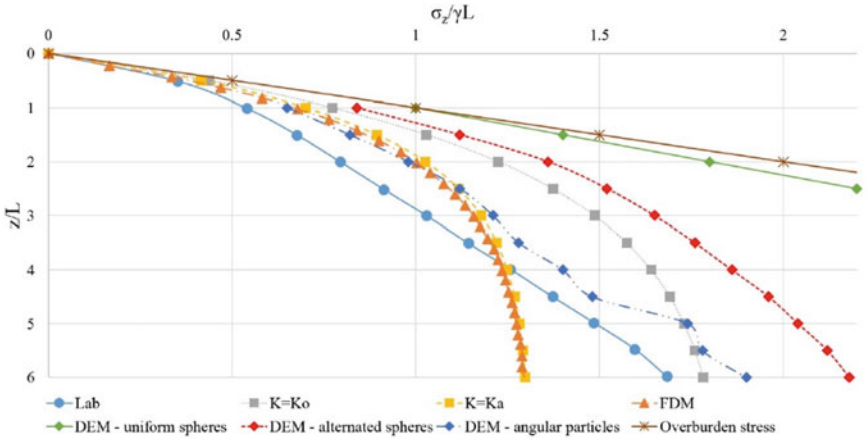

Fig. 1.4 DEM simulation of average vertical stress within a granular fill (*Source* To and Sivakugan [64])

Table 1.1 Evolution of analytical solutions for determining vertical stresses within backfills

Proposer	Material properties	Application	Result	K value	δ
Janssen [41]	Granular	Corn-filled silo	Average vertical normal stress		
Marston [36]	Granular (e.g., hydraulic fills)	2D plane strain loading (e.g., Trenches—very long narrow stopes)	Average vertical normal stress	K_a from Rankine	Between $1/3\ \phi$ and $2/3\ \phi$
Terzaghi [40]	Any material (both granular and cohesive)	2D plane strain loading (e.g., Trenches—very long narrow stopes)	Average vertical normal stress	K from Krynine	Equal to ϕ
Aubertin et al. [44]-Modified Marston's theory	Granular (e.g., hydraulic fills)	2D plane strain loading (e.g., Trenches—very long narrow stopes)	Average vertical normal stress	Three cases; K_a and K_p from Rankine's expressions K_0 from Jaky's expression	Equal to ϕ
Pirapakaran and Sivakugan [31]	Any material (both granular and cohesive)	3D mine fill stopes and storage vessels with rectangular, square and circular cross sections	Average vertical normal stress	K_0 from Jaky	Equal to $2/3\ \phi$
Handy [25], Li and Aubertin [59], Singh et al. [65]	Any material (both granular and cohesive)	2D inclined mine stopes	Maximum vertical normal stress	K_0 from Jaky	Equal to $2/3\ \phi$

The evolution of analytical solutions accounting the arching theory in determining vertical normal stresses within material filled structures is shown in Table 1.1.

1.3.7 Laboratory Modelling of Backfilled Stopes

According to Jayakodi et al. [66], a laboratory model apparatus was used to study the arching effect on the stresses within the hydraulic fill. Figure 1.5a shows a photograph of the laboratory model stope set up called the 'arching apparatus' and it is schematically drawn in Fig. 1.5b. High strength steel wires were used to suspend

the model to which a load cell was connected from the top of the frame. The model is positioned vertically such that the minimum possible gap between the stope and balance becomes 0.5 mm, ensuring that there is no any load registered on the balance. When the model is filled in layers with dry hydraulic fill of weight $(m+n)$, a fraction of the fill load is recorded on the balance at the bottom and the rest is registered on the load cell as the fill load carried by the walls. The load cell records the fill load transferred to the wall (m) and the balance reflects the fill load transferred to the bottom (n), given that the balance and load cell readings were zero at the start of the test. At any stage of filing, m and n can be measured separately through this setup. A square shape stope with breath $(B) = 150$ mm and height $= 900$ mm with an open bottom, was tested and the wall condition was varied from rough to smooth, to simulate underground mine wall roughness or a grain silo. Since the stope walls are very rough after blasting, the interfacial friction angle (δ) can be taken as the friction angle of the fill (ϕ) as the failure occurs on the fill-fill interface, not the fill-wall interface. Hence, a similar condition was created using a very rough sandpaper attached to the stope walls of the model, and acrylic planes were used as the smooth walls to represent the condition of a grain silo.

Figure 1.6 shows a dimensionless analysis to compare the laboratory result to that of Marston's equation (Eq. 1.4). Marston's analytical equation was used to express the stress variation for both K_a and K_0 cases separately. The ratio of vertical stress to the product of unit weight and the stope width/breath (i.e., $\sigma/\gamma B$) is plotted against

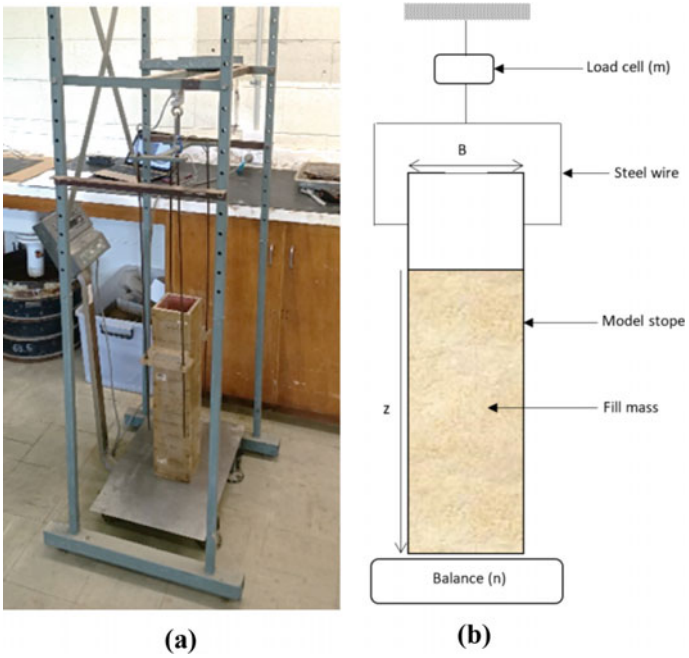

Fig. 1.5 Laboratory model stope setup **a** photograph **b** schematic diagram

the fill depth and stope breath ratio (i.e., z/B). The dimensionless analysis allows for the comparison of varying stope sizes and fill properties. Figure 1.6 depicts that the Marston's equation with $K = K_a$ largely overestimates the stresses whereas, $K = K_0$, $\delta = \phi$ condition gives more reasonable approximation to the laboratory results. Hence, the at-rest lateral earth pressure coefficient (K_0) is more reliable in Marston's equation (Eq. 1.4) to predict the stress at a depth approaching 6*B*, and this was reiterated by Pirapakaran and Sivakugan [23], however $\delta = 0.67\ \phi$ was applied. The mine stope walls are generally more competent and hence the wall movement is not expected in a backfill system. Therefore, the backfill can be considered more stable suggesting that K_0 is more realistic to use in the Marston's equation. Laboratory results from both rough and smooth wall conditions confirmed that the vertical stress is continuously increasing through to 6*B* depth, however the analytical solutions suggested an asymptotic value for the stress at a depth as low as 4*B*.

Sivakugan et al. [2] presented two distinct ways of developing the variation of vertical normal stress within the dry granular fill with the depth of the stope through numerical modelling, which give different values of stresses as shown in the dimensionless plot in Fig. 1.7.

Method 1: Vertical stress at the stope bottom for each fill layer, replicating the laboratory model test above (stress variation is measured only at the stope bottom).

Method 2: Vertical stresses at corresponding depths for each layer added, determined when filling the entire stope is completed.

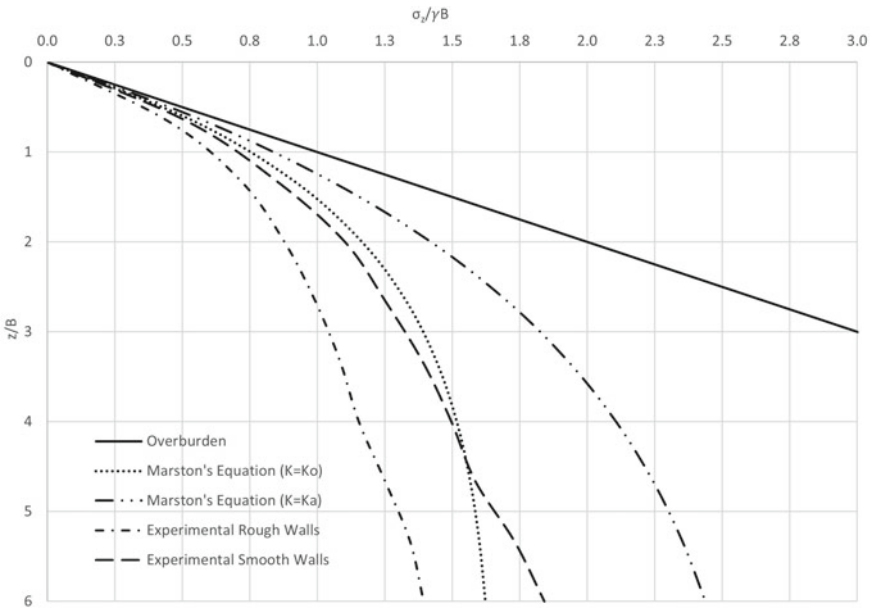

Fig. 1.6 Comparison of laboratory results and Marston's analytical solutions

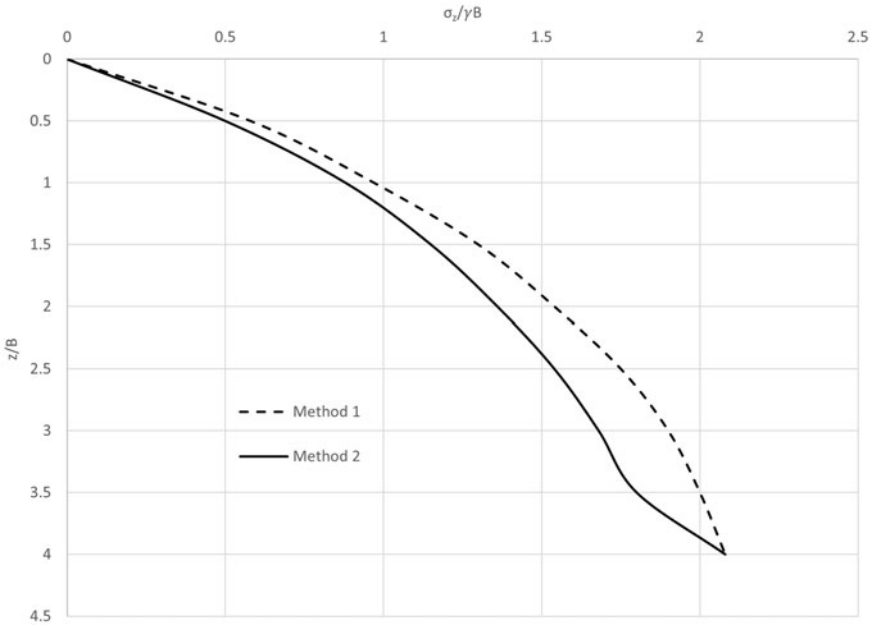

Fig. 1.7 Vertical stresses within granular fill in the stope

According to Sivakugan et al. [2], the two methods give significantly different vertical stress profiles except for the top and the bottom of the stope (see Fig. 1.7). The difference in the stress profiles is attributed to restricting the movement of stope bottom, implying zero displacement in any direction, assumed in numerical modelling.

In Method 2, downward movement of the fill is not restricted for all layers except for the bottom layer and hence, the friction along the wall is fully mobilised in the upper layers. When the fill movement is fully restricted for the bottom layer, more fill load is transferred to the bottom due to partial frictional mobility, which causes a sudden increase in the vertical normal stress closer to the bottom. This behaviour is clearly evident in the numerical modelling work carried out by Fahey [56], Kuganathan [57], Li and Aubertin [4], Pirapakaran and Sivakugan [23], and Ting et al. [67]. This approach is useful to estimate the vertical normal stresses at any depth of the fill, once the filling process has been completed.

In Method 1, the vertical normal stress is determined only at the stope bottom when the fill accumulates, unlike in Method 2. Therefore, the effect of the zero displacement of the stope bottom (i.e., partial mobilisation of shear stresses) is accounted for every layer, and hence, the sharp increase in vertical stress near the bottom, observed in Method 2, is not seen in Method 1. This method is more suitable in situations where the stresses at the bottom of the stope are required throughout the stope filling. For example, from engineering perspective, it is more important to determine the vertical stresses near the underground structure like barricade or at the bottom of the trench/

stope over the course of filling than knowing the vertical stress profile for the entire stope after filling is completed.

The stress patterns obtained from both methods show similar trends for stopes or trenches with different aspect ratios. In the case of Method 1, all the stress profiles obtained for any aspect ratio fall over an approximately similar path and hence, the use of a single stress curve is accepted. Although, a considerable deviation in stresses is observed with regard to the Marston's equation, Method 1 appears to follow the trend of the analytical (Marston) curve, which does not have the sudden increase in stresses near the stope floor known as 'kink', unlike in the curves from Method 2.

1.4 Loadings on Drive Barricades

1.4.1 General

In underground mines, the horizontal access drives that are connected to the mine stope at different sub-levels, are generally barricaded with strong retaining walls before backfilling the stope. The barricades are designed to be free draining such that they allow the water in the fill to seep through while retaining the fill. The construction of a barricade with special porous bricks is shown in Fig. 1.8. Realistic determination of the vertical stresses within the mine stope and correct estimation of loadings onto barricades can be a successful and correct approach to improving the design of barricades. The failure of the barricade can be catastrophic, with in-rush of wet hydraulic fill into the mines, trapping the miners and machinery. Between 1980 and 1997, 11 barricade failures were recorded at Mount Isa Mines in both HFs and CHFs [18]. In 2000, three fatalities were reported due to barricade failure at the Normandy Bronzewing Mine in Western Australia and later that same year, two barricade brick failures were reported as a result of HF contaminant at Osborne Mine in Queensland, Australia [3].

1.4.2 Design of Fill Barricades in Underground Mines

The construction of mine fill barricades is largely associated with the properties of barricade bricks and the stress state of the fill material in the stope and drive. According to Thompson et al. [68], it is anticipated that the horizontal normal stress acting on the barricade below 100 kPa will have a great chance to avoid failure. However, a proper evaluation of the stress state along the drive is essential to carry out safe barricade design work and also to determine the appropriate filling schedule. Analysing barricade stress behaviour for design and construction purposes by means of analytical equations, laboratory tests, and validating with numerical modelling is significantly important for safe and sustainable mining practice.

Fig. 1.8 Barricade being constructed using specially made very porous bricks

Analytical equations are useful for rational assessment of barricade performance for fill loads, however, the solutions are constrained by assumptions for barricade-rock interface properties, geometry simplifications, etc. Unlike in some analytical models that consider the arching of the fill load across the entire barricade, field observations indicate that the likelihood of barricade failure with punching shear at the center area of the wall is high [12, 18]. Kuganathan [69] expresses an analytical equation to determine the stresses on fill barricade as below.

$$\sigma_b = \sigma_o \times exp\left(-\frac{PLK_0 \tan \phi}{A}\right) \tag{1.21}$$

where, σ_b the horizontal stress at the barricade, σ_o the horizontal stress at the drive entrance, P the drive perimeter, A the barricade cross sectional area, L the barricade offset distance, and ϕ the friction angle of the fill.

1.4.3 Laboratory Modelling of Stress State at Drive Barricade

Jayakodi et al. [66] used, a laboratory model barricade comprising 310 mm diameter vertical stope and several drive attachments in the model tests (Fig. 1.9). The granular soil mass in the model has been subjected to surcharge loads (q) ranging from 30 to 900 kPa, and the soil pressures were recorded at the stope centre, stope edge and on the barricade face using three Earth Pressure Cells (EPC) attached in the model. The fill height within the vertical stope was 450 mm. A schematic diagram of the testing apparatus is shown in Fig. 1.10, clearly showing the three EPC locations.

Square (SD) and circular (CD) cross section drives of 100 mm and 150 mm width have been tested using the apparatus shown in Fig. 1.8 to determine the effect of drive shape and size on vertical and horizontal stress distribution. The barricade offset or

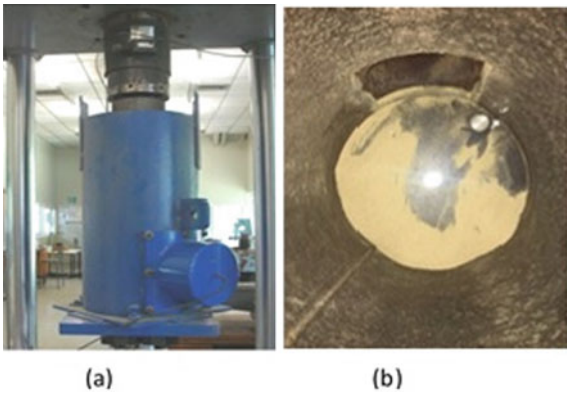

Fig. 1.9 **a** Drive barricade model apparatus **b** EPCs attached to the stope base

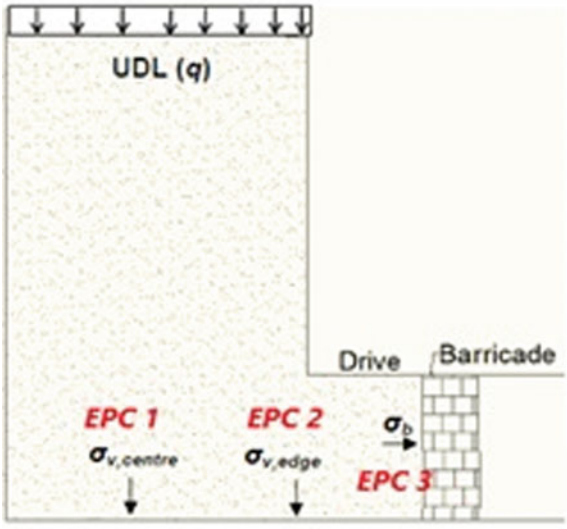

Fig. 1.10 Schematic diagram of the barricade testing apparatus

setback distance (L) has been set at four different positions (0, 25, 50, 75 mm) for each drive size and shape to determine the stress function as offset increases.

Figure 1.11 displays the recorded barricade pressure at each offset tested for the 100 mm drive with circular cross-section (CD100). The plot displays a definite correlation between barricade pressure and offset distance. As the barricade is constructed at an increasing distance from the stope brow, the stress reduces. This relationship has been apparent for all four offsets and it confirms that the reduction of lateral load acting on the barricade with increasing offset distance, encouraging miners to install the barricade as far as possible from the stope brow. However, the common industry practice is to keep the barricade offset distance equal to the drive height to reduce the drainage time of the fill [4].

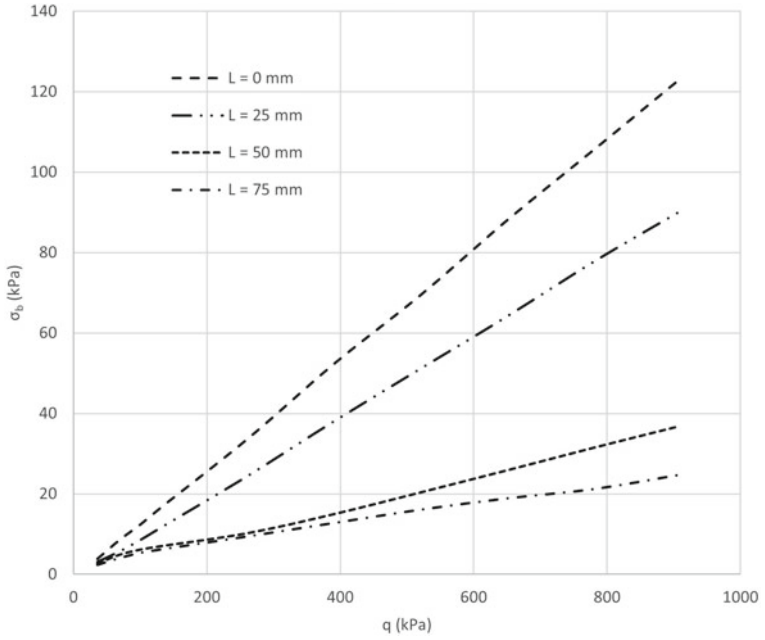

Fig. 1.11 Barricade stress variation with surcharge pressure q for different offset distances L, for CD100

Laboratory results were compared with the Kuganathan's equation (Eq. 1.21) in a dimensionless analysis as shown in Fig. 1.12. The analytical solutions show an overestimation of barricade stresses at an offset (L) approaching the drive height (D) for both active and at-rest earth pressure coefficients, however, the at-rest condition is more comparable with the experimental results justifying the same behaviour as in Fig. 1.6. Furthermore, Kuganathan solutions also verified that the trend of barricade stress reduction with offset distance is non-linear.

A novel laboratory model of square-shaped drive barricade apparatus (Fig. 1.13) has been built recently at James Cook University, Australia to study the arching within drives and to analyse the stress developments on the fill barricade. The vertical stope model apparatus (the 'arching apparatus' referred in Sect. 3.7) will be integrated with the new barricade apparatus to understand the behaviour of fill stresses in a full-scale mine stope through laboratory model simulations. The locations of the soil pressure sensors in the stope are shown in Fig. 1.14.

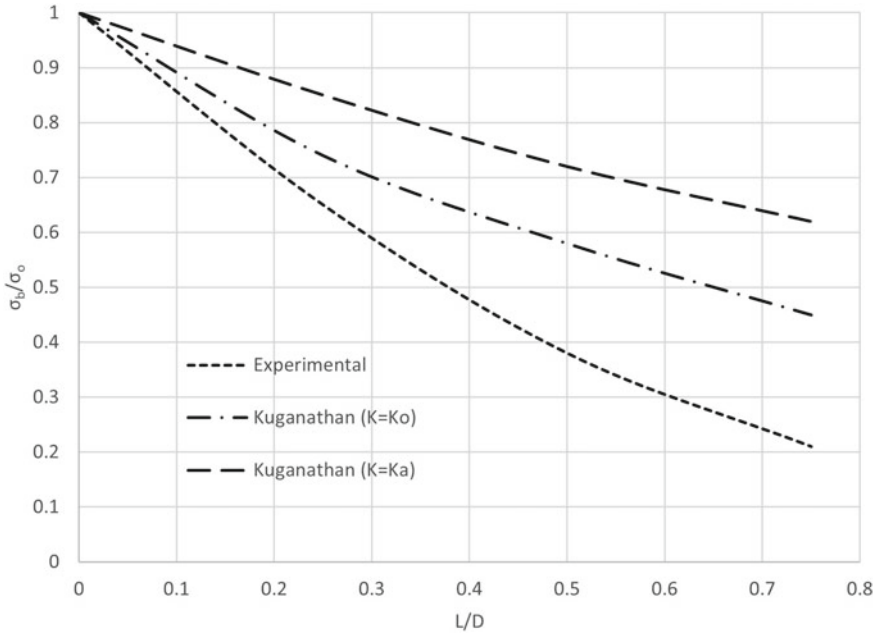

Fig. 1.12 Analytical and experimental comparison of barricade stresses

1.4.4 General Properties of Barricade Bricks

Drive barricades are constructed either using special porous bricks or shotcrete method with drain pipes in place to allow drainage. The porous bricks are composed of gravel, sand, cement and water in the approximate ratio of 40:40:5:1 respectively by weight. It is believed by mining professionals that the porous bricks used for underground barricade construction are susceptible to strength variabilities due to rheological properties of the backfill slurry [18, 70]. The porous bricks with average porosity values of 18–24% and specific gravity values of 2.39–2.59 are designed such that the barricade facilitates free draining of any excess water in the fill. The extensive laboratory testing carried out by Berndt et al. [70] have concluded that the bricks have permeability values significantly higher than that of the hydraulic fill. Typical permeability values of hydraulic fill vary from 2×10^{-4} to 35×10^{-4} cm/s while the permeability for barricade bricks ranges between 1.2×10^{-2} and 3.1×10^{-1} cm/s, which confirms that porous bricks are 2–3 orders of magnitude more permeable than the fill. It has been concluded that the drainage of the backfill system is not influenced by the brick permeability and hence, assuming that the barricade is not affecting the pore pressure development within the fill for numerical modelling exercises is reasonable. Porous bricks that were specially made for the use of barricade construction are shown in Fig. 1.15.

Fig. 1.13 Newly built square stope-drive barricade laboratory model apparatus

Fig. 1.14 Inside view of the model stope and locations of soil pressure sensors

Fig. 1.15 Special porous barricade bricks

1.5 Summary

Mine tailing management through mine backfilling is an important part of the underground mining operation which should be done as the mining progresses. Backfilling provides numerous benefits for sustainable mining. Geotechnical aspects of mine backfilling including properties of different backfill types with more focus on hydraulic fills and paste fills, stress developments within backfilled stopes, and the stresses on drive barricades were discussed extensively in this chapter. An accurate estimation of the stress state within the full mine stope is critically important to design safe and competent barricades and to prevent potential barricade failures. Behaviour of a backfill system has been researched over the past few decades through analytical modelling and laboratory modelling. Numerical model simulations have become popular nowadays in an attempt to study the backfill system conveniently. Most of the research on backfill modelling conducted thus far are based on continuum modelling and are limited to vertical stopes. Hence, the particulate approach for backfill modelling is highly recommended and further research on backfill stresses within drive and on barricade are highly encouraged for better designing of barricades. The comprehensive review on geotechnical considerations of mine backfilling and the research based solutions for geotechnical issues and challenges arising when designing a safe backfill system, presented in this chapter will be useful to many stakeholders including researchers, academics, industry professionals and policy makers.

References

1. Minerals Council of Australia. Retrieved May 2, 2023, from https://minerals.org.au/resources/mcas-2020-21-pre-budget-submission/.
2. Sivakugan, N., Widisinghe, S., & Wang, V. Z. (2014). Vertical stress determination within backfilled mine stopes. *International Journal of Geomechanics, 14*(5), 06014011.
3. Grice, T. (2001). Recent minefill developments in Australia. In *7th International Symposium on Mining with Backfill*, Seattle, Washington.
4. Li, L., & Aubertin, M. (2009a). Horizontal pressure on barricades for backfilled stopes. Part I: Fully drained conditions. *Canadian Geotechnical Journal, 46*(1), 37–46.
5. Potvin, Y., Thomas, E., & Fourie, A. (2005). Handbook on mine fill. *Australian Centre for Geomechanics.*
6. Boger, D. V. (1998). Environmental rheology and the mining industry. In *7th International Symposium on Mining with Backfill: Minefill '98*, Australia (pp. 15–17).
7. Rankine, R., Pacheco, M., & Sivakugan, N. (2007). Underground mining with backfills. *Soils and Rocks, 30*(2), 93–101.
8. Piciullo, L., Storrøsten, E. B., Liu, Z., Nadim, F., & Lacasse, S. (2022). A new look at the statistics of tailings dam failures. *Engineering Geology, 303*, 106657.
9. Bloss, M. L. (2014). An operational perspective of mine backfill. In *Minefill 2014: 11th International Symposium on Mining with Backfill* (pp. 15–30).
10. Chileshe, M. N., Syampungani, S., Festin, E. S., Tigabu, M., Daneshvar, A., & Odén, P. C. (2020). Physico-chemical characteristics and heavy metal concentrations of copper mine wastes in Zambia: Implications for pollution risk and restoration. *Journal of Forestry Research, 31*(4), 1283–1293.

11. Nyenda, T., Gwenzi, W., & Jacobs, S. M. (2021). Changes in physicochemical properties on a chronosequence of gold mine tailings. *Geoderma, 395*, 115037.
12. Rankine, K., Sivakugan, N., & Cowling, R. (2006). Emplaced geotechnical characteristics of hydraulic fills in a number of Australian mines. *Geotechnical and Geological Engineering, 24*(1), 1–14.
13. Sivakugan, N., Rankine, R. M., Rankine, K. J., & Rankine, K. S. (2006). Geotechnical considerations in mine backfilling in Australia. *Journal of Cleaner Production, 14*(12–13), 1168–1175.
14. Pettibone, H. C., & Kealy, C. D. (1971). Engineering properties of mine tailings. *Journal of the Soil Mechanics and Foundations Division, ASCE, 97*(SM9), 1207–1225.
15. Herget, G., & De Korompay, V. (1978). In-situ drainage properties of hydraulic backfills. *Proceedings of Mining with Backfill, Research and Innovations, CIM Special, 19*, 117–123.
16. Grice, T. (1998). Underground mining with backfill. In *2nd Annual Summit-Mine Tailings Disposal Systems* (pp. 1–14).
17. Brady, A. C., & Brown, J. A. (2002). Hydraulic fill at Obsorne mine. In *Proceedings of the 8th Underground Operators' Conference*, Townsville, Australia (pp. 161–165).
18. Kuganathan, K. (2001). Mine backfilling, backfill drainage and bulkhead construction–A safety first approach. *Australian Mining Monthly* (February), 58–64.
19. Pullum, L. (2003). Pipeline performance. In *International Seminar on Paste and Thickened Tailings, Australian Center for Geomechanics* (pp. 1–13).
20. Robinsky, E. I. (1975). Thickened discharge—A new approach to tailings disposal. *CIM Bulletin, 68*, 47–53.
21. Jewell, R. J., Fourie, A. B., & Lord, E. R. (2002). Paste and thickened tailings-a guide. *Australian Center for Geomechanics*, 152.
22. Clough, G. W., Sitar, N., Bachus, R. C., & Rad, N. S. (1981). Cemented sands under static loading. *Journal of Geotechnical Engineering Division, ASCE, 107*(6), 799–817.
23. Pirapakaran, K., & Sivakugan, N. (2007). Arching within hydraulic fill stopes. *Geotechnical and Geological Engineering, 25*(1), 25–35.
24. Dalvi, R. S., & Pise, P. J. (2008). Effect of arching on passive earth pressure coefficient. In *Proceedings of 12th IACMAG Conference*, Goa, India (pp. 236–243).
25. Handy, R. L. (1985). The arch in soil arching. *Journal of Geotechnical Engineering, 111*(3), 302–318.
26. Take, W. A., & Valsangkar, A. J. (2001). Earth pressures on unyielding retaining walls of narrow backfill width. *Canadian Geotechnical Journal, 38*(6), 1220–1230.
27. Caceras, C. A. (2005). *Effect of delayed backfill on open stope mining methods.* MASc Thesis, University of British Columbia, Vancouver, Canada.
28. Iglesia, G. R., Einstein, H. H., & Whitman, R. V. (1999). Determination of vertical loading on underground structures based on an arching evolution concept. In C. Fernandez & R. A. Bauer (Eds.), *Geo-Engineering for underground facilities* (pp. 495–506). Geo-Institute of ASCE.
29. Li, L., Aubertin, M., Simon, R., Bussière, B., & Belem, T. (2003). Modeling arching effects in narrow backfilled stopes with FLAC. In *3rd International Symposium on FLAC and FLAC3D Numerical Modelling in Geomechanics*, Ontario, Canada (pp. 211–219).
30. Ladanyi, B., & Hoyaux, B. (1969). A study of the trap-door problem in a granular mass. *Canadian Geotechnical Journal, 6*(1), 1–14.
31. Pirapakaran, K., & Sivakugan, N. (2007). A laboratory model to study arching within a hydraulic fill stope. *Geotechnical Testing Journal ASTM, 30*(6), 496–503.
32. Sivakugan, N., & Widisinghe, S. (2013). Stresses within granular materials contained between vertical walls. *Indian Geotechnical Journal, 43*(1), 30–38.
33. Bosscher, P. J., & Gray, D. H. (1985). Soil arching in sandy slopes. *Journal of Geotechnical Engineering, ASCE, 112*(6), 626–635.
34. Low, B. K., Tang, S. K., & Choa, V. (1994). Arching in piled embankments. *Journal of Geotechnical Engineering, ASCE, 120*(11), 1917–1937.
35. Shelke, A., & Patra, N. R. (2008). Effect of arching on uplift capacity of pile groups in sand. *International of Geomechanics, ASCE, 8*(6), 347–354.

36. Marston, A. (1930). The theory of external loads on closed conduits in the light of the latest experiments. *Bulletin 96 of the Iowa Engineering Experiment Station*, 138–170.
37. McCarthy, D. F. (1988). *Essentials of soil mechanics and foundations: Basic geotechnics.* Prentice Hall.
38. Shukla, S. K., & Sivakugan, N. (2013). Load coefficient for ditch conduits covered with geosynthetic-reinforced granular backfill. *International Journal of Geomechanics, 10*(106), 76–82.
39. Spangler, M. G. (1962). Culverts and conduits. In G. A. Leonards (Ed.), *Foundation engineering* (pp. 965–999). McGraw-Hill
40. Terzaghi, K. (1943). *Theoretical soil mechanics* (pp. 66–99). Wiley and Sons.
41. Janssen, H. (1895). Versuche uber Getreidedruck in Silozellen. *Zeitschrift des Vereines deutscher Ingenieure, 39*, 1045–1049.
42. Walters, J. K. (1973). A theoretical analysis of stresses in silos with vertical walls. *Chemical Engineering Science, 28*, 13–21.
43. Mitchell, R., Olsen, R., & Smith, J. (1982). Model studies on cemented tailings used in mine backfill. *Canadian Geotechnical Journal, 19*(1), 14–28.
44. Aubertin, M., Li, L., Arnoldi, S., Belem, T., Bussière, B., Benzaazoua, M., & Simon, R. (2003). Interaction between backfill and rock mass in narrow stopes. In *12th Pan American Conference on Soil Mechanics and Geotechnical Engineering* (pp. 1157–1164).
45. Rankine, W. J. M (1857). On the stability of loose earth. *Philosophical Transactions of the Royal Society, 147*, 9–27. http://doi.org/10.1098/rstl.1857.0003
46. Krynine, D. P. (1945). Discussion of stability and stiffness of cellular cofferdams by K. Terzaghi. *ASCE Transactions, 110*, 1175–1178.
47. Jaky, J. (1944). The coefficient of earth pressure at rest. *Journal of the Society of Hungarian Architects and Engineers, 7*(2), 355–358.
48. Singh, S., Sivakugan, N., & Shukla, S. K. (2010). Can soil arching be insensitive to phi? *International Journal of Geomechanics, ASCE, 10*(3), 124–128.
49. Bloss, M. L. (1992). *Prediction of cemented rock fill stability design procedures and modelling techniques.* Ph.D. Thesis, University of Queensland, Brisbane.
50. Pierce, M. E. (2001). Stability analysis of paste back fill exposes at Brunswick mine. In *Proceedings of 2nd International FLAC Symposium*, Lyon, France (pp. 147–156).
51. Rankine, R. M., Rankine, K. J., Sivakugan, N., Karunasena, W., & Bloss, M. (2001). A numerical analysis of the arching mechanism in paste fills throughout a complete mining sequence. *Proceedings of the 1st Asian Pacific Congress on Computational Mechanics* (pp. 461–466).
52. Belem, T., Harvey, A., Simon, R., & Aubertin, M. (2004). Measurement and prediction of internal stresses in an underground opening during its filling with cemented fill. In *5th International Symposium on Ground Support in Mining and Underground Construction* (pp. 619–630).
53. Knutsson, S. (1981). Stresses in the hydraulic backfill from analytical calculations and in situ measurements. In *Application of Rock mechanics to Cut and Fill mining* (pp. 261–268). Institution of Mining and Metallurgy.
54. Thompson, B. D., Grabinsky, M. W., Bawden, W. F., & Counter, D. B. (2009). In situ measurements of cemented paste backfill in long-hole stopes. In M. Diederichs & G. Grasselli (Eds.), *ROCKENG09; 3rd CANUS Rock Mechanics Symposium*, Toronto.
55. Thompson, B. D., Bawden, W. F., & Grabinsky, M. W. (2012). In situ measurements of cemented paste backfill at the Cayeli Mine. *Canadian Geotechnical Journal, 49*(7), 755–772.
56. Fahey, M., Helinski, M., & Fourie, A. (2009). Some aspects of the mechanics of arching in backfilled stopes. *Canadian Geotechnical Journal, 46*(11), 1322–1336.
57. Kuganathan, K. (2005). Hydraulic fills. In Y. Potvin, E. D. Thomas, & A. Fourie (Eds.), *Handbook on Mine Fill* (pp. 23–47).
58. Li, L., Aubertin, M., & Belem, T. (2005). Formulation of a three dimensional analytical solution to evaluate stresses in backfilled vertical narrow openings. *Canadian Geotechnical Journal, 42*(6), 1705–1717.

59. Li, L., & Aubertin, M. (2008). An improved analytical solution to estimate the stress state in subvertical backfilled stopes. *Canadian Geotechnical Journal, 45*(10), 1487–1496.
60. Mitchell, R., & Roettger, J. (1984). Bulkhead pressure measurements in model fill pours. *CIM Bulletin, 77*(888), 50–55.
61. Ting, C. H., Sivakugan, N., & Shukla, S. K. (2012). Laboratory simulation of the stresses within inclined stopes. *Journal of Geotechnical Testing, 35*(2), 1–15.
62. Widisinghe, S. D. (2014). *Stress developments within a backfilled mine stope and the lateral loading on the barricade.* Ph.D. thesis, James Cook University.
63. To, P., & Sivakugan, N. (2018a). Arching of granular flow under loading in silos. In *Proceedings of the 9th European Conference on Numerical Methods in Geotechnical Engineering (NUMGE)* (pp. 857–862). CRC Press.
64. To, P., & Sivakugan, N. (2018b). Boundary stress distribution in silos filled with granular material. In *Proceedings of the 9th European Conference on Numerical Methods in Geotechnical Engineering (NUMGE)* (pp. 863–868). CRC Press.
65. Singh, S., Shukla, S., & Sivakugan, N. (2011). Arching in inclined and vertical mine stopes. *Geotechnical and Geological Engineering, 29*(5), 685–693.
66. Jayakodi, J. D. S. U., Bennett, R. J., Reddicliffe, A. J., Sivakugan, N., & To, P. (2021). Laboratory modelling of stresses within the minefills and loads on barricades. In *Proceedings of 3rd International Conference in Geotechnical Engineering,* Colombo, Sri Lanka (pp. 247–252).
67. Ting, C. H., Shukla, S. K., & Sivakugan, N. (2011). Arching in soils applied to inclined mine stopes. *International Journal of Geomechanics, 11*(1), 29–35.
68. Thompson, B. D., Hunt, T., Malek, F., Grabinsky, M. W., & Bawden, W. F. (2014). In situ behaviour of cemented hydraulic and paste backfills and the use of instrumentation in optimising efficiency.
69. Kuganathan, K. (2002). A method to design efficient mine backfill drainage systems to improve safety and stability of backfill bulkheads and fills. In *8th Underground Operators' Conference, Growing Our Underground Operations* (pp. 181–188).
70. Berndt, C. C., Rankine, K. J., & Sivakugan, N. (2007). Materials properties of barricade bricks for mining applications. *Geotechnical and Geological Engineering, 25*(4), 449–471.
71. Geoscience Australia. Retrieved Sept 15, 2021, from https://www.ga.gov.au/education/classroom-resources/minerals-energy/australian-mineral-facts.